INVESTIGATING THE LONG-TERM EFFECTS OF SPIKE-TIMING-DEPENDENT PLASTICITY AND THE ACTIVITY-DEPENDENCE OF cFOS EXPRESSION IN HIPPOCAMPAL PYRAMIDAL NEURONS USING OPTOGENETICS

Dissertation
zur Erlangung des Doktorgrades
an der Fakultät für Mathematik, Informatik und Naturwissenschaften
Fachbereich Physik
der Universität Hamburg

vorgelegt von
Margarita Anisimova

Hamburg, 2020

Gutachter der Dissertation	Prof. Dr. Thomas G. Oertner
	Prof. Dr. Claus C. Hilgetag
Zusammensetzung der Prüfungskommision	Prof. Dr. Peter Schmelcher
	Prof. Dr. Robert H. Blick
	Prof. Dr. Wolfgang Parak
	Prof. Dr. Thomas G. Oertner
	Prof. Dr. Claus C. Hilgetag
Vorsitzender der Prüfungskommision	Prof. Dr. Peter Schmelcher
Datum der Disputation	24.11.2020
Vorsitzender des Fach-Promotionsausschusses Physik	Prof. Dr. Günter H. W. Sigl
Leiter des Fachbereichs Physik	Prof. Dr. Wolfgang Hansen
Dekan der Fakultät MIN	Prof. Dr. Heinrich Graener

Моим родителям Владимиру и Ольге Анисимовым
Für meinen Mann Lennart Sobirey
And to my green iguana Ryuuketzu

CONTENTS

ABSTRACT i
ZUSAMMENFASSUNG iii
PUBLICATIONS vi

I Introduction 1
1 The Hippocamus 3
  1.1 Trisynaptic excitatory circuit 3
  1.2 Organotypic hippocampal slice cultures 4
2 Synaptic plasticity 5
  2.1 NMDAR-dependent long term potentiation and long term depression 5
3 Spike-timing-dependent plasticity 9
4 Channelrhodopsin family 11
5 Immediate early gene cFos 13
6 Objectives 15

II Materials and methods 17
7 Animal experiments and expression of channelrhodopsins 19
  7.1 Organotypic hippocampal slice cultures 19
  7.2 Expression of channelrhodopsins in neurons 20
  7.3 Viral vector-based transfection 20
  7.4 Single-cell electroporation 21
8 Electrophysiology 23
  8.1 Electrophysiology setup 23
  8.2 Patch-clamp measurement configurations 24
9 Optogenetics 29
  9.1 Channelrhodopsins functional characterization 29
  9.2 Light evoked spiking threshold 30
  9.3 oSTDP: Causal and Anti-causal pairing 30
  9.4 oSTDP during whole-cell recordings 31
  9.5 In-incubator light stimulation 32
  9.6 Special stimulation conditions for in-incubator oSTDP 33
  9.7 Read-out procedure for in-incubator oSTDP 33
  9.8 Slope analysis for oSTDP 34
10 Immunohistochemistry and imaging 37
  10.1 Immunohistochemistry 37
  10.2 Confocal microscopy 38
  10.3 Stimulated emission depletion (STED) microscopy 38
  10.4 Data analysis in IMARIS 39

III Optogenetic induction of spike-timing-dependent plasticity 41
11 Expression and characterization of spectrally separated channelrhodopsins 45
  11.1 Functional characterization of ChrimsonR and CheRiff 45
  11.2 Light evoked action potentials in CheRiff-CA1 neurons 47

11.3 Optimal number of ChrimsonR-CA3 neurons 47
12 Optogenetic induction of spike-timing-dependent plasticity 51
12.1 Optogenetic induction of STDP during whole-cell patch clamp 51
12.2 Input strength 3 days after in-incubator oSTDP induction 53
12.3 NMDA and pairing frequency dependence of late LTP 56
12.4 Absence of tLTD 3 days after in-incubator oSTDP induction 56
12.5 Input strength 3 hours after in-incubator oSTDP induction 57
12.6 Calmodulin washout role in early tLTD 58
12.7 Activity dependence of late LTP 59
12.8 Intrinsic excitation of postsynaptic neurons 61
12.9 Dendritic spines morphology 3 days after oSTDP induction 62
13 Discussion and perspectives 65
13.1 Short-term vs long-term consequence of oSTDP 65
13.2 Patch-clamp associated problems in plasticity induction 66
13.3 Increase in filopodia spines number after light stimulation 67

IV Characterization of activity-dependent cFos upregulation after light stimulation 69
14 cFos upregulation after neuronal activity 73
14.1 cFos protein expression window in neuronal nuclei in OHSCs 73
14.2 Viral expression of opsins over extended period of time leads to cFos expression 74
14.3 Optimal light stimulation protocol for ChrimsonR transduced pyramidal neurons 75
14.4 cFos expression depends on the firing frequency. 76
14.5 cFos expression depends on the number of spikes 79
14.6 cFos expression in PCP4-CA2 neurons 82
15 Discussion and perspectives 85
CONCLUSION 87

V Appendix 89

APPENDIX A:

CFOS EXPRESSION DEPENDS ON THE FIRING FREQUENCY: DATA PER HIPPOCAMPAL REGION 91

APPENDIX B:

CFOS EXPRESSION DEPENDS ON THE NUMBER OF SPIKES: DATA PER HIPPOCAMPAL REGION 94

APPENDIX C:

CFOS EXPRESSION DEPENDS ON THE MAPK SIGNALING PATHWAY 97
LIST OF FIGURES 104
LIST OF TABLES 105
ACRONYMS 107
BIBLIOGRAPHY 125
STATEMENT OF CONTRIBUTION 127
ACKNOWLEDGEMENTS 129
DECLARATION 131

ABSTRACT

The strengthening or weakening of synapses that occurs after coincident activity of pre and postsynaptic neurons is called spike-timing-dependent plasticity (STDP) and is thought to be a key mechanism underlying the formation of memories. However, to control postsynaptic firing, the neurons need to be recorded from which consequently limits what we know about STDP to about 60 minutes after the induction. Using two colors of light, I was able to overcome this issue and optogenetically induce STDP (oSTDP) between hippocampal CA3 and CA1 neurons expressing the channelrhodopsins ChrimsonR and CheRiff and observe both timing-dependent potentiation (tLTP) and timing-dependent depression (tLTD). I then induced oSTDP in the incubator without patching the neurons and quantified the results three days later. Surprisingly, three days after inducing oSTDP only tLTP was evident regardless of whether pre- or postsynaptic neurons fired first. The late tLTP depended on NMDA receptors and unperturbed spontaneous activity was necessary in the two days following oSTDP induction. My data suggest that tLTD at Schaffer collateral synapses may be a transitory phenomenon or, potentially, a recording artifact of patch-clamp experiments.

In addition, I investigated the action potential-induced expression pattern of the immediate early gene cFos. As expected, cFos was strongly and specifically activated in the CheRiff-CA1 neurons during induction of oSTDP (300 EPSPs at 5 Hz paired with 300 bursts of 3 action potentials at 50 Hz). However, 300 single spikes at 5 Hz failed to elevate cFos level in CA3 neurons. To understand this, I investigated the relationship between cFos expression and neuronal firing pattern. Neurons expressing ChrimsonR were stimulated at various frequencies and a clear U-shaped frequency dependence was observed. cFos was induced by 300 action potentials at 0.1 Hz and 50 Hz, whereas almost no cFos upregulation was evident at 1 Hz, 5 Hz and 10 Hz. I then investigated how many action potentials (i.e. spikes) fired by a neuron are sufficient to upregulate cFos. Interestingly, 3 light-induced action potentials were enough to induce cFos expression in CA1 neurons, but less sufficient in case of CA3 or Dentate gyrus, whereas 10 action potentials were not sufficient to induce cFos expression in any region. 30 and 300 spikes at 50 Hz resulted in similar cFos expression pattern across the organotypic hippocampal slice culture.

ZUSAMMENFASSUNG

Die Stärkung oder Schwächung von Synapsen, die nach einer gleichzeitigen Aktivität von prä- und postsynaptischen Neuronen auftritt, wird als 'spike-timing-dependent plasticity' (STDP) bezeichnet und als Schlüsselmechanismus für die Bildung von Erinnerungen angesehen. Um die postsynaptische Aktivität zu kontrollieren, müssen jedoch die Neuronen gepatcht werden, wodurch das, was wir über STDP wissen, auf etwa 60 Minuten nach der Plastizitätsinduktion begrenzt wird. Mit zwei Lichtfarben konnte ich dieses Problem überwinden. Die optogenetisch induzierte STDP (oSTDP) zwischen CA3- und CA1-Pyramidenzellen des Hippocampus, die mit den Channelrhodopsinen ChrimsonR und CheRiff transduziert beziehungsweise transfektiert wurden, produzierte sowohl eine zeitabhängige Langzeitpotenzierung (tLTP) als auch eine zeitabhängige Langzeitdepression (tLTD). Ich induzierte oSTDP im Inkubator, ohne die Neuronen zu patchen, und quantifizierte die Ergebnisse drei Tage später. Überraschenderweise war drei Tage nach Induktion von oSTDP nur tLTP offensichtlich, unabhängig davon, ob prä- oder postsynaptische Neuronen zuerst feuerten. Das Vorhandensein von tLTP nach drei Tagen hing von NMDA-Rezeptoren ab und eine ungestörte spontane Aktivität war in den zwei Tagen nach der oSTDP-Induktion notwendig. Meine Daten legen nahe, dass tLTD an Schaffer-Kollateral-Synapsen ein vorübergehendes Phänomen oder möglicherweise ein Aufzeichnungsartefakt von Patch-Clamp-Experimenten sein kann.

Zusätzlich untersuchte ich das aktivitätsinduzierte Expressionsmuster des unmittelbaren frühen Gens cFos. Wie erwartet wurde cFos in den CheRiff-CA1-Neuronen während der Induktion von oSTDP stark und spezifisch aktiviert (300 EPSPs bei 5 Hz gepaart mit 300 Bursts mit 3 Aktionspotentialen bei 50 Hz). 300 einzelne Spikes bei 5 Hz konnten jedoch das cFos-Expressionsniveau in CA3-Neuronen nicht erhöhen. Um dieses Verhalten zu verstehen, untersuchte ich die Beziehung zwischen der cFos-Expression und dem neuronalen Feuermuster. ChrimsonR transduzierte Neuronen wurden bei verschiedenen Frequenzen stimuliert und eine deutliche, U-förmige Frequenzabhängigkeit wurde beobachtet. cFos-Expression wurde durch 300 Aktionspotentiale bei 0.1 Hz und 50 Hz induziert, während bei 1 Hz, 5 Hz and 10 Hz fast keine cFos-Hochregulation erkennbar war. Ich untersuchte weiterhin, wie viele von einem Neuron ausgelöste Aktionspotentiale ausreichen, um cFos hoch zu regulieren. Interessanterweise reichten 3 lichtinduzierte Aktionspotentiale aus, um die cFos-Expression in CA1-Neuronen zu induzieren, während CA3-Neuronen oder Granularzellen des Gyrus dentatus mehr benötigten. Mit 10 Aktionspotentialen konnte dagegen in keiner Region des Hippokampus cFos-Expression induziert werden. 30 und 300 Aktionspotentiale bei 50 Hz führten zu einem ähnlichen cFos-Expressionsmuster in der organotypischen Hippocampus-Schnittkultur.

PUBLICATIONS

- **Long vs short-term synaptic learning rules after optogenetic spike-timing-dependent plasticity**
  M. Anisimova, B. van Bommel, J. S. Wiegert, M. Mikhaylova, T. G. Oertner, C. E. Gee
  bioRxiv:863365
- **Firing frequency dependence of cFos expression in hippocampal neurons**
  M. Anisimova, P. Lamothe Molina, T. G. Oertner, C. E. Gee
  in prep.

Part I

INTRODUCTION

1 THE HIPPOCAMUS

The hippocampus is an important part of the brain limbic system and is known to play a crucial role in various types of memory, such as short-term and spatial. The hippocampus has two main regions: dentate gyrus and *Cornu Ammonis* (CA), which has 3 distinct subfields (CA1, CA2 and CA3). Each region has inhibitory and excitatory (with mostly unidirectional pathways) circuitry. It is known on the famous case of H.M., than without the hippocampi it is impossible to form any new declarative memories [1], which makes it an attractive model to study synaptic plasticity and memory. in addition, the hippocampus is one of the few brain regions with adult neurogenesis [2, 3] and has an architecture convinient for various types of electrophysiological experiments.

1.1 Trisynaptic excitatory circuit

The trisynaptic excitatory circuit or loop – is a unidirectional pathway in hippocampus, originally described by Santiago Ramon y Cajal in 1911 [4]. It consists of three major cell groups: granule cells in dentate gyrus and pyramidal neurons in CA3 and CA1 areas. The first synaptic connection (Figure 1.1) is made between the entorhinal cortex and dentate gyrus via perforant pathway fibers. Then the signal transmission goes from dentate gyrus via mossy fibers to CA3 pyramidal neurons in *stratum lucidum*. The axonal terminals from CA3 pyramidal neurons then form synapse onto CA1 pyramidal neurons in *stratum radiatum* via Schaffer collaterals. As last, CA1 pyramidal neurons send axons back to entorhinal cortex, completing the loop. Apart from the mentioned loop there is a variety of inhibitory and other excitatory circuits which all together make the whole connectivity picture in hippocampus more complicated [2].

For my study the Schaffer collateral part of trisynaptic excitatory circuit is chosen due to unidirectionality and well defined pre- and postsynaptic structure, which allowed me to precisely control plasticity induction between selected pre- and postsynaptic partners.

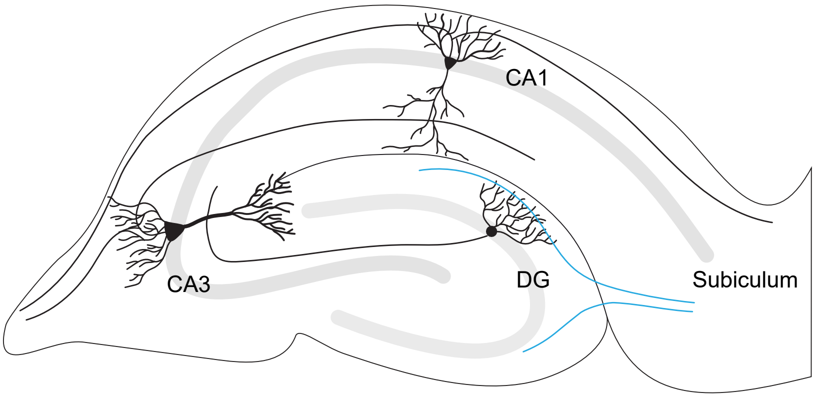

Figure 1.1: Trisynaptic circuit. Illustrated are the granule cells in dentate gyrus (DG) and pyramidal neurons in CA3 and CA1. The entorhinal cortex projections are shown in blue.

1.2 Organotypic hippocampal slice cultures

In vivo studies are considered to be preferential in the field of neuroscience, however many questions would not be possible to address due to complicated experimental procedures and limited access within the intact brain. The other extreme, dissociated neuronal cultures, however, tend to oversimplify the organ model and lack the defined structure, which can greatly impact the outcome of the study. Organotypic hippocampal slice cultures (OHSCs) have various advantages to both *in vivo* and dissociated cell culture. As the name suggests, the cultured tissue continues to develop *in vitro* as it would *in vivo* [5, 6].

As described in section 1.1, one of the important features of hippocampus is a unique set of unidirectional pathways. Those pathways are well preserved in OHSCs through the culturing time and thus OHSCs could be used as a model for long-term studies of neuronal plasticity [5, 6]. Sterile OHSCs are viable for at least 30 days, which allows genetic and pharmacological manipulations on a cellular level with relatively easy access to the neuronal network. In present work I am interested in long-term changes in synaptic strength, which was possible to observe due to long-term stability of OHSCs.

OHSC - organotypic hippocampal slice culture

2 SYNAPTIC PLASTICITY

> *"Activity-dependent synaptic plasticity is induced at appropriate synapses during memory formation, and is both necessary and sufficient for the information storage underlying the type of memory mediated by the brain area in which that plasticity is observed."* [7]

The synaptic plasticity and memory hypothesis.

Hippocampal synapses are plastic, which mean that they can respond to a specific pattern of activity in the circuit with long-lasting changes in their efficacy. Synaptic plasticity is classified by the time of lasting changes (short term and long term) and by the type of those changes (potentiation, when synaptic strength increased, and depression, when it decreased).

Short term synaptic plasticity is believed to be important for synaptic transmission adaptation on milliseconds to seconds level and happens as a response to brief neuronal activity, which leads to calcium influx into the synaptic terminal. This influences the changes in the neurotransmitter release probability, leading to facilitation or depression of the synaptic transmission [8, 9].

Long term plasticity was originally described in 1973 [10, 11]. It was shown that the repetitive presynaptic stimulation at 100 Hz (tetanic) leads to a significant increase in the synaptic transmission efficiency hours to days after stimulation. That was the first experimental evidence of long term potentiation (LTP) in hippocampal reagion dentate gyrus and became a well-studied phenomenon since then. LTP, together with long term depression (LTD), is believed to be one of the major cellular mechanisms underlying learning and memory [12].

2.1 NMDAR-dependent long term potentiation and long term depression

LTP and LTD are the prime candidate mechanisms underlying bidirectional control of activity dependent persistent changes in synaptic strength. High frequency stimulation (HFS) is traditionally used to induce LTP, whereas prolonged low-frequency stimulation (LFS) is found to induce LTD (Figure 2.1) [8, 10–13].

LTP - long term potentiation
LTD - long term depression

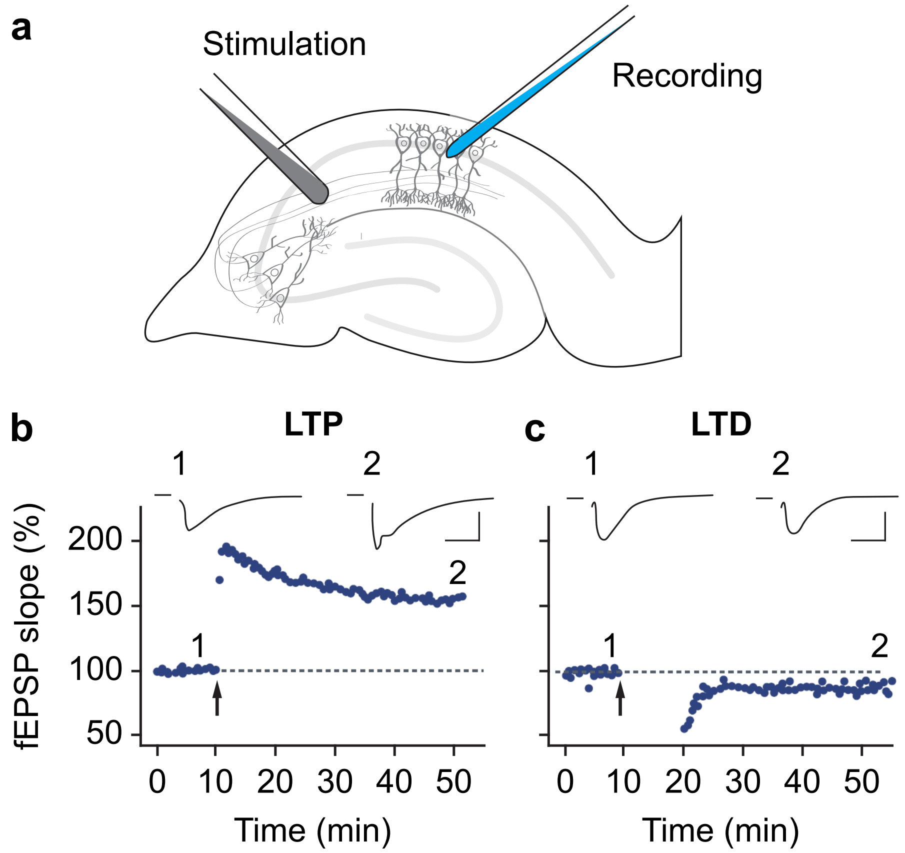

Figure 2.1: NMDAR-dependent LTP and LTD at hippocampal CA1 synapses. a, A schematic diagram of the rodent hippocampal slice preparation, demonstrating the CA1 and CA3 regions as well as the dentate gyrus. Typical electrode placements for studying synaptic plasticity at Schaffer collateral synapses onto CA1 neurons are indicated. **b and c,** Sample experiments illustrating LTP and LTD in the CA1 region of the hippocampus. Synaptic strength, defined as the initial slope of the field excitatory postsynaptic potential (fEPSP; normalized to baseline) is plotted as a function of time. **b,** LTP elicited by high-frequency tetanic stimulation (100 Hz stimulation for 1 s; black arrow). **c,** LTD elicited by low-frequency stimulation (5 Hz stimulation for 3 min given twice with a 3 min interval; black arrow). Data traces were taken at the times indicated by the numbers on the graphs (Scale bars - 0.5 mV; 10 ms). *Figure and legend are based on* [8].

fEPSP - field excitatory postsynaptic potential

Among many different types of the plasticity mechanisms, NMDAR-dependent LTP and LTD in the hippocampal region CA1 is one of the most studied and well understood phenomena and also discussed in this dissertation. The schematic representation of the mechanisms underlying NMDAR-dependent LTP and LTD is shown on Figure 2.2. NMDA receptors are believed to play a role of a ’coincidence detector’ with millisecond precision: glutamate is released in a response to presynaptic activity and postsynaptic depolarization frees the NMDA receptor pore from [Mg^{2+}] block [14–16]. To summarize, in case of LTP, a significant rapid calcium influx through the NMDA receptors in dendritic spine activates the intracellular signaling cascade, which leads to an increase in the single-channel conductance of AMPA receptors and promotes the integration of additional AMPA receptors into the PSD [17–20]. Alongside, the structural plasticity leads to the dendritic spine growth and drives an increase of the presynaptic ac-

NMDAR - N-methyld-aspartate receptor
AMPAR - α-amino-3-hydroxy-5-methylisoxazole-4- propionic acid receptor
PSD - postsynaptic density

tive zone size [8, 21–23]. Whereas during LTD the prolonged modest rise in calcium concentration leads to preferential activation of protein phosphatases and to removal of AMPA receptors from the PSD and their further endocytoses and degradation [17, 19, 24]. Thus, during LTD due to the loss of receptors, structural plasticity leads to decrease in dendritic spine size [23, 25–27].

CaMKII - calcium/calmodulin-dependent kinases II
PP1 - protein phosphatases 1

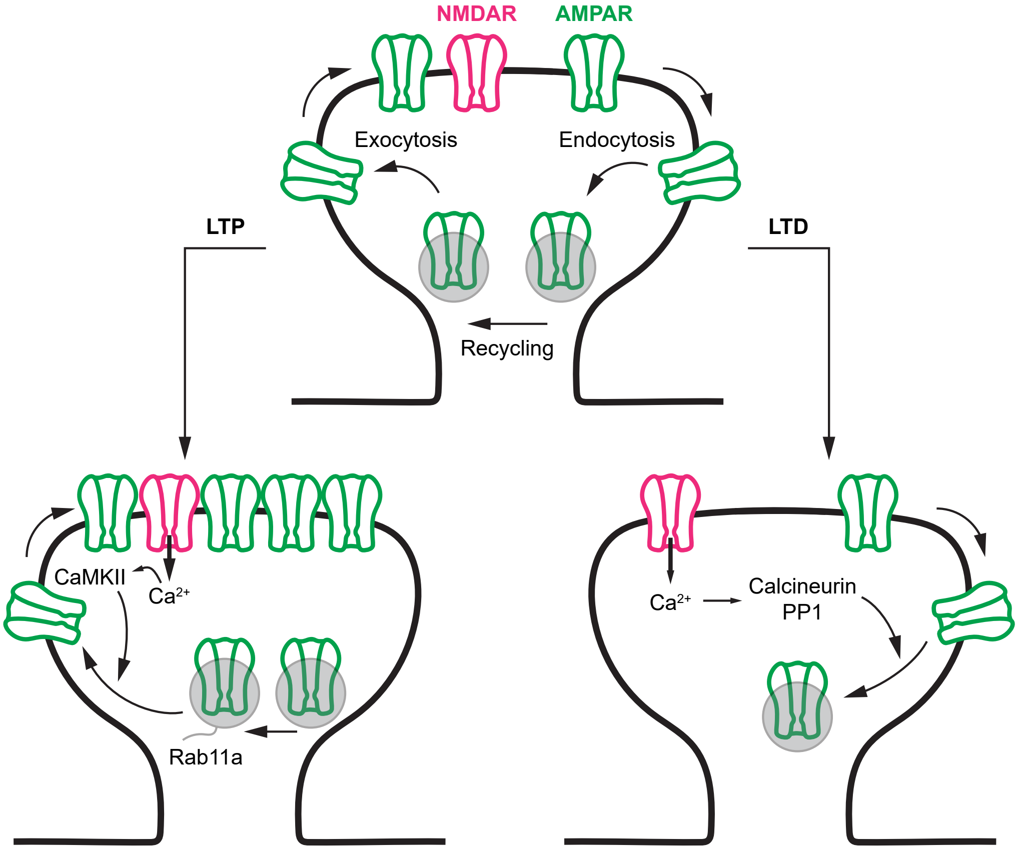

Figure 2.2: Model of AMPAR trafficking during LTP and LTD. In the basal state (depicted on top), receptors cycle between the postsynaptic membrane and intracellular compartments. This is achieved through lateral mobility of the receptors out of the synapse into endocytic zones, where they are endocytosed into early endosomes in a clathrin- and dynamin-dependent manner. Following induction of LTP, there is enhanced receptor exocytosis and stabilization at the synapse through a calcium-driven process that involves CaMKII and fusion of recycling endosomes mediated by Rab11a. Following the induction of LTD, enhanced endocytosis at extrasynaptic sites occurs in a process that is calcium-dependent and involves protein phosphatases, primarily calcineurin and PP1. While in the basal state endocytosis is presumably balanced by receptor recycling, following LTD receptors are retained within the cell, and perhaps degraded. *Figure and legend are based on* [8].

3 SPIKE-TIMING-DEPENDENT PLASTICITY

Spike-timing-dependent plasticity (STDP) is one of the physiologically relevant forms of activity-dependent plasticity, thought to underlie learning and memory formation in the brain [13, 28–32]. Its existence was originally implied in a hypothesis by Canadian psychologist Donald Hebb in 1949:

> *"Let us assume that the persistence or repetition of a reverberatory activity (or "trace") tends to induce lasting cellular changes that add to its stability.... When an axon of cell A is near enough to excite a cell B and repeatedly or persistently takes part in firing it, some growth process or metabolic change takes place in one or both cells such that A's efficiency, as one of the cells firing B, is increased."* [33]

This hypothesis later became known as a Hebb's postulate or Hebbian learning rule. It took about 50 years until the importance of causality in activity of pre- and postsynaptic partners, which determines the direction of synaptic strength modification, was experimentally proven by Guo-Qiang Bi and Mu-Ming Poo in dissociated neuronal cultures [34], Dominique Debanne and coauthors in organotypic slice cultures [35] and Bert Sakmann and coauthors in acute slices [36, 37]. Further studies have demonstrated the diversity of STDP rules for different brain regions and types of synaptic connections (Figure 3.1) [38–45].

Same as for HFS and LFS, timing-dependent LTP and LTD (tLTP and tLTD) also depend on NMDA receptors activation and changes in postsynaptic $[\mathrm{Ca}^{2+}]$ [34, 35, 46–49], which play a role in shaping the STDP window. In addition, STDP also depends on the precise timing of action potentials and firing mode during plasticity induction [30, 50–53], location of the spines along the dendritic tree [50, 54–58], and on the dendritic spikes [50, 53, 56, 59].

HFS - high frequency stimulation
LFS - low frequency stimulation

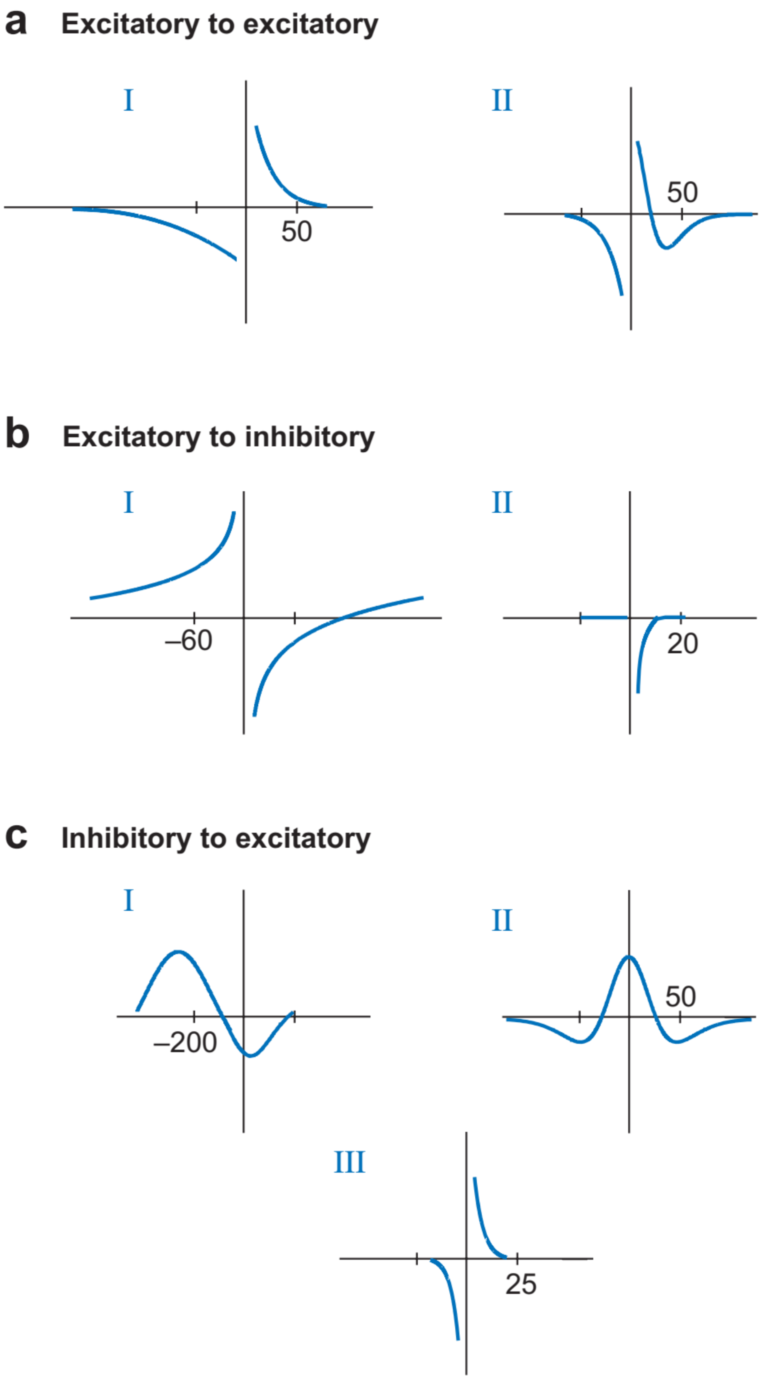

Figure 3.1: Diversity of temporal windows for STDP induction. **a,** Windows for excitatory to excitatory connections. **I,** Classical STDP curve. **II,** STDP with an additional tLTD window due to EPSP coinciding with the afterdepolarization, which leads to a moderate $[\mathrm{Ca}^{2+}]$ influx. Observed in CA1 pyramidal neurons. **b,** Windows for excitatory to inhibitory connections. **I,** Excitatory inputs to Purkinje-like GABAergic neurons. **II,** Mouse brain stem slices by pairing parallel fiber stimulation with cartwheel neuron spiking. **c,** Windows for inhibitory to excitatory connections. **I,** Inhibitory inputs to neocortical L2/3 pyramidal neurons. **II,** GABAergic synapses onto CA1 pyramidal neurons. **III,** The entorhinal cortex GABAergic inputs to layer II excitatory stellate cells. Temporal axis is in milliseconds. *Figure and legend from* [28].

GABA - gamma aminobutyric acid

4 CHANNELRHODOPSIN FAMILY

Channelrhodopsin-1 (ChR1) and Channelrhodopsin-2 (ChR2), the first members of the now big channelrhodopsin family, were initially discovered from the model organism *Chlamydomonas reinhardtii* by the group of Prof. Dr. Peter Hegemann in 2002 [60, 61]. Shortly after both variants became publicly available, several groups in Germany, USA and Japan successfully used them to control neuronal activity with light [62–65], starting the new field of Optogenetics.

Using light to manipulate the neuronal activity is a very attractive idea nowadays widely used in neuroscience [66–68]. The obvious advantages of less invasive experiments generate a constant demand for new types of optogenetic tools with different functions [69–72], ion selectivity [70–75], kinetics [69, 71, 72, 76–81] and absorption spectra [71, 77, 79–82]. In recent years genetic engineering together with ongoing large-scale sequencing of algal and marine microorganisms' genomes and use of machine learning algorithms have provided a number of new rhodopsins families with more advantageous characteristics (Figure 4.2) [68, 74, 80, 81, 83–85].

Out of this richness, the spectrally shifted channelrhodopsins (Figure 4.1) are of the great interest, since, when combined, they can be used to investigate more complex behavior-relevant mechanisms [71, 72, 80]. In this work I am using the combination of blue-light sensitive CheRiff [81] and red-light sensitive ChrimsonR [80] to independently activate two separate groups of hippocampal neurons with a millisecond precision to study the spike-timing-dependent plasticity over behavior-relevant timescale.

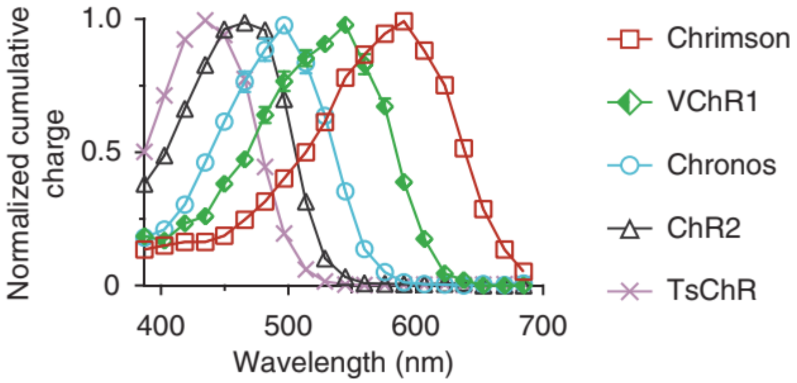

Figure 4.1: Novel channelrhodopsin spectral classes discovered through algal transcriptome sequencing. Channelrhodopsin action spectra measured in HEK293 cells ($n = 6$–8 cells) using equal photon fluxes, ~2.5×10^{21} photons/(s m^2). *Figure and legend from* [80].

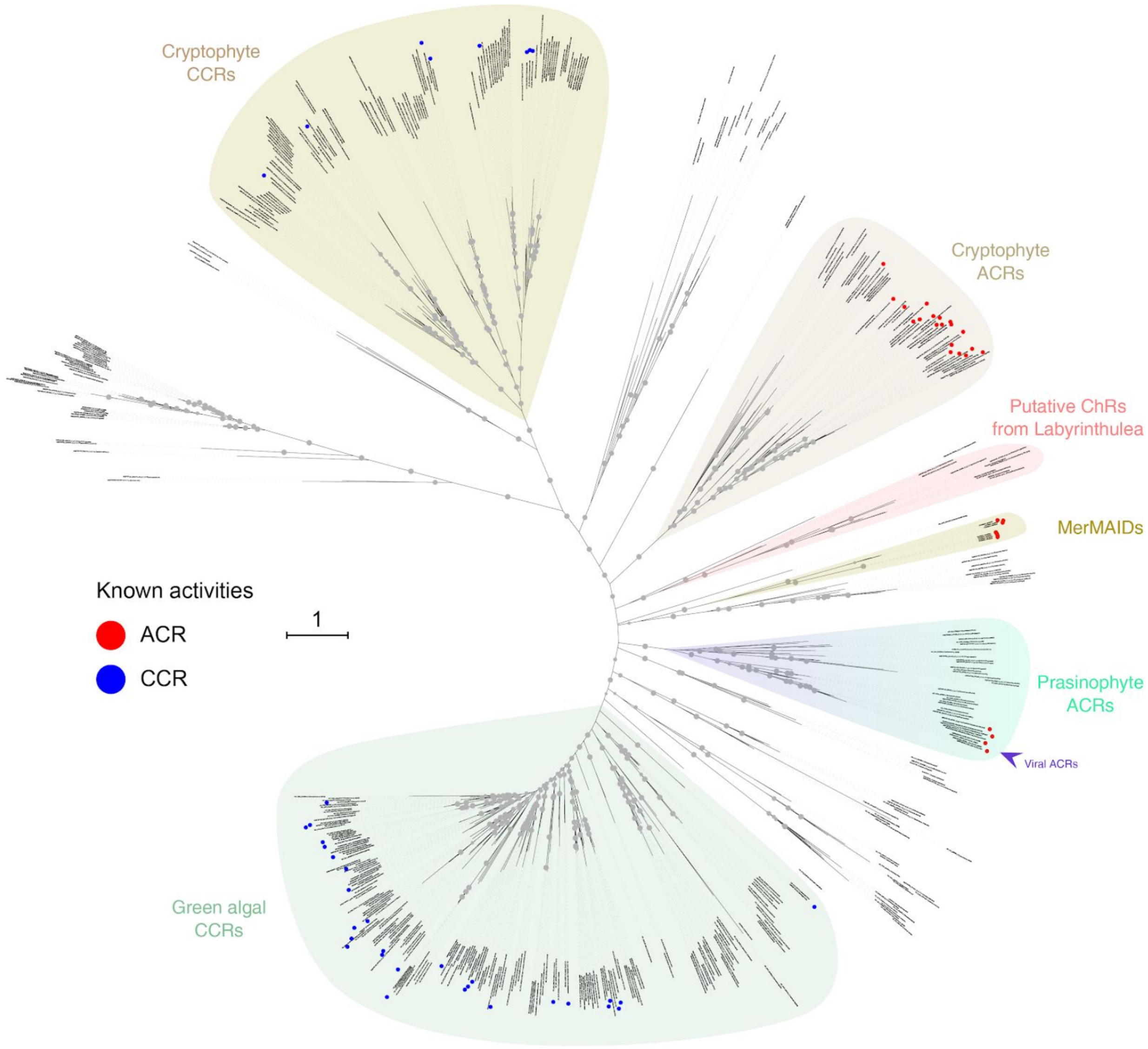
Cryptophyte CCRs
Cryptophyte ACRs
Putative ChRs from Labyrinthulea
MerMAIDs
Prasinophyte ACRs
Viral ACRs
Green algal CCRs
Known activities
● ACR
● CCR
1

Figure 4.2: Phylogenetic analysis of known and putative channelrhodopsins. The prasinophyte and viral ACRs form a well-supported clade not nested in any of the described families of channelrhodopsins. The ultrafast bootstrap support values are indicated by circles (70 to 100 range). *Figure and legend from* [83].
Interactive version is avaliable at: `https://itol.embl.de/tree/1326924345362481586852545`.

ACR - anion-conducting channelrhodopsin
CCR - cation-conducting channelrhodopsin

5

IMMEDIATE EARLY GENE CFOS

Neuronal activity related transcription of immediate early genes (IEGs) is believed to be necessary for many forms of synaptic plasticity induction and its maintenance [86–91]. Out of this large variety, the IEG cFos is particularly interesting, since it codes a transcription factor which participates in a variety of adaptive responses in neurons, such as long-term structural and functional regulation of neuronal properties, stress, neurotransmitter receptors activation and long-term changes in synaptic strength [89, 92–94], but also cFos expression can provide a valuable information about the specific changes in neuronal activity which is widely used in modern neuroscience [86–88, 95–103].

***Immediate early gene* (*IEG*)** *- a gene, such as cFos, that is induced rapidly and transiently in the absence of de novo protein synthesis.*

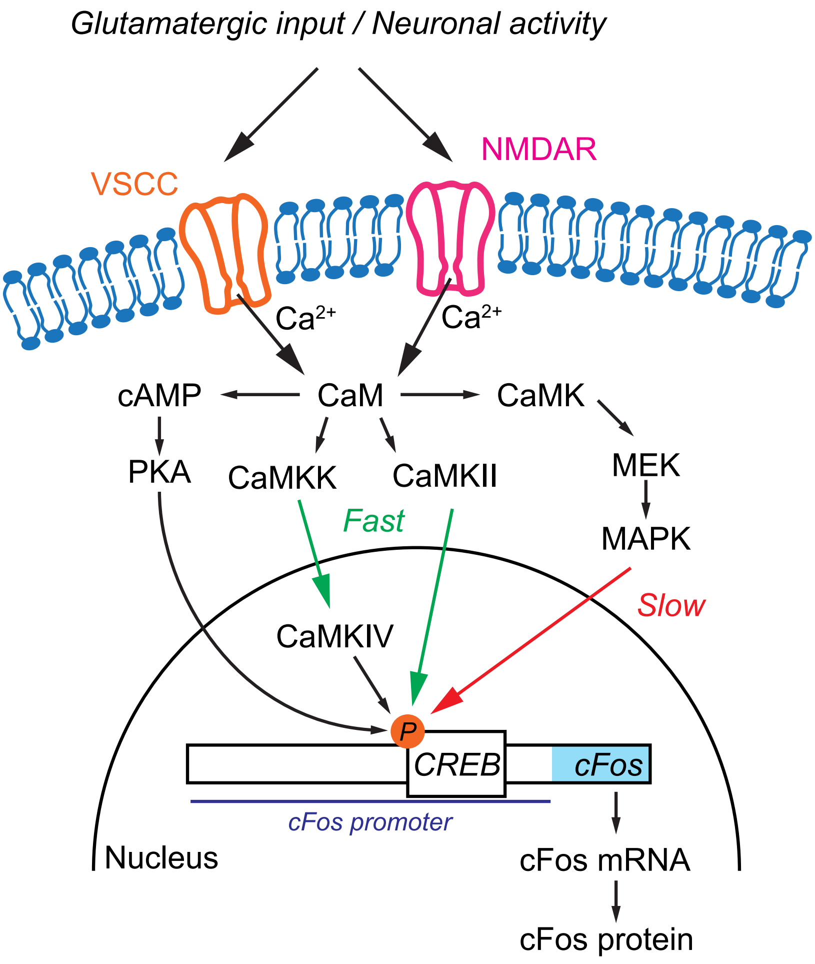

Figure 5.1: A schematic representation of activity dependent-activation of cFos signaling pathway. Shown are fast (green) CaMKII and CaMKIV dependent CREB phosphorylation pathway; slow (red) CaMK-dependent MAPK signaling pathway and cAMP-dependent pathway. Together those pathways are controlling early and late CaM-dependent CREB phosphorylation, which with a recruitment of translational cofactors leads to the cFos protein production. *Modified from* [104] *and* [105].

VSCC - voltage-sensitive calcium channels
CaM - calmodulin
CaMK - calcium/calmodulin-dependent kinase
CaMKK - calcium/calmodulin-dependent kinase kinase
CaMKII and CaMKIV - calcium/calmodulin- dependent kinases II and IV
MEK - mitogen-activated protein kinase (**MAPK**)/extracellular signal-regulated kinase (**ERK**) kinase
cAMP - cyclic adenosine monophosphate
PKA - cAMP-dependent protein kinase A
CREB - cAMP response element binding protein

Action potential dependent gene regulation, together with associated $[\mathrm{Ca}^{2+}]$ transients, lead to the activation of the specific signaling pathway with appropriate temporal dynamics [90, 95, 97, 98]. It is known that the combined activation of MAPK pathway and phosphorylation of CREB cause high cFos expression in neurons [90, 98, 100, 106–109], however it is still unclear, how the multiple second messenger pathways associated with action potential signaling influence gene transcription. Thus, a simplified signaling pathway for cFos expression is shown on Figure 5.1.

6 OBJECTIVES

Spike-timing-dependent plasticity (STDP) is a candidate mechanism for information storage in the brain. However, it has been practically impossible to assess the long-term consequences of STDP since the patch-clamp recordings from postsynaptic neurons last at most one hour. Since my main objective was to study the effects of STDP on the behavior relevant timescale (i.e. days after induction), I established the all-optical noninvasive STDP (oSTDP) induction protocol. To do so, I first had to determine and characterize opsins suitable for independently spiking CA3 and CA1 pyramidal neurons (Chapter 11.1). Then, it was essential to optimize the transfection/transduction method to achieve desired firing pattern in CA3-CA1 circuit (Chapter 11.3). It was also important to make sure, that the new all-optical protocol works in the same way as when tLTP/tLTD were induced by electrical stimuli (Chapter 12.1). When the protocol was established for the short-term (~30 min) STDP, I further developed and validated a normalization strategy for reading out synaptic strength days after induction (Chapter 9.7). Finally, I explored the synaptic mechanisms of late-oSTDP (Chapters 12.2 to 12.8). Additionally, I used super resolution microscopy (STED) to investigate the postsynaptic dendritic spines density and spine morphology 3 days after in-incubator oSTDP induction (Chapter 12.9).

tLTP - timing-dependent long term potentiation

tLTD - timing-dependent long term depression

STED - stimulated emission depletion

Furthermore, I aimed at characterizing the activity-dependent IEG cFos expression in hippocampal pyramidal neurons. To do so, I first established a virus drop protocol to homogeneously express ChrimsonR in the whole OHSC and characterized the light-induced firing activity in CA3 and CA1 neurons (Chapter 14.3). To identify the cFos-positive pyramidal neurons I tested different antibodies and staining protocols. I then optimized the settings for the image acquisition and established the data analysis routine (Chapter 10). Then the ChrimsonR-expressing OHSC were light-stimulated to evoke action potentials at different frequencies with different number of repetitions. In addition, I compared the cFos upregulation in the different hippocampal regions, to investigate cell-type specific expression pattern (summarized in Chapters 14.4 and 14.5). At last, I investigated how low and high frequency firing induce cFos expression in PCP4-positive and PCP4-negative CA2 neurons (Chapter 14.6).

IEG - immediate early gene

PCP4 - Purkinje cell protein 4

Thus, this study is the first to report a long-term (3 days) consequence of spike-timing-dependent plasticity at Schaffer-collateral synapses. It shows that the late-STDP results in synaptic potentiation regardless of the exact temporal sequence. This finding impacts our understanding of STDP-like mechanism involved in the memory consolidation process on the behavior relevant timescale. This study also reports the results of the first detailed analysis of the activity-dependent cFos expression in hippocampal pyramidal neurons. It shows that the experimental results with cFos as an activity marker should be interpreted carefully, since not each firing pattern leads to the cFos expression in pyramidal neurons.

Part II

MATERIALS AND METHODS

7

ANIMAL EXPERIMENTS AND EXPRESSION OF CHANNELRHODOPSINS

Animal experiments: all experiments were performed in accordance with the Animal Welfare Law of the Federal Republic of Germany (Tierschutzgesetz der Bundesrepublik Deutschland, TierSchG) with the approval of the Behörde für Gesundheit und Verbraucherschutz Hamburg, Fachbereich Veterinärwesen and the animal care committee of the UKE.

Sample size: For the oSTDP experiments, the minimum sample size I aimed at was 5 CheRiff-CA1 neurons (+ 8 NT-CA1 neurons for normalization) from at least 3 OHSC per group. For the cFos characterization experiments, the aim was 5 OHSC per stimulation condition. In general, the data collection for both experiments took approximately 4 years. To ensure blinding (see below) and reduce the influence of external factors, experimental groups were interspersed, which resulted in the uneven group sizes for both projects.

UKE - University Medical Center Hamburg-Eppendorf

oSTDP - optogenetically induced spike-timing-dependent plasticity

CheRiff-CA1 - CheRiff expressing CA1 pyramidal neurons

NT - non transfected pyramidal neurons

OHSC - organotypic hippocampal slice culture

Blinding: For all in-incubator experiments in both projects, I was blind to the treatment of the OHSCs until the analysis of the selected data was finished and decision on whether to include the particular data point into the final results was made. Unblinding occurred when it was necessary to assign the individual measurements to their respective treatment groups.

7.1 Organotypic hippocampal slice cultures

All experiments described in this dissertation were performed using organotypic hippocampal rat slices (OHSC). Here, a modified long-term tissue culturing process with adjusted culturing medium composition, initially described in [5], was used. The detailed protocol used for slices preparation can be found in [110].

In brief, Wistar rat pups were sacrificed at postnatal day 5 to 7. Hippocampus was dissected and cut into 400 µm thick slices with a tissue chopper. If not indicated otherwise, hippocampal slices were cultured in pairs on 30 mm membrane inserts in the incubator at 37 °C with 5 % CO_2. The membranes were placed in 6-well plates on top of 1 ml of culturing medium. The plates were kept in sterile conditions throughout the experiments to avoid usage of antibiotics, which are known to induce epileptic-like spiking in the OHSCs [111]. The medium was partially changed 2 times a week under yellow light, especially after the expression of opsins, to prevent unwanted light activation.

Solutions

Culture medium, 37 °C
(pH 7.28 , 320 mOsm/kg)

79 %	MEM (Sigma; M7278)
20 %	heat-inactivated horse serum (Gibco; 16050122)
13 mM	D-glucose (Fluka; 49152)
109 mM	NaCl (Sigma; S5150-1L)
0.8 mM	$MgSO_4$ (Fluka; 63126-1L)
1.8 mM	$CaCl_2$ (Fluka; 21114-1L)
1 mM	L-glutamine (Gibco; 25030-024)
6 µM	ascorbic acid (Fluka; 11140)
0.01 mg/ml	insulin (Sigma; I6634)

Essential Equipment and Materials

Membrane inserts
Millicell Cell Culture Insert, pore size 0.4 µm; PICMORG50

Yellow light
Osram LUMILUX CHIP control T8

7.2 Expression of channelrhodopsins in neurons

As described in Chapter 3, STDP relies on independent and precise control of pre- and postsynaptic partners. As one of the goals of this thesis was to achieve non-invasive plasticity induction, the preference was given to spectrally-separated channelrhodopsins. The approach for the transfection of pre- and postsynaptic partners was different due to the experimental design. To achieve reliable light-controlled input into CA1 neurons, I aimed at transfecting at least 30 neurons in a central region of CA3. Adeno-associated viral vector-based (AAV) transduction is the most suitable method in this case. For CA1 region I used single cell electroporation to be able to compare opsin-expressing CA1 pyramidal neurons to their non-transfected neighbors, since this method allows targeted and precise DNA delivery. In general, I aimed at transfecting both CA3 and CA1 neurons on the same day, when slices were 12 to 14 DIV.

DIV - days *in vitro*

7.3 Viral vector-based transfection

The viral vectors were made in the Vector Core facility of the UKE (listed in Table 7.1). The plasmid pAAV-syn-ChrimsonR-TdTomato was packed into AAV viral particles with serotype Rh10. The viral vector was diluted to 7.22×10^{13} vg/ml and stored at −80 °C.

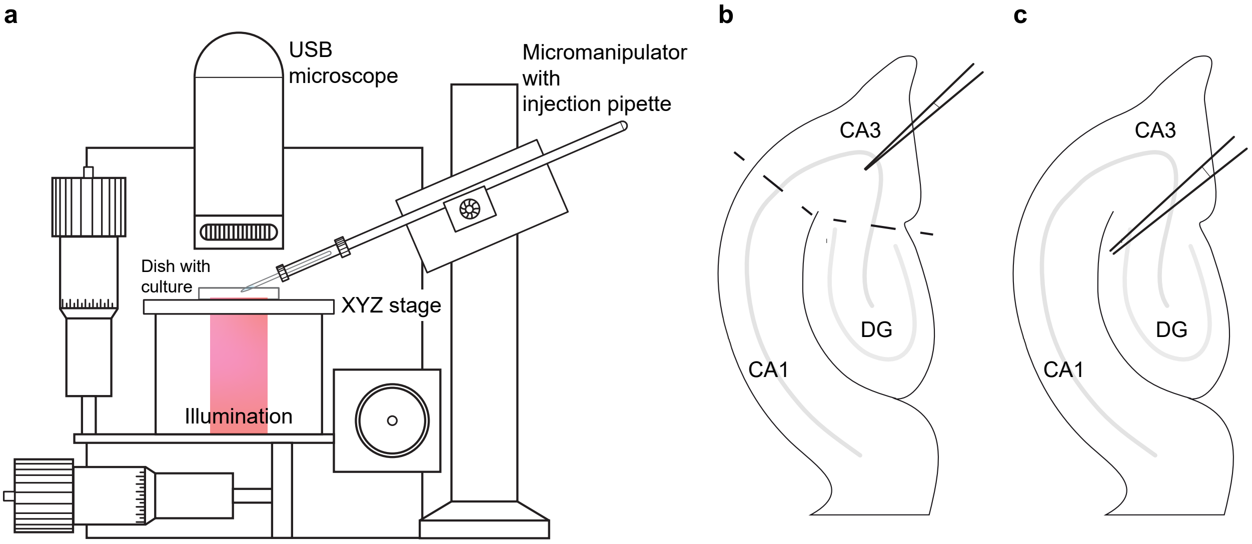

Figure 7.1: DNA expression in organotypic hippocampal slice culture by viral vector transduction. a, Schematic representation of the virus injection setup. **b,** Pipette placement for local virus injection. Dashed line indicates the border of CA3 region. **c,** Pipette placement for the virus drop. Note the difference in the pipette tip size.

The schematic of sterile virus-injection setup is shown in Figure 7.1 a. Sharp thin-walled borosilicate glass micropipettes were broken under the visual control to a diameter of approximately 10 µm and then loaded with 1 µl of viral vector solution. A membrane insert with OHSCs was transferred into sterile HEPES-buffer solution warmed up to 37 °C. In every OHSC I aimed to inject approximately in the middle of CA3 region (Figure 7.1 b). It was important for the injection to be local, as if the majority of CA3 neurons were transduced, light-driven input into CA1 neurons was sufficient to cause complex spiking, which could induce plasticity on its own. Thus, I injected each slice with 2 to 5 pressure pulses (Picospritzer settings: 2 bar, 50 ms to 100 ms pulse). A detailed protocol for viral-vector injection and how to maintain sterility is published in [112].

To express the opsin in the whole slice, I established the virus drop technique. In this case, the sharp thin-walled borosilicate glass micropipette was broken to a diameter of approximately 25 µm to 35 µm and then loaded with 2 µl to 3 µl of viral vector in virtue of having ~125 nl of viral vector solution per OHSC. I aimed to place the micropipette to approximately the middle of the slice (Figure 7.1 c) and to gently touch the surface. I then gave 1 or 2 pressure pulses (Picospritzer settings: 2 bar, 30 ms to 60 ms pulse) to form a drop on top of the slice.

Solutions

HEPES-buffer, 30 °C
(pH 7.4 , 318 mOsm/kg)

145 mM	NaCl (Sigma; S5886-500G)
10 mM	HEPES (Sigma; H4034-100G)
25 mM	D-glucose (Fluka; 49152)
2.5 mM	KCl (Fluka; 60121-1L)
1 mM	NaH_2PO_4 (Sigma; S5011-100G)
1 mM	$MgCl_2$ (Fluka; 63020-1L)
2 mM	$CaCl_2$ (Honeywell; 21114-1L)

Essential Equipment and Materials

Microscope camera
USB microscope, dnt DigiMicro Profi

Micromanipulator
PatchMan NP2, Eppendorf

Microelectrode holder
WPI MPH6S

Picospritzer
Picospritzer III, Parker Hannafin

Thin-walled borosilicate glass
TW150F-3, World Precision Inst.

7.4 Single-cell electroporation

All plasmids used for single cell electroporation (listed in Table 7.2) were diluted in intracellular solution. Optimal DNA concentration used in oSTDP experiments was previously determined by Christine E. Gee to ensure that neurons remain healthy and viable weeks after electroporation and that the light evoked spiking threshold remains stable from 7 days to several weeks following electroporation. Thin-walled borosilicate glass pipettes (10 MΩ to 15 MΩ) were loaded with 1 µl of DNA mixture, containing either 0.5 ng/ml pAAV-hsyn-CheRiff-eGFP and 10 ng/ml pCI-syn-mKate2 (for oSTDP experiments), or 0.5 ng/ml pAAV-hsyn-CheRiff-eGFP and 10 ng/ml pEGFP-N1 (for STED experiments); 0.5 ng/ml pAAV-hsyn-CheRiff-eGFP (for oSTDP-cFos experiments). The membrane insert with slices was transferred to the sterile removable microscope chamber filled with 1 ml of HEPES-buffer solution warmed to 37 °C, then 2 ml of the solution were added on top. The chamber was transferred to the electroporation setup under the HEPA-filtered hood, then a few neighboring pyramidal-looking neurons were electroporated (25 pulses, −12 V, 500 µs, 50 Hz). A detailed protocol for single-cell electroporation is published in [113].

Solutions

Intracellular solution
(pH 7.2 , 295 mOsm/kg)

135 mM	K-gluconate (Sigma; G 4500-100G)
0.2 mM	EGTA (Sigma-Aldrich; E0396-10G)
10 mM	HEPES (Sigma; H4034-100G)
4 mM	$MgCl_2$ (Fluka; 63020-1L)
4 mM	Na_2-ATP (Aldrich; A26209-1G)
0.4 mM	Na-GTP (Sigma; G8877-100MG)
10 mM	Na_2-phosphocreatine (Sigma; P7936-1G)
3 mM	ascorbate (Sigma; A5960-100G)

Essential Equipment and Materials

Electrophysiology setup:

Body
Zeiss Axioscope with IR-DIC

Single-cell electroporator
Axoporator 800A, Molecular Devices

Headstage
AP-1A-1MU, Axon Instruments

Micromanipulator
Luigs and Neumann

Camera
ImagingSource CCD camera with 0.5-2.0x zoom

Table 7.1: List of viral vectors

Viral vector	Capsid serotype	Internal number	Titer
pAAV-syn-ChrimsonR-TdTomato	ssAAV$_{\mathrm{Rh10}}$	V11 (V54)	7.22×10^{13} vg/ml
AAV-hsyn-CheRiff-eGFP	ssAAV9	V29	1.93×10^{12} vg/ml

Table 7.2: List of plasmids

Plasmid	Producer (code)	Internal number	Concentration
pAAV-syn-ChrimsonR-TdTomato	Addgene (59171)	E14-27	
AAV-hsyn-CheRiff-eGFP	Addgene (51697)	AD-015	0.5 ng/µl
pCI-syn-mKate2	By I. Ohmert	57	10 ng/µl
pEGFP-N1	Clontech (6085-1)	E18-130	10 ng/µl

8

ELECTROPHYSIOLOGY

8.1 Electrophysiology setup

A schematic representation of the electrophysiology setup is shown in Figure 8.1. The setup is based on the Olympus BX61W1 microscope fitted with Dodt contrast, epifluorescence and CCD-camera on a dual camera port, shared with the LEDs, coupled via a 1 mm multimode fiber and a collimator. Light intensities of the LEDs were calibrated through a 40x objective in the specimen plane using a silicone photodiode power meter.

The on-axis field of view (40x water immersion objective) was chosen such that most CheRiff-CA1 neurons would fit, as well as at least 5 of their NT neighbors (Figure 8.2). It was essential to be able to directly stimulate the CA3 region while recording from CA1 for both induction of oSTDP and the read-out after in-incubator oSTDP. Thus, to locally activate CA3 transduced neurons, which are outside the on-axis field of view (~1.5 mm away), an off-axis stimulation pathway was required [114]. The 594 nm laser was coupled to an optical fiber with a collimator and mounted on a swinging arm with 2 degrees of freedom. Thus, this construction allowed us to point the laser beam though the condenser at any part of the OHSC and locally, with minimum scattering, excite the transfected neurons. Therefore, the laser position was set to be in the middle of ChrimsonR-CA3 neurons (positioned using 5x air objective without moving specimen). However, since this construction was coupled through the condenser, stage movement during the experiments would mean that the illumination field will also be moved. To ensure the stimulation of the exact same region the stage was fixed after the laser position was determined.

Freshly pulled 3 MΩ to 4 MΩ patch electrodes, filled with 1 µl of intracellular solution right before the patch-clamp experiments were used for electrophysiological recordings. A membrane with OHSC was carefully cut from the insert and transferred into the recording chamber. A horseshoe shaped flattened gold wire was used on top of the membrane to hold it in place during the recording to prevent drifting. It was important to leave the OHSC to settle in the chamber for approximately 30 min before starting the recordings due to tissue compression in the bath solution.

Essential Equipment and Materials

Electrophysiology setup

Body
Olympus BX61WI microscope

Illumination
Dodt contrast and epifluoresence

CCD-camera
DMK23U274, The Imaging Source

LEDs
Mightex Systems, wavelengths 625 nm, 530 nm, 470 nm and 400 nm

Laser
Omicron LightHub, 594 nm

40x objective water
Plan-Apochromat 1.0 NA DIC VIS-IR, Zeiss, illuminated field ⌀557 µm

10x objective water
UMPlanFL 0.30 NA W, Olympus, illuminated field ⌀2.65 mm

5x objective air
FLUAR 0.25 NA, Zeiss

Condenser oil
NA 1.4, Olympus

Hg lamp
U-RFL-T, Olympus

Headstage
CV203BU, Axon Instruments

Micromanipulator
ROE-200, Sutter Instruments

Multimode optical fibers
RM38L01 200 µm 0.39 NA, Thorlabs

Collimator
Thorlabs

Filters
mKate2, GFP

Amplifier
Axopatch 200B, Axon Instruments

In-line heater
Warner Instruments

A/D boards
National Instruments

Power meter

Sensor
918D-ST-UV, Newport

Power meter
1936R, Newport

Thick-walled borosilicate glass

1B150F-3, World Precision Inst.

Gold wire

99.99 %, 7440-57-5, Chempur

Perfusion and pump

All recordings were performed in the Ephus [115] software in Matlab environment. For all experiments pre-warmed (30 °C to 33 °C) recording solution was supplied with humidified carbogen (95 % O_2 / 5 % CO_2), circulated through the perfusion system into the recording chamber and recycled for up to 4 hours and then refreshed to avoid osmolality or pH fluctuations.

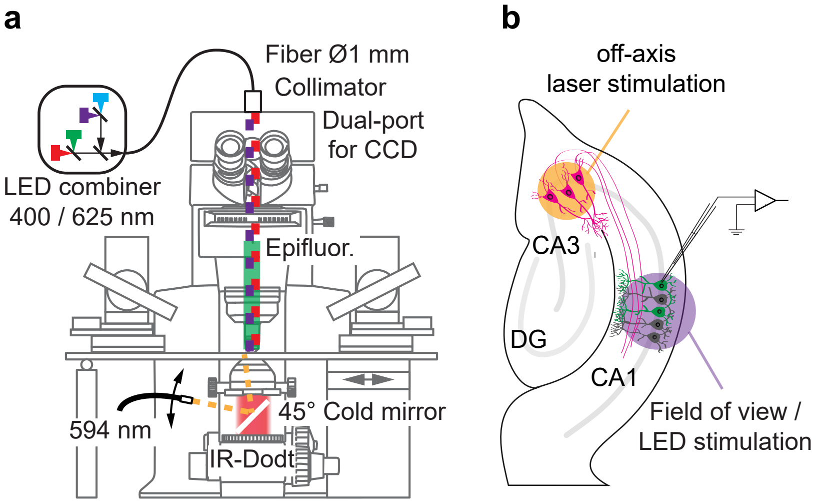

Figure 8.1: Electrophysiology setup. a, Schematic representation of the microscope. **b,** Off- and on-axis stimulation position. Magenta – ChrimsonR-CA3 neurons; Green – CheRiff-CA1 neurons; Black – NT-CA1 neurons.

EPSC - Excitatory postsynaptic current
IPSC - Inhibitory postsynaptic current
LJP - Liquid junction potential
Rs - Series resistance

During the experiments CA1 neurons were voltage-clamped at −70 mV to ensure clear separation between EPSCs and IPSCs (LJP corrected, see Extra 8.3) and all critical cell parameters (see Extra 8.2) were monitored with an external Matlab script for Ephus (OnlineAnalysis) written by a former PhD student of the laboratory. All recordings with unstable (change more than 30 % from the start of the experiments) or high (more than 25 MΩ) Rs were terminated. Importantly, Rs compensation was only used in current-clamp mode for current injections.

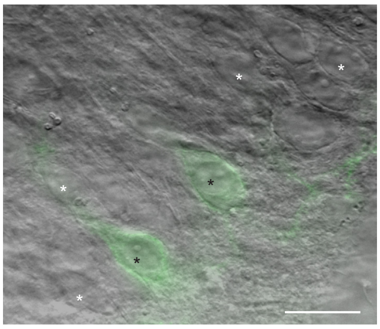

Figure 8.2: Field of view of 40x objective during patch-clamp experiments. Shown is an overlay of the Dodt contrast image and epifluorescence of the CheRiff-eGFP (in green – CheRiff-CA1 neurons). Asterisks are indicating neurons suitable for patching. Scale bar - 25 µm.

8.2 Patch-clamp measurement configurations

Here, two patch-clamp measurement configurations were used: cell-attached or whole-cell patch. The main difference between the two configurations is schematically illustrated in Figure 8.3. In the cell-attached mode the neuronal membrane is intact and the glass pipette is tightly sealed on it. This configuration allows to record the activity of individual or groups of ion channels, located directly under the glass pipette. The cell-attached is usually followed by the whole-cell configuration: when the neuronal membrane under the pipette is broken and there is a direct access to the intracellular space of the neuron. With whole-cell access it is possible to record and externally control the global electrical activity in the entire neuron. However, in oppose to the cell-attached, here the pipette solution will start defusing and mixing together with the intracellular solution of the neuron diluting it and causing the processes known as *washout* [116–118].

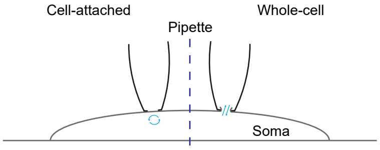

Figure 8.3: Patch-clamp measurement configurations. Note that in contrast to the cell-attached configuration the neuronal membrane in whole-cell configuration is broken and there is a diffusion process happening between the patch-pipette and intracellular solutions.

Extra 8.1: Electrical Equivalent Circuits [117, 119, 120]

For better understanding of the basic principal, the patch-clamp procedure itself could be represented through electrical equivalent circuits, consisting of batteries (E), resistors (R) and capacitors (C). A patch-clamp amplifier is represented by the voltage source E_{am}, in series with a resistor R_{am}, both shunted by an input capacitance C_{am} (Figure 8.4). In case of cell-attached patch, the patch pipette with resistance R_p and capacitance C_p is tightly sealed (Giga-seal, R_{seal}) on the cell membrane. In this case there is no direct input to measure the cell parameters, since the pipette opening is closed off by the high resistance (R_{ca}) of the patch of cell membrane under the electrode tip. When the membrane under the pipette is broken (referred as *breaking-in*), the high resistance R_{ca} is replaced with access resistance R_{acc}, which provides the full access to measure the cell parameters (membrane resistance R_m, membrane capacitance C_m and membrane voltage E_m) under the whole-cell patch.

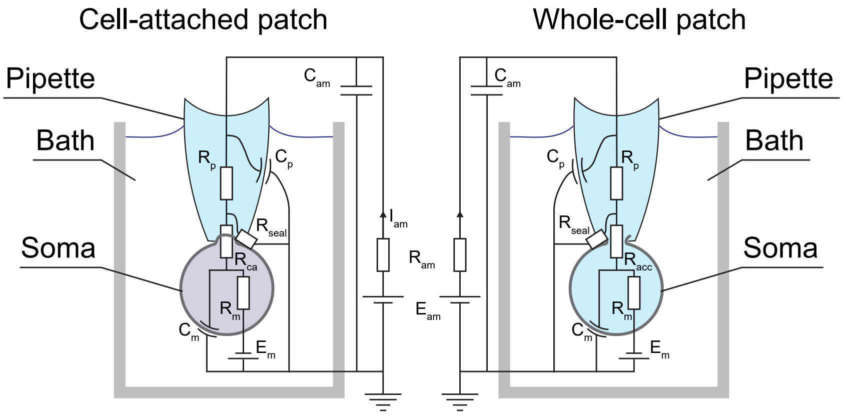

Figure 8.4: Electrical equivalent circuits of patch-clamp measurement configurations. Cell-attached and whole-cell patch as an ERC-circuit. *Figure and legend based on* [119].

To visualize how the whole-cell configuration can be obtained in terms of electrical equivalent circuits, the two simple ERC-circuits from the Figure 8.4 can be combined together by introducing the switches (S, Figure 8.5). When the pipette enters the bath solution, first switch S_p (on scheme: double switch S_{cp} and S_{rp}) is closed. When the switch S_{seal} is opened, the current will flow through lower resistance R_{seal}, creating the cell-attached configuration. From this state to achieve the whole-cell patch, the last switch S_{acc} should be closed (break-in into the cell), shortening the R_{ca} with access resistance R_{acc}.

The quality of the pipette and the patch (giga-seal) in both configurations can be monitored by applying a series of square step pulses (test pulses) to the pipette and measuring the resulting current I_{am}.

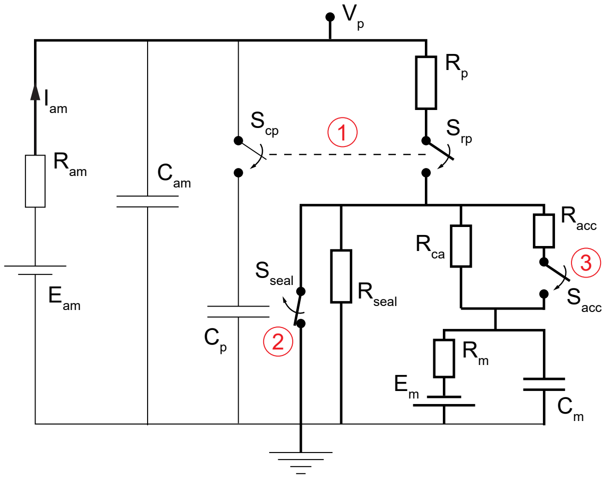

Figure 8.5: Patch-clamp process as an ERC-circuit. 1. First configuration: Pipette in the bath solution. Double switch S_p is closed, current flows through the capacitance C_p and switch S_{seal}. **2.** Second configuration: Cell-attached with giga seal. Now switch S_{seal} is open and the current flows through resistance R_{seal}, while $R_{seal} \ll R_{ca}$. **3.** Third configuration: Whole-cell patch. Now switch S_{acc} is open and the R_{ca} is shortened with R_{acc}. *Figure and legend based on* [119].

Extra 8.2: How to calculate cell parameters from the test pulse [121, 122]

Cell parameters during whole-cell patch-clamp experiments can be calculated from the square test pulse, given in the beginning of each recording. Usually the following parameters are measured and reported: series resistance (the sum of all the resistances between the input of patch-clam amplifier and the cell membrane, determines the quality of patch; $R_s = R_{acc} + R_{seal} + R_p$, Extra 8.1), membrane resistance (R_m), input resistance ($R_{in} = R_s + R_m$) and membrane capacitance (C_m).

Since cell membrane is a leaky capacitor (the capacitor shunted by resistance), the Ohm's law together with Kirchhoff's current law can be used to calculate the main circuit parameters. Thus (Figure 8.6):

$$R_s = \frac{V_t}{I_p} \tag{8.1}$$

$$R_{in} = \frac{V_t}{I_s} \tag{8.2}$$

$$R_m = R_{in} - R_s \tag{8.3}$$

$$C_m = \frac{\tau * (R_s + R_m)}{R_s * R_m} \tag{8.4}$$

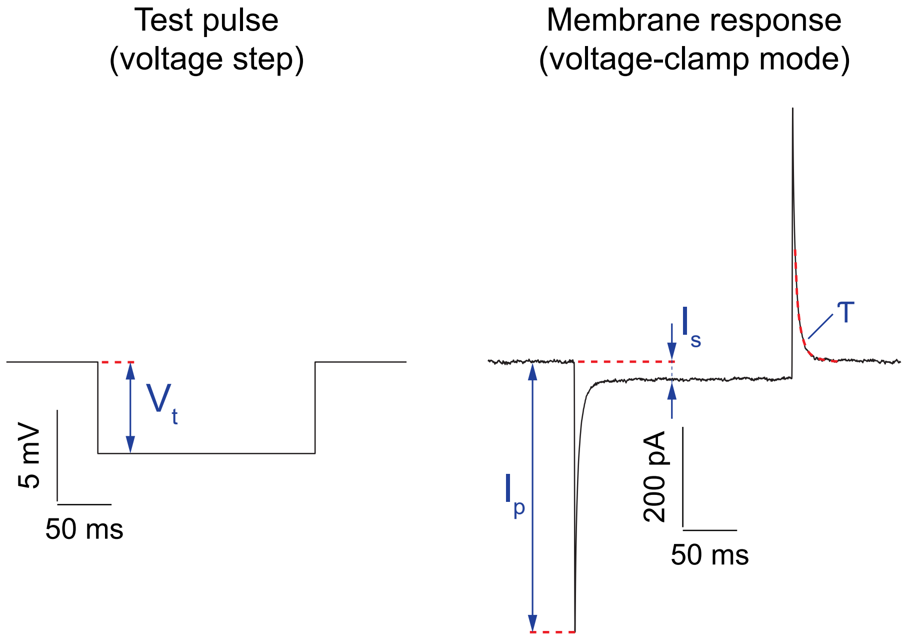

Figure 8.6: How to calculate cell parameters from a test pulse. Cell membrane response (right) to the test pulse (left). V_t - test pulse step size; I_p - peak current; I_s - current response to a voltage step; τ - RC time constant, here calculated as exponential fit of capacitor discharge current.

Extra 8.3: Liquid junction potential measurement [123, 124]

In every electrophysiological experiment involving patch-clamp a significant error of voltage measurements is present due to the formation of a liquid junction potential (LJP), which develops at the interface between two ionic solutions with different compositions due to a difference in the ion's mobility. This voltage offset between pipette and bath solutions should always be measured and compensated prior to patch-clamp experiments.

Here, the LJP was experimentally measured (following [124]) for each relevant bath solution every time the new stock of pipette solution was made. A well-chlorided silver wire was connected to the ground and placed in the small diameter silicone tube filled with 1 % agarose mixed with 3 M KCl solution (agarose bridge). Patch pipette was filled with intracellular solution and placed on the amplifier headstage with freshly chlorided silver wire. The recording chamber with agarose bridge and patch pipette was first filled with same intracellular solution. The pipette offset was set to zero, using the current-clamp mode of the patch amplifier. If the voltage reading did not change significantly in the following minute, the current bath solution was fully exchanged to the solution of interest and the tip (~1 cm) of agarose bridge was cut to prevent errors due to ion exchange. Otherwise, if the zero offset was unstable, the wires were rechlorided and zero offset was set again. The resulting voltage difference displayed by the amplifier showed the LJP for the current pair of bath and pipette solutions. To measure another pair, bath solution was yet again fully changed back to the pipette solution and the tip of the agarose bridge was cut to make sure, that displayed voltage is back to zero. Afterwards the measuring procedure was repeated.

9

OPTOGENETICS

9.1 Channelrhodopsins functional characterization

As a first step, functional characterization of channelrhodopsins was performed to ensure that there is no co-activation of the CheRiff-CA1 and ChrimsonR-CA3 during the oSTDP. To cover the visible spectrum, a 16 channel CoolLED with a narrow band filter (to isolate the 550 nm peak wavelength from the broad-spectrum LED installed inside the apparatus) was used. The CoolLED was operated in F1 mode, which allows triggering from the Ephus software through the A/D board. A TTL pulse was used to control the time and length of the light flash and an analog pulse to control the intensity. Each channel was calibrated in the specimen plane through a 40x objective by silicone photodiode power meter and then individual intensity map sequences were made (the stimulation was set to go from the lowest to the highest intensity). Each sequence was triggered through PulseJacker (module of Ephus software [115]) with 20 s in between sweeps with additional 1 min between each sequence.

The OHSCs were virus injected and single cell electroporated in same way as used for oSTDP experiments. The light evoked currents were recorded in the ACSF 4/4 with fast synaptic transmission and action potentials blocked by CPPene, picrotoxin, NBQX and TTX (Table 9.1). An intensity map for each wavelength was recorded 4 times (7 CheRiff-CA1 and 11 ChrimsonR-CA3 neurons). The peak current of the light evoked responses was automatically detected, averaged together and plotted for each wavelength using a custom Matlab script.

ACSF - Artificial cerebrospinal fluid

Essential Equipment and Materials:

Electrophysiology setup modification

LEDs
pE-4000, s/n 0453, CoolLED Ltd.
Narrow band filter
525 nm to 575 nm, Thorlabs
Neutral density filters

Solutions:

ACSF 4/4, 30 °C

(LJP −14.3 mV, pH 7.4, 308 mOsm/kg to 316 mOsm/kg)

119 mM	NaCl (Sigma; S5886-500G)
26.2 mM	$NaHCO_3$ (Sigma; S5761-500G)
11 mM	D-glucose (Sigma; G7528-250G)
2.5 mM	KCl (Fluka; 60121-1L)
1 mM	NaH_2PO_4 (Sigma; S5011-100G)
4 mM	$MgCl_2$ (Fluka; 63020-1L)
4 mM	$CaCl_2$ (Honeywell; 21114-1L)

Table 9.1: List of drugs for pharmacological manipulation

Formula	Short name	Brief description	Producer (code)	Concentration
$C_8H_{15}N_2O_5P$	CPPene	Potent, competitive NMDA receptor antagonist	Tocris biosci. (1265)	10 µM
$C_{12}H_8N_4O_6S$	NBQX	Competitive AMPA receptor antagonist	Tocris biosci. (1044)	10 µM
$C_{30}H_{34}O_{13}$	Picrotoxin	Non-competitive GABA receptor antagonist	Sigma (P1675-1G)	100 µM
$C_{11}H_{17}N_3O_8$	TTX	Sodium channel blocker	HelloBio (HB1035)	1 µM
$C_3H_7NO_3$	D-Serine	Potent agonist at the glycine site of the NMDA (NR1) receptor	Tocris biosci. (0226)	30 µM
$C_{18}H_{16}N_6S_2$	U0126	Potent, selective and non-competitive MAP2K inhbitor.	HelloBio (HB2246)	10 µM

9.2 Light evoked spiking threshold

To characterize the threshold light intensity for evoking action potentials I expressed ChrimsonR or CheRiff by virus drop for 7 − 9 days. To minimize the effect of changes in Rs and Rm, I recorded from neurons in the cell-attached mode. The whole-cell current-clamp mode was used in the end of each experiment to verify the cell type from the spiking pattern (current steps injection). Here, to mimic the in-incubator conditions, recordings were done in the warmed-up to 33 °C modified cell culture medium: the horse serum was removed and replaced by minimal essential medium (MEM) to prevent foaming of the solution during the circulation through the perfusion. To eliminate network effects, fast synaptic transmission was blocked by CPPene, picrotoxin and NBQX (Table 9.1).

First, the spiking threshold was verified for 1 ms to 2 ms light flash (405 nm to activate CheRiff and a 625 nm to activate ChrimsonR) in CA1 or CA3. Light flashes with different intensity were given every 20 s to ensure that the channels were fully closed before reopening. Importantly, spiking threshold did not change for ChrimsonR-neurons expressing virus for 10 or 12 days after injection, which shows that the virus expression was stable during this time ($P = 0.22$, Kolmogorov-Smirnov test; Figure 9.1). Then, I checked how well the neurons can follow the repetitive light stimulation: 1 ms of violet or red light was flashed 10 times at 5 Hz, 10 Hz and 50 Hz. The results are quantified in Chapter 14.3.

Solutions:

Recording medium, 33 °C

(LJP −15.3 mV, pH 7.28 , 308 mOsm/kg to 316 mOsm/kg)

99 %	MEM (Sigma; M7278)
13 mM	D-glucose (Fluka; 49152)
109 mM	NaCl (Sigma; S5150-1L)
0.8 mM	$MgSO_4$ (Fluka; 63126-1L)
1.8 mM	$CaCl_2$ (Fluka; 21114-1L)
1 mM	L-glutamine (Gibco; 25030-024)
6 µM	ascorbic acid (Fluka; 11140)
0.01 mg/ml	insulin (Sigma; I6634)

ddH_2O to adjust the osmolality

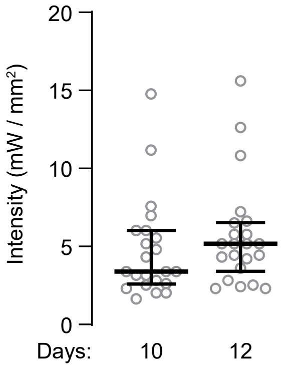

Figure 9.1: Light induced spiking threshold of ChrimsonR-CA3 neurons. There was no significant difference in the light induced spiking threshold for ChrimsonR-CA3 neurons between day 10 and day 12 after virus injection ($n_{10} = 22$, $n_{12} = 22$; $P = 0.22$, Kolmogorov-Smirnov test). Plotted are individual data points, median and 25 % to 75 % interquartile range.

9.3 oSTDP: Causal and Anti-causal pairing

To optically induce spike-timing-dependent plasticity, spike to burst pairing was used: a single action potential in ChrimsonR-CA3 neurons was paired with 3 action potentials at 50 Hz in CheRiff-CA1 neurons. Pairing was either causal, when EPSP from the ChrimsonR-CA3 neurons arrived before the action potentials were fired in CheRiff-CA1 neuron, or anti-causal, when the CheRiff-CA1 neuron fired action potentials before the EPSP from ChrimsonR-CA3 arrived (Figure 9.2). The pairing timing Δt was set either between EPSP and the first action potential fired (causal pairing), or between the last action potential fired and EPSP (anti-causal pairing). The stimulation parameters for causal and anti-causal pairings are listed in Table 9.2.

EPSP - Excitatory postsynaptic potential

Table 9.2: oSTDP pairing parameters

Causal/Anti-causal Δt (ms)	Rep. frequency (Hz)	Number of rep.	Duration (sec)
+10 / -10	0.1	360	3600
	5	300	60
+50 / -50	5	300	60

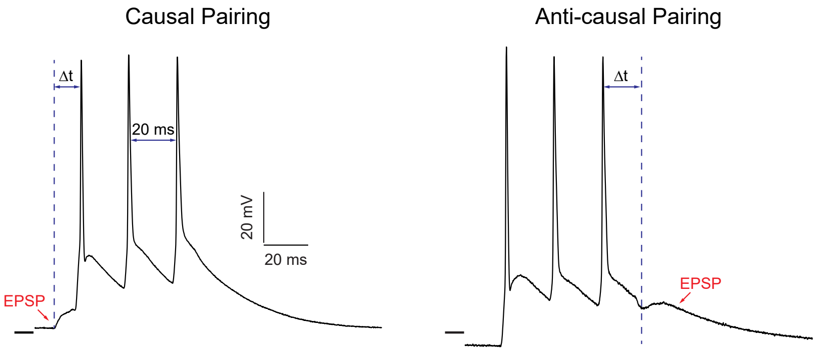

Figure 9.2: Causal and anti-causal pairing. Shown one pairing trace, recorded in the current-clamp mode. Δt - spike-timing delay between EPSP (red) and first or last action potential. Postsynaptic burst contained 3 action potentials at 50 Hz. The black ticks are at −75 mV.

9.4 oSTDP during whole-cell recordings

To verify if it is possible to use light evoked spiking to induce STDP, I recorded EPSCs from OHSCs 8 - 11 days after transfection. Here, experiments were performed in the recording medium with D-serine (Table 9.1). To induce oSTDP 405 nm light through the objective (~1 mW/mm^2) and a condenser-coupled yellow laser together with a 625 nm LED through the objective (combined illumination ~7 mW/mm^2) were used. CheRiff-CA1 (or NT-CA1) pyramidal neurons were voltage-clamped at −65.3 mV (LJP corrected), where inhibitory currents were clearly outward. Baseline EPSCs (1 ms laser flash to activate ChrimsonR-CA3 neurons) were recorded at 0.05 Hz in whole-cell voltage-clamp mode for no longer than 5 min after break-in followed by the oSTDP induction in current-clamp mode. To maximize the illumination area, a 10x objective was carefully moved into position instead of the 40x objective before plasticity induction. Afterwards, the baseline stimulation at 0.05 Hz was continued for at least 30 min.

Initially the delay between spike-burst stimuli was set to be −10 ms or +10 ms. However, after analysis of the first 9 experiments it became clear that the actual median delay from the last action potential to EPSP onset was −14.2 ms during anti-causal pairing and from EPSP to the first action potential was +6.8 ms during causal pairing. Therefore, the delay was adjusted by 2 ms for the remaining experiments, which resulted in more symmetrical timing distribution (median timing −12.4 ms during anti-causal pairing and +8.8 ms during causal pairing; Figure 12.1 f). To determine whether tLTP or tLTD occurred in an individual experiment, the baseline EPSCs slope (5 min before pairing) was compared to the post pairing EPSCs slope (between 20 and 25 min after pairing) with a Kolmogorov-Smirnov test (significance $P < 0.05$). This test was also used to verify whether the baseline-normalized EPSC slopes were different between the anti-causally and causally paired groups. Plots and statistical analysis were done using Matlab or GraphPad Prism.

9.5 In-incubator light stimulation

To induce plasticity noninvasively by light in the incubator atmosphere, a stimulation tower with two high power LEDs was constructed (Figure 9.3). Each tower contained an injection-molded reflector to collimate the 630 nm LED and an aspheric condenser lens to collimate the 405 nm LED. The LEDs were powered and controlled from outside the incubator by a two-channel stimulator, two constant-current drivers and a timer.

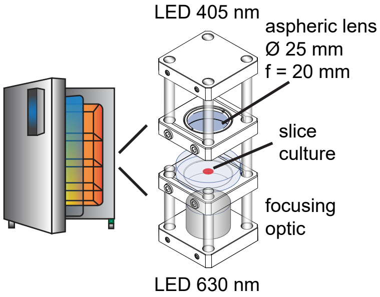

Figure 9.3: In-incubator stimulation tower. The schematic representation of two-color in-incubator stimulation tower with a centered OHSC in 35 mm dish.

OHSCs were either single cultured per well or were separated 4 days before stimulation and transferred to the new membrane insert. The last medium change was performed 1 day before stimulation*, and on the same day, the transfected OHSCs were moved to the dedicated incubator, and shielded from external light sources (referred as *dark incubator*) close to the incubator with the stimulation towers (referred as *stimulation incubator*). Importantly, all light stimulations were performed in incubator conditions in the culturing medium, which should minimize any external influence. After pairing, OHSCs were transferred back into the dark incubator and left there until the recording day (oSTDP) or fixation time (cFos characterization). During that time the medium was not changed to prevent unwanted increase of spontaneous activity in neurons, if not specified otherwise.

* *For cFos characterization experiments OHSCs were treated with fast synaptic transmission blockers (CPPene, picrotoxin and NBQX, Table 9.1) before transferring to the dark incubator overnight.*

On the day of stimulation, the closed petri dish containing centered OHSC was placed in an illumination tower. The stimulation parameters were either set using data obtained from on-cell oSTDP (see Table 9.3) or set according the light induced spiking threshold (for cFos characterization, Figure 14.4). To ensure a nonbiased outcome (blinding approach), all in-incubator stimulations were done by Christine E. Gee or Sabine Graf. OHSCs were letter coded and stimulations or treatments groups were inter-mixed to ensure the blinding and to minimize the influence of batch specific factors. The letter code was broken after all the data in current groups was collected and analyzed (see sample size). No single measurements were denied after unblinding.

Essential Equipment and Materials

LEDs
630 nm - Cree XP-E red
405 nm - Roschwege Star-UV

Reflector
10034, Roithner LaserTechnik

Condenser lens
ACL2520U-A, Thorlabs

Stimulator
Grass S8800

Current driver
RCD-24-1.20, RECOM

Table 9.3: In-ncubator tower LEDs parameters

Experiment	LEDs (nm)	Light flash (ms)	Light intensity (mW/mm^2)
oSTDP	405	2	1.2
	630	2	8
cFos Characterization	630	1	7

9.6 Special stimulation conditions for in-incubator oSTDP

For the oSTDP experiments, a few additional handling procedures were established. First, for the +CPPene experiments, the potent NMDA receptor antagonist was mixed into the culture medium and applied to the OHSCs overnight, before the slices were transferred to dark incubator. On the next day, one hour after the end of pairing protocol, the CPPene containing medium was carefully replaced with previously collected culturing medium. An additional drop of medium was carefully placed on top of the slice and then removed to allow the washout of the drug. Afterwards treated OHSCs were returned to the dark incubator until the recording day.

Second, 3 h to 4 h after the oSTDP induction, fresh warm medium with 1 µM TTX was pipetted on top of the membrane insert to immediately prevent neurons from action potential firing in the entire OHSC. The medium under membrane insert was then aspirated, replaced with the TTX containing medium and the medium on top of the slice was removed before returning the slice to the dark incubator. Two days later, the TTX was washed out by gently aspirating and replacing the medium 3 times, and the OHSCs were returned to the dark incubator until the following recording day. For the medium change condition, OHSCs were handled identically, except the medium never contained TTX.

9.7 Read-out procedure for in-incubator oSTDP

The main limitation of the optogenetic in-incubator plasticity induction without patching the postsynaptic neuron is the unavailability of the baseline synaptic strength between selected pre- and postsynaptic partners. Thus, it was essential to find an alternative way to assess the changes in synaptic strength after in-incubator oSTDP induction. It is well known that each single CA3 neuron makes connections to a number of CA1 neurons [2]. Thus, on average, the neighboring CA1 neurons should have similar input from a selected subset of CA3 neurons. Thereby, during oSTDP-induction all neighboring CA1 neurons should have received an equivalent EPSPs from light activated ChrimsonR-CA3 neurons, but only CheRiff-CA1 neurons were forced to fire action potentials and thus were actually undergoing the pairing. Taking that into account, the average slope of EPSCs in close by NT-CA1 neurons evoked by ChrimsoR-CA3 light stimulation was used as a baseline to normalize the EPSCs slope in CheRiff-CA1 neurons.

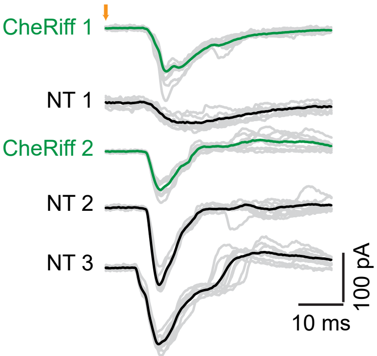

Figure 9.4: Typical set of recorded EPSCs in a given OHSC. Averaged EPSCs recorded in pseudorandom order from non-paired slice. Orange arrow indicates time of light stimulation.

The OHSC were transferred to the recording chamber of the setup 1 h or 3 days after the in-incubator oSTDP induction. For every CA1 neuron in the cell-attached configuration before whole-cell access was obtained, one blue light flash (405 nm, 1 ms, 1.2 mW/mm^2) was given. As expected, none of the NT-CA1 neurons fired a spike. However, if a fluorescent CheRiff-CA1 neuron did not respond to the light stimulation, the recording was discontinued (4.25 %, 9 out of 212 neurons). Of the remaining 203 responsive CheRiff-CA1 neurons 190 responded with single spikes and 13 with 2 or 3 (6.4 %), all 405 nm responsive CheRiff-CA1 neurons were used for analysis.

The EPSCs from at least one CheRiff-CA1 and at least two NT-CA1 neurons were sequentially recorded in pseudorandom order (Figure 9.4). EPSC onset in CA1 neurons after light stimulation of ChrimsonR-CA3 (594 nm, 1 ms, repetition rate 0.05 Hz) was typically 6 ms to 8 ms, if the delay was 15 ms or longer, the response was assumed to be polysynaptic and the recording was not analyzed. For all neurons in a given OHSC EPSCs were recorded at 3 d to 4 different laser intensities with at least 10 recorded EPSCs per intensity.

To verify the cell type, a series of current injections with different amplitude (from −600 pA to +600 pA) was given in current-clamp mode at the end of each set of recordings per given cell. All neurons without pyramidal-like firing patterns (i.e high action potentials frequency, large amplitude after-hyperpolarization etc) were eliminated from the analysis.

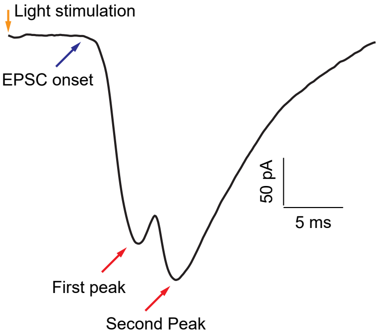

Figure 9.5: Multipeak EPSC in a responce to the presynaptic light stimulation.

9.8 Slope analysis for oSTDP

All data analysis was performed in a custom Matlab script. For each OHSC, I had a set of EPSCs recorded at different laser intensities per CA1 neuron (CheRiff and NT). One laser intensity was chosen to analyze the EPSCs recorded from the neurons in one OHSC. This was the lowest of the three laser intensities used that evoked similar sized EPSCs of at least −20 pA amplitude in the NT neurons. After selecting the intensity, any individual EPSC recordings in which a spontaneous EPSC or IPSC occurred in the 10 ms preceding the laser flash were removed. If the remaining number of EPSCs for a given neuron were fewer than 4, the neuron was excluded from the analysis.

Further analysis was performed automatically for selected laser intensity. All individual EPSCs from the NT neurons in the given slice were averaged together, then the (first*) peak amplitude and time of (first) peak were measured. The slope was measured as a linear fit between 20 % and 60 % of the peak amplitude (Figure 9.6). If the time of the peak for the neurons in the same slice varied by more than 5 ms, the data set was excluded, as that suggested a mixture of mono and polysynaptic responses within the data set. The input strength calculated for each CheRiff-CA1 neuron, is the average EPSC slope of the CheRiff-CA1 neuron divided by the slope of the combined average EPSC recorded from the $\geqslant 2$ NT-CA1 neurons in that slice.

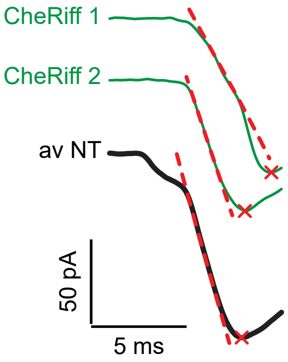

Figure 9.6: Peak and slope detection example. Analyized EPSCs from Figure 9.4 are shown. Red x indicates automatically detected peak; Red dashed line indicates a linear fit between 20 % and 60 % of the peak value. Note that the traces from NT neurons were first averaged together.

* ***Why "first" peak?*** *Sometimes the light activation of subset of ChrimsonR-CA3 neurons caused the recurrent activity in CA3, resulting in a few desynchronized EPSPs arriving to CA1 with millisecond delay. In this case only first peak of EPSC is the direct response to the light stimulation, Figure 9.5.*

Extra 9.1: Post synaptic potentials and currents (EPSP, IPSP, EPSC, IPSC)

There are two types of synaptic potentials which are transferred from the presynaptic to the postsynaptic neuron and make the postsynaptic neuron more or less likely to fire an action potential in a response to it. The postsynaptic membrane potential depolarization, caused by the positively charged ion flow into it, increases the likelihood of the action potential firing. This postsynaptic potential is referred to as excitatory postsynaptic potential (EPSP). The opposite process of postsynaptic membrane hyperpolarization, which makes the action potential firing less likely is caused by the inhibitory postsynaptic potential (IPSP). The flow of ions causing an EPSP or IPSP is an excitatory or inhibitory postsynaptic current (EPSC or IPSC). Both EPSPs and IPSPs have an additive effect, which means that when the multiple postsynaptic events occur close in time on a single patch of the postsynaptic membrane, their combined effect results in the sum of the individual potentials [125].

As described in the Chapter 8.2, patch-clamp technique allows to record the electrical events in the postsynaptic neuron in two configurations: voltage- and current-clamp. The currents passing through the open ion channels (postsynaptic currents, EPSCs or IPSCs) can be recorded in the voltage-clamp mode, when the membrane voltage of the postsynaptic neuron is kept constant. To record the changes in the membrane potential induced by the opening and closing of the ion channels (postsynaptic potentials, EPSPs or IPSPs), the current-clamp mode should be used (Figure 9.7) [116].

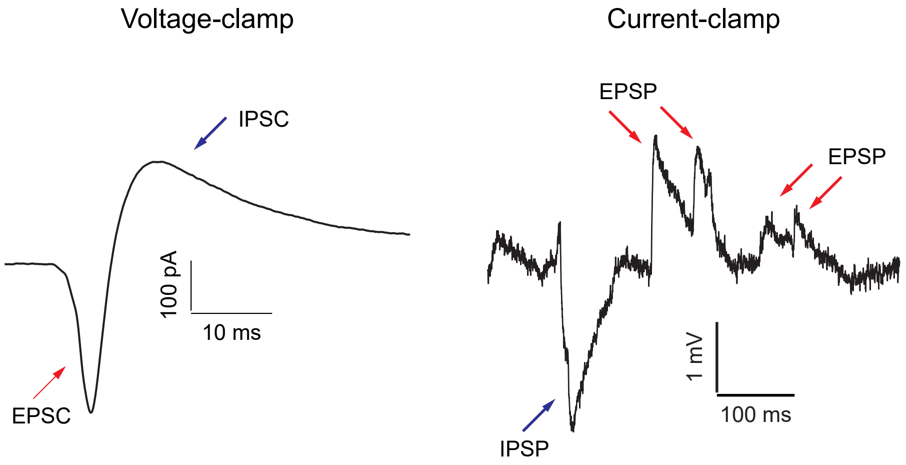

Figure 9.7: Currents and potentials in voltage- and current-clamp mode. Inhibitory currents and potentials are indicated with blue arrows. Excitatory currents and potentials are indicated with red arrows. Note, that in voltage-clamp mode the inhibitory currents are positive (excitatory currents are negative), whereas in current-clamp mode inhibitory potentials are negative and hyperpolarize the neuron (excitatory potentials are positive and depolarize the neuron).

10

IMMUNOHISTOCHEMISTRY AND IMAGING

10.1 Immunohistochemistry

If not stated otherwise, an hour after stimulation (light or chemical) OHSCs were fixed for 30 min in 500 µl paraformaldehyde (4 % PFA in PBS). Then, they were washed 3 times in PBS for 10 min and incubated in blocking solution for 2 h at room temperature. Afterwards incubated overnight in carrier solution with primary antibodies at 4 °C. Next morning, OHSCs were washed 3 times with PBS for 10 min and incubated for 2 h in carrier solution with secondary antibodies (concentrations are listed in Table 10.1). Then, OHSCs were again washed 3 times in PBS for 10 min before they were mounted with a Shandon Immu-Mount under the glass coverslip. Mounted OHSCs were left to dry for at least 3 h at room temperature in darkness before the edges of the coverslip were sealed with nail-polish. This last step prevented OHSCs from drying out for at least a week after mounting. Mounted slices were kept in darkness at 4 °C until imaged.

For STED microscopy, OHSCs were fixed and blocked as described above either 9 days after virus injection and single-cell electroporation (not-paired) or 3 days after in-incubator stimulation (10−12 days after transfection, causal pairing or post only stimulation). OHSCs were incubated overnight at 4 °C with conjugated primary nanobodies in carrier solution (Table 10.1). Next morning, they were washed 3 times for 10 min in PBS and mounted in Mowiol, prepared according to manufacturer's protocol with anti-fading reagent DABCO.

PBS - Phosphate buffered solution

Solutions:

Blocking solution
10 % Donor goat serum
0.2 % Boverin Serum Albumin
0.3 % Triron^{TM} X-100
All dissoved in 1x PBS

Carrier solution
1 % Donor goat serum
0.2 % Boverin Serum Albumin
0.3 % Triron^{TM} X-100
All dissoved in 1x PBS

STED - Stimulated emission depletion microscopy

Chemicals for the mounting:

Mounting solutions
Shandon Immu-Mount
(Thermo Scientific; 9990402)
Mowiol
(Mowiol 4-88, Roth; 0713.2)

Anti-fading reagent
DABCO
(Sigma-Aldrich; D27802)

Table 10.1: List of antibodies

Immunogen	Host	Label	Producer (code)	Internal number	Dilution
c-Fos(4)	rabbit	none	Santa Cruz Inc. (sc-52)	P005	1:500
PCP4	mouse	none	Sigma (AMAb91359)	P022	1:500
GFP	camelid	Atto647N	NanoTag (X4, N0304-At647N)	PC002	1:250
RFP	camelid	AbberiorStar580	NanoTag (Q, N0401-Ab580)	PC004	1:250
Rabbit	goat	Alexa Fluor 488	Life Technologies (A11008)	S002	1:1000
Rabbit	goat	Alexa Fluor 568	Life Technologies (A11011)	S003	1:1000
Rabbit	goat	Alexa Fluor 647	Invitrogen (A27040)	S007	1:2000
Mouse	goat	Alexa Fluor 488	Invitrogen (A11029)	S009	1:1000

10.2 Confocal microscopy

The mounted slice cultures were imaged on an Olympus F1000 confocal microscope, using a 20x oil immersion objective. Depending on the experiment, a different combination of lasers (488 nm, 559 nm and 635 nm) was used. The filter setting used in the experiments are listed in Table 10.2. The imaging parameters were adjusted for each set of experiments and kept unchanged throughout. Z-series (5 slices) stacks with 3 µm z-step at a 1024 × 1024 pixel resolution (zoom 1x) scanning at 12.5 µs per pixel were taken and analyzed in IMARIS software. Fiji/ImageJ [126] was used to project the z-series and overlay channels.

Table 10.2: Confocal excitation/emission settings

Fluorophore	Excitation laser	Olympus emission filter	Range
Alexa Fluor 488 / eGFP	488 nm	Alexa Fluor 488	500 nm to 545 nm
Alexa Fluor 568 / TdTomato	559 nm	Alexa Fluor 568	570 nm to 625 nm
Alexa Fluor 647	635 nm	Alexa Fluor 647	655 nm to 755 nm

10.3 Stimulated emission depletion (STED) microscopy

STED microscopy was performed at the UKE Imaging facility (UMIF) with a kind help of Dr. Virgilio Failla, who has also provided the methodology, written below.

Gated-2D-STED images were acquired using an Abberior expert-line STED microscope. The microscope was controlled by Abberior Inspector software. Samples were placed on a Nikon TI microscope body, equipped with a 60x objective. At first, fluorophores were excited with 561 nm and 640 nm laser lines. Both channels, red and far-red were acquired in confocal mode. In addition, the far-red channel was resolved with 2D-STED by use of a 775 nm depletion laser. For both, confocal and 2D-STED acquisitions the pinhole was set to 1 au. Fluorescence was collected on avalanche photodetectors through emission filters 615/20 (red channel) and 685/70 (far-red channel). Gating was obtained with a Becker and Hickl SPC150 TCSPC board. Gates were set to 8 ns width, starting with a delay of 781.3 ps for both confocal and STED. Acquisitions were obtained sequentially with a 20 nm × 20 nm pixel size. Confocal images were the result of 6 accumulations, STED images of 18 accumulations acquired by line-mode. Files were saved in a 16-bit format. Confocal and STED images were merged and analyzed in Fiji/ImageJ. For representation, the lookup table is linearly adjusted for each channel.

Essential Equipment:

Confocal microscope

Body
Olympus F1000

Objective
20x UPLSAPO 0.85 NA, Olympus

STED microscope

Body
Gated-2D-STED, Abberior Inst.

Objective
60x P-Apo 1.4NA, Nikon

10.4 Data analysis in IMARIS

IMARIS software was used to count cFos positive nuclei and to measure their intensity. The settings for automatic counting were first set using a few images from the CA1 region (*'High Potassium'* condition), then tested on images from different regions and conditions and adjusted accordingly to maximize the accuracy of detection. Each 3D stack was visually inspected after using automatic detection. All spots detected outside of the pyramidal cell layer, cFos positive nuclei of glial cells, as well as of ChrimsonR-negative neurons were removed. If the cFos positive nuclei from ChrimsonR-positive neuron in pyramidal cell layer was skipped, the detection spot was manually added. The final settings for automatic detection were: cFos channel lookup table was set as min 250 and max 1000, spot size diameter was 8 µm (CA1 and DG) or 10 µm (CA3 and CA2) and detection quality (the signal to noise ratio within the spot) above 122.

Part III

Optogenetic induction of spike-timing-dependent plasticity

OPTOGENETIC INDUCTION OF SPIKE-TIMING-DEPENDENT PLASTICITY

As described in Chapter 3, STDP relies on independent and precisely timed spiking of pre- and postsynaptic partners. The classical method of STDP induction involves whole-cell patch or intracellular recordings and electrical stimulation. In this case, the plasticity observation time is limited by many factors, such as the quality of the patch, the health of the cell after break-in, the washout process and others. Typical recordings last for up to an hour, which makes it almost impossible to study synaptic plasticity consolidation on behavior relevant time scale [127–131]. Thus, the classical method is not sufficient to study how the input strength changes over days.

In Part III, I first present a new way of STDP induction – two-color optogenetic STDP (oSTDP). Then, using this method, I show how the input strength changes over days following the plasticity induction.

This part was partialy published in:

Long vs short-term synaptic learning rules after optogenetic spike-timing-dependent plasticity
M. Anisimova, B. van Bommel, J. S. Wiegert, M. Mikhaylova, T. G. Oertner, C. E. Gee
bioRxiv:863365

11 EXPRESSION AND CHARACTERIZATION OF SPECTRALLY SEPARATED CHANNELRHODOPSINS

To achieve the controlled, precise and independent noninvasive spiking of two selected groups of neurons in OHSC I expressed light activated channelrhodopsins in pyramidal neurons. At the time this project was planned, the most promising pair was ChrimsonR [80] and CheRiff [81], red- and blue-light sensitive channelrhodopsins respectively. As described in Chapter 7.2, the different approach of opsin expression was used for pre- and postsynaptic groups: local virus injection [112] for CA3 pyramidal neurons and single-cell electroporation [113] for CA1 (Figure 11.1). All experiments were performed at least 7 days after transfection to ensure stable expression of both channelrhodopsins.

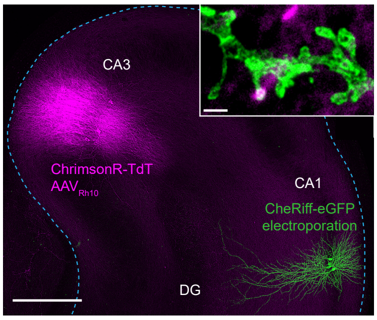

Figure 11.1: ChrimsonR and CheRiff expression in OHSC. Confocal image (maximum intensity projection) of an OHSC transfected with ChrimsonR and CheRiff to independently control spiking in CA3 and CA1 neurons, respectively. Insert: STED reconstruction of a Cheriff-CA1 oblique dendrite (green) and confocal image of presynaptic boutons (magenta) with a putative synaptic contact. Scale bar - 500 µm, insert - 1 µm.

11.1 Functional characterization of ChrimsonR and CheRiff

It is expected that the threshold for light induced action potentials is not only channelrhodopsin dependent but also depends on cell type, expression level and the technique used for the DNA delivery. Therefore, a detailed analysis of the spectral sensitivity of ChrimsonR-CA3 (virus injection) and CheRiff-CA1 (single-cell electroporation) pyramidal neurons was performed. ChrimsonR has a broad activation spectrum, while CheRiff is insensitive to all wavelengths above 550 nm. Taking this spectral difference in consideration, the following light stimulation parameters were used: 405 nm at 1.2 mW/mm^2 to activate CheRiff-CA1 neurons and 630 nm at 8 mW/mm^2 for ChrimsonR-CA3 neurons (Table 9.3, Figure 11.3). ChrimsonR is not fully insensitive to 405 nm light, however 2 ms light pulse with 1.2 mW/mm^2 intensity is not sufficient to spike ChrimsonR-CA3 neurons and does not lead to strong depolarization (0 mV to 3 mV, Figure 11.2). As already mentioned, light with wavelengths above 550 nm does not cause photocurrents in CheRiff-CA1 neurons for intensities up to 100 mW/mm^2 (Figure 11.3) making yellow epifluorescence light, used to visualize mKate2 and to target laser beam to CA3 safe to use. Thus, there was no unwanted co-activation (spiking or strong depolarization) of pre- and postsynaptic neurons outside the pairing window, when OHSC were stimulated with both 405 nm and 630 nm.

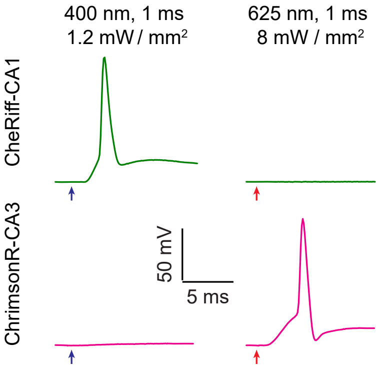

Figure 11.2: Light induced spiking of ChrimsonR and CheRiff expressing neurons. Example membrane responses of CheRiff-CA1 (upper traces) and ChrimsonR-CA3 (lower traces) neurons to 405 nm (violet arrows) and 625 nm (red arrows) light. Note that 405 nm light evokes action potential in the CheRiff expressing neuron and only slight depolarization of the ChrimsonR-CA3 neuron. 625 nm light induced an action potential in the ChrimsonR-CA3 neuron with no effect on the CheRiff-CA1 neuron.

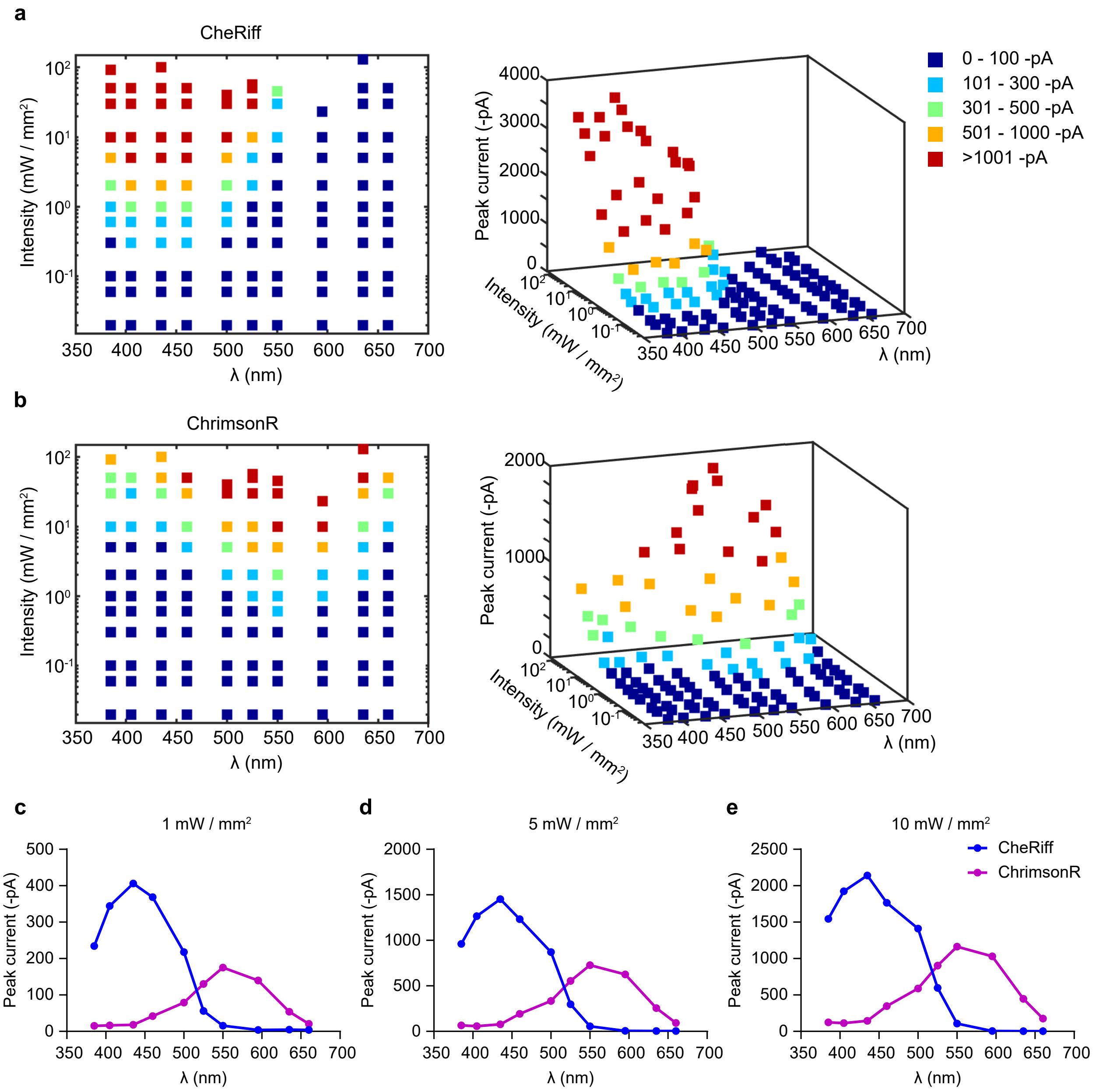

Figure 11.3: CheRiff and ChrimsonR functional characterization. a and b, Average ($n = 4$ cells per point) light evoked EPSC peaks from CheRiff-CA1 neurons (electroporated) and ChrimsonR-CA3 neurons (AAV transduced) in response to stimulation with different wavelengths at different intensities. Color code indicates average peak current amplitude. Note that CheRiff-CA1 neurons were completely non-responsive to light with wavelengths longer than 550 nm and ChrimsonR-CA3 neurons were only modestly responsive to 405 nm light. Peak current vs wavelength at: **c,** 1 mW/mm^2, **d,** 5 mW/mm^2 and **e,** 10 mW/mm^2 for CheRiff-CA1 and ChrimsonR-CA3 neurons. Note different y-axis scales.

11.2 Light evoked action potentials in CheRiff-CA1 neurons

As depolarization induced increase in postsynaptic calcium is critical for plasticity induction [46, 47], a possible prolonged light induced depolarization of the postsynaptic CA1 neurons is expected to affect STDP. Therefore, it was necessary to compare light evoked and electrically evoked action potentials in CheRiff-CA1 neurons (Figure 11.4). As opposed to Channelrhodopsin2 [132], light-evoked actions potentials of CheRiff-CA1 neurons were not significantly prolonged relative to electrically-evoked ones, the amplitude and half-widths were also similar. Thus, driving action potentials with 405 nm light in CheRiff-CA1 neurons instead of somatic current injections should not alter STDP induction rule.

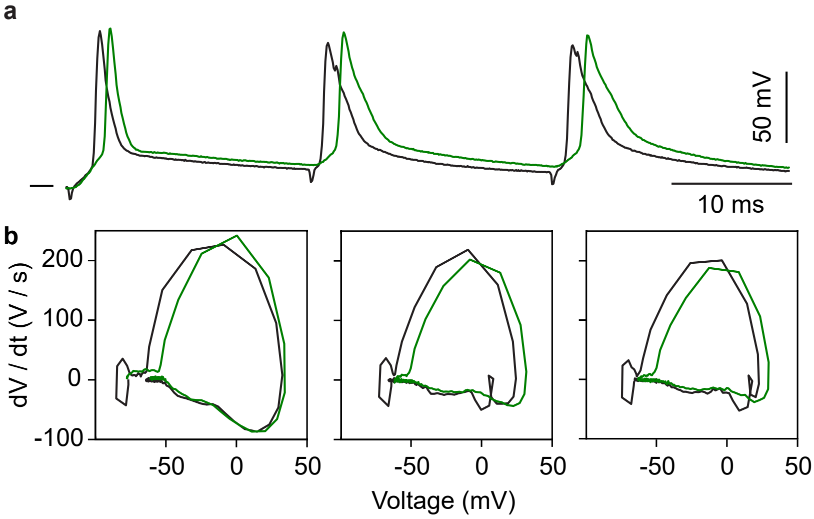

Figure 11.4: Light vs electrically induced action potentials in CheRiff-CA1 neuron. **a,** Action potentials induced by somatic current injection (black trace, 3 nA, 2 ms) or by optical stimulation (green trace, 405 nm, 1.2 mW/mm^2, 2 ms) of a CheRiff-CA1 pyramidal neuron. Electrical stimulation artefacts appear at 0 ms, 20 ms and 40 ms. Black tick is at −80 mV. **b,** Phase plots of the corresponding action potentials from **a**.

11.3 Optimal number of ChrimsonR-CA3 neurons

The number of transduced CA3 neurons is important: too few ChrimsonR-CA3 neurons would not provide similar synaptic input to neighboring CA1 neurons, while too many would directly drive majority of CA1 to complex bursting-firing, which alone may already induce plasticity. In case of whole-cell oSTDP it was easy to monitor activity pattern in the postsynaptic neuron (CheRiff or NT) and keep only those recordings, where no complex bursting was observed. However, there was no possibility to directly record the neuronal activity during the light stimulation inside the incubator. Since immediate early gene cFos is upregulated in burst-firing neurons [133] and in neurons which have undergone LTP [134], I reasoned that the expression pattern of cFos can be used to determine whether the selected neuron was active during the stimulation or not. Thus, to optimize the number of ChrimsoR-CA3 neurons for in-incubator oSTDP, I injected OHSC with different amount of viral vector, then 10 days later they were causally paired (Figure 9.2, Table 9.2) and fixed in 4 % PFA and stained against cFos (for details see Chapter 10). There was no cFos upregulation in ChrimsonR-CA3 or NT-CA3 neurons (9/9 slices, Figure 11.5), indicating that they were not driven to bust-fire by either single light flashes at 5 Hz (300 flashes, 630 nm at 8 mW/mm^2) or high frequency triplets at 5 Hz (300 bursts of 3 flashes at 50 Hz, 12 ms delay, 1 mW/mm^2).

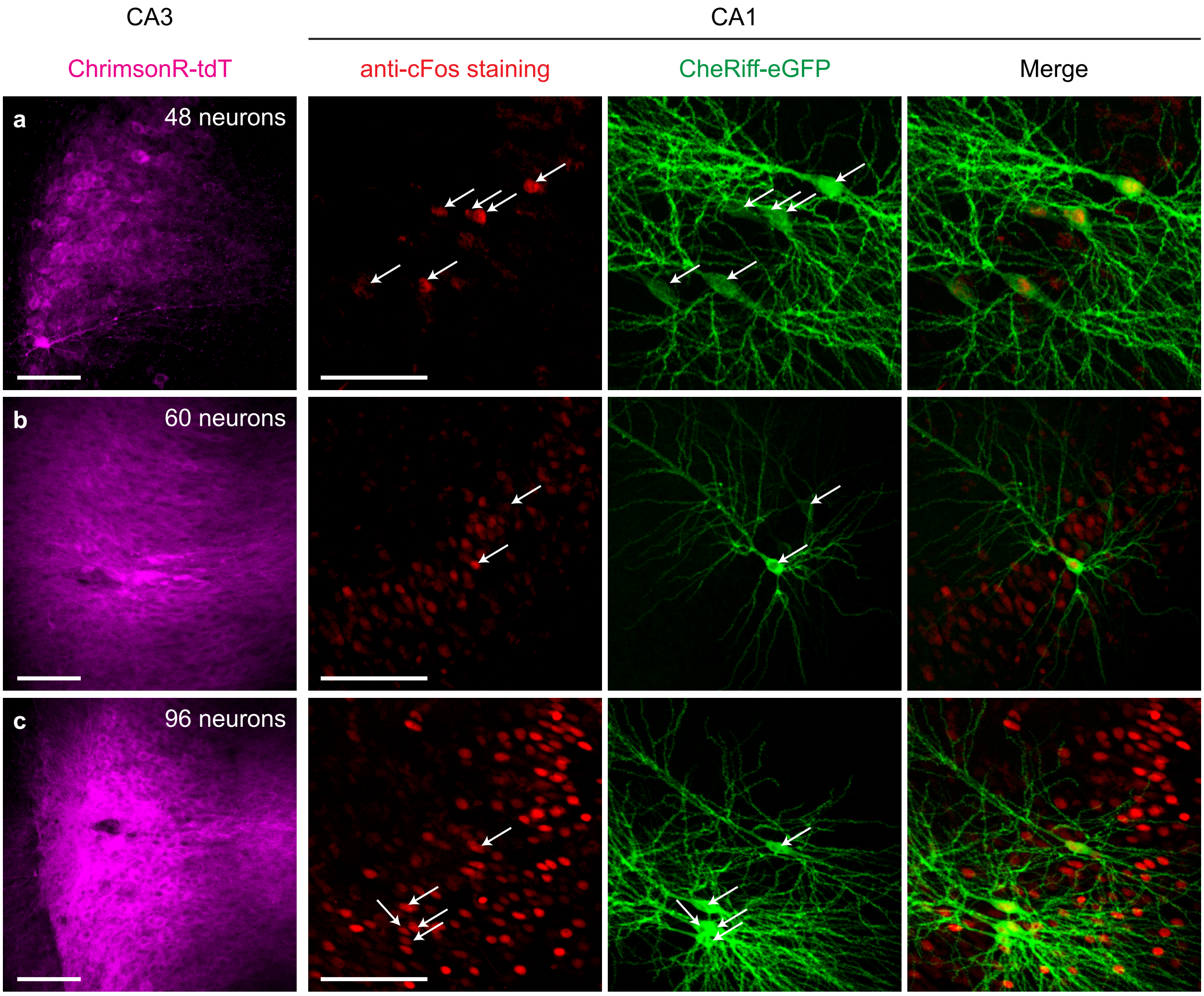

Figure 11.5: cFos expression pattern after causal pairing vs number of ChrimsonR-CA3 neurons. Confocal images (average intensity projection) of CA3 and CA1 areas in a given slice culture. White arrows are showing the soma of CheRiff-CA1 neurons. Scale bars - 100 µm. **a,** Expected cFos expression pattern in CA1 after causal pairing: Only directly light stimulated CheRiff-CA1 express cFos (5 out of 6). **b and c,** Number of ChrimsonR-CA3 neurons enough to induce complex spiking in CA1, which lead to cFos expression in NT-CA1 neurons.

To validate this approach, ChrimsonR-CA3 neurons were intentionally driven to burst-fire* by three light flashes at 50 Hz, repeated 300 time at 5 Hz (630 nm at 8 mW/mm^2). Now, cFos was expressed in approximately half of the burst-stimulated ChrimsonR-CA3 neurons (Figure 11.6), indicating that burst-firing is necessary for cFos upregulation in pyramidal neurons.

** Here the fast synaptic transmission was blocked by CPPene, picrotoxin and NBQX overnight (Table 9.1) to avoid the induction of recurrent activity in CA3, and to visualize the cell-autonomous effect of high frequency light stimulation*

After causal pairing, 83 % of CheRiff-CA1 neurons were expressing cFos, indicating that they were directly driven to burst-fire (7 slices: 30/36 neurons; Figure 11.5). In case of NT-CA1 neurons the expression of cFos strictly depended on the number of ChrimsonR transduced neurons. Thus, in 5 OHSCs ($36 - 53$ ChrimsonR-CA3 neurons) there were no cFos upregulation in NT-CA1 neurons (Figure 11.5 a). In 2 slices (~60 ChrimsonR-CA3 neurons) some NT-CA1 neurons were expressing cFos and in another 2 slices (96 or more ChrimsonR-CA3 neurons) the cFos was upregulated throughout the entire CA1 region (Figure 11.5 b, c), meaning that ChrimsonR-CA3 light stimulation at 5 Hz was sufficient to directly drive NT-CA1 neurons to burst-fire.

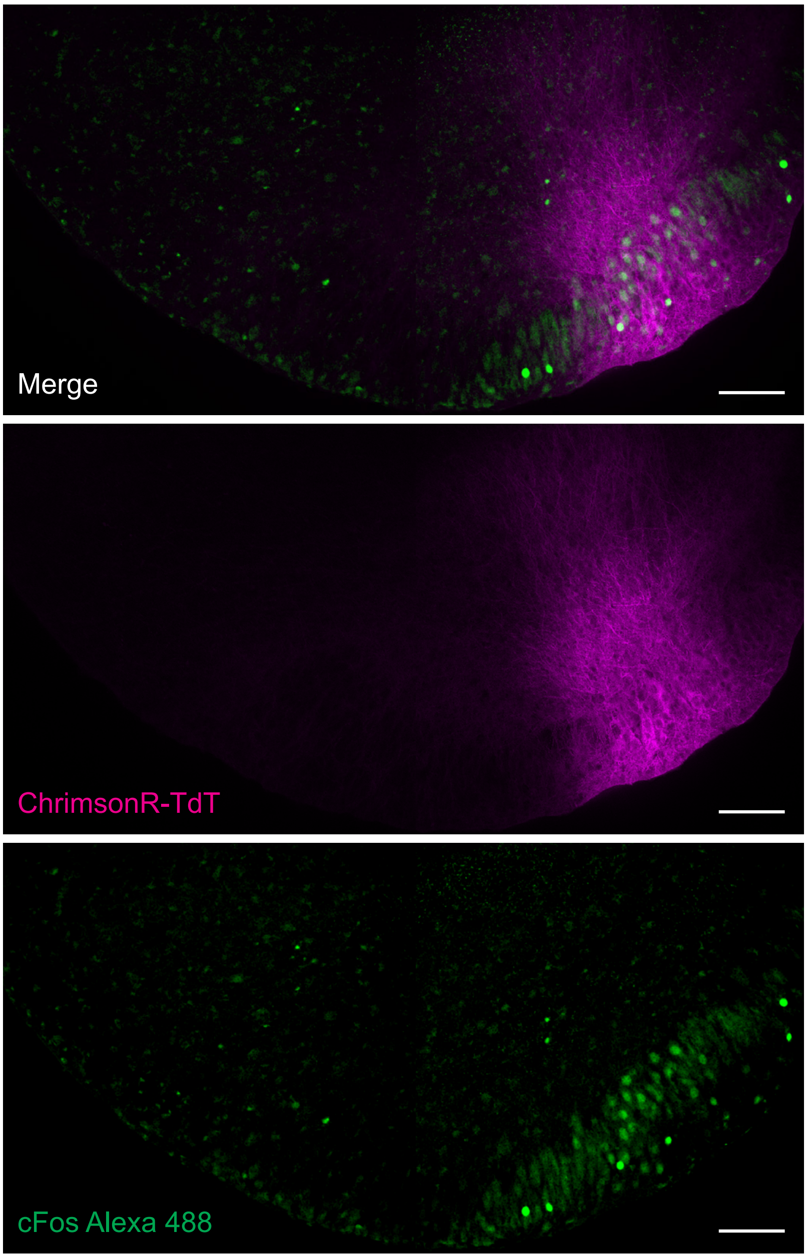

Figure 11.6: CA3 neurons express cFos after burst firing. Confocal images of CA3 area of a hippocampal slice culture fixed 90 min after burst stimulation. The ChrimsonR-tdTomato channel (magenta) is a minimum intensity projection to visualize transfected neurons and a median intensity projection was used for anti-cFos immunostaining (green). Approximately half of the burst-stimulated ChrimsonR-CA3 neurons were cFos-positive as were several non-transduced spontaneously active CA3 neurons. Scale bars - 100 µm.

12 OPTOGENETIC INDUCTION OF SPIKE-TIMING-DEPENDENT PLASTICITY

The main goal of this work is to induce STDP noninvasively and follow the plasticity consolidation over behavior-relevant time scale (3 days). To do so, I first investigate the short-term timing rules and compare it to classical STDP. Then I present the synaptic plasticity consolidation results 3 days after no-patch oSTDP.

12.1 Optogenetic induction of STDP during whole-cell patch clamp

To assess the early changes in input strength after oSTDP, I performed optogenetic spike-burst pairing while patched on a postsynaptic neuron (either CheRiff-CA1 or NT-CA1). The total recording length was set to 30 min, including a 5 min baseline. Light induced EPSCs were recorded in the patch-clamped neuron, while ChrimsonR-CA3 somas were optically stimulated with a condenser-coupled laser (594 nm, 2 ms, see Chapter 8.1) at 0.05 Hz. After a five minute baseline, I switched from voltage- to current-clamp mode. Single presynaptic ChrimsonR-CA3 spikes (300 flashes at 5 Hz, 2 ms duration, see Chapter 9.3) led or followed spike bursts by about 10 ms in the CheRiff-CA1 postsynaptic neurons (3 flashes at 50 Hz, 2 ms duration, Figure 12.1 a-c, Table 9.2 and 9.3). In CheRiff-CA1 neurons, causal pairing resulted in tLTP induction ($n = 12$ experiments; $P = 0.0002$, Kolmogorov-Smirnov test, Figure 12.1 d, f) and anti-causal pairing, as expected, induced tLTD ($n = 11$ experiments, $P = 0.0009$, Kolmogorov-Smirnov test, Figure 12.1 e, f). The two groups were significantly different from each other ($P = 0.003$, Kolmogorov-Smirnov test). Importantly, causal pairing in NT-CA1 neurons had no overall effect ($\text{median} = 1.06$, $n = 6$ experiments, $P = 0.09$, Kolmogorov-Smirnov test, Figure 12.1 c, f), showing that oSTDP induction was specific to CheRiff-CA1 neurons. Evidently, light-induced spiking in pre- and postsynaptic neurons produces STDP with similar timing rules as was previously shown for electrical stimulation [34, 35, 38, 46–48, 135].

To exclude the initial EPSC size influence on the plasticity induction, I performed the correlation analysis of the size of initial EPSC slope (baseline, before pairing) to the amount of plasticity induced (fold change after pairing). Evidently, there was no correlation neither for causal nor for anti-causal pairing (Figure 12.2, Pearson correlation coefficient: $R^2_{\text{Causal}} = 0.02$, $R^2_{\text{Anti-causal}} = 0.005$.).

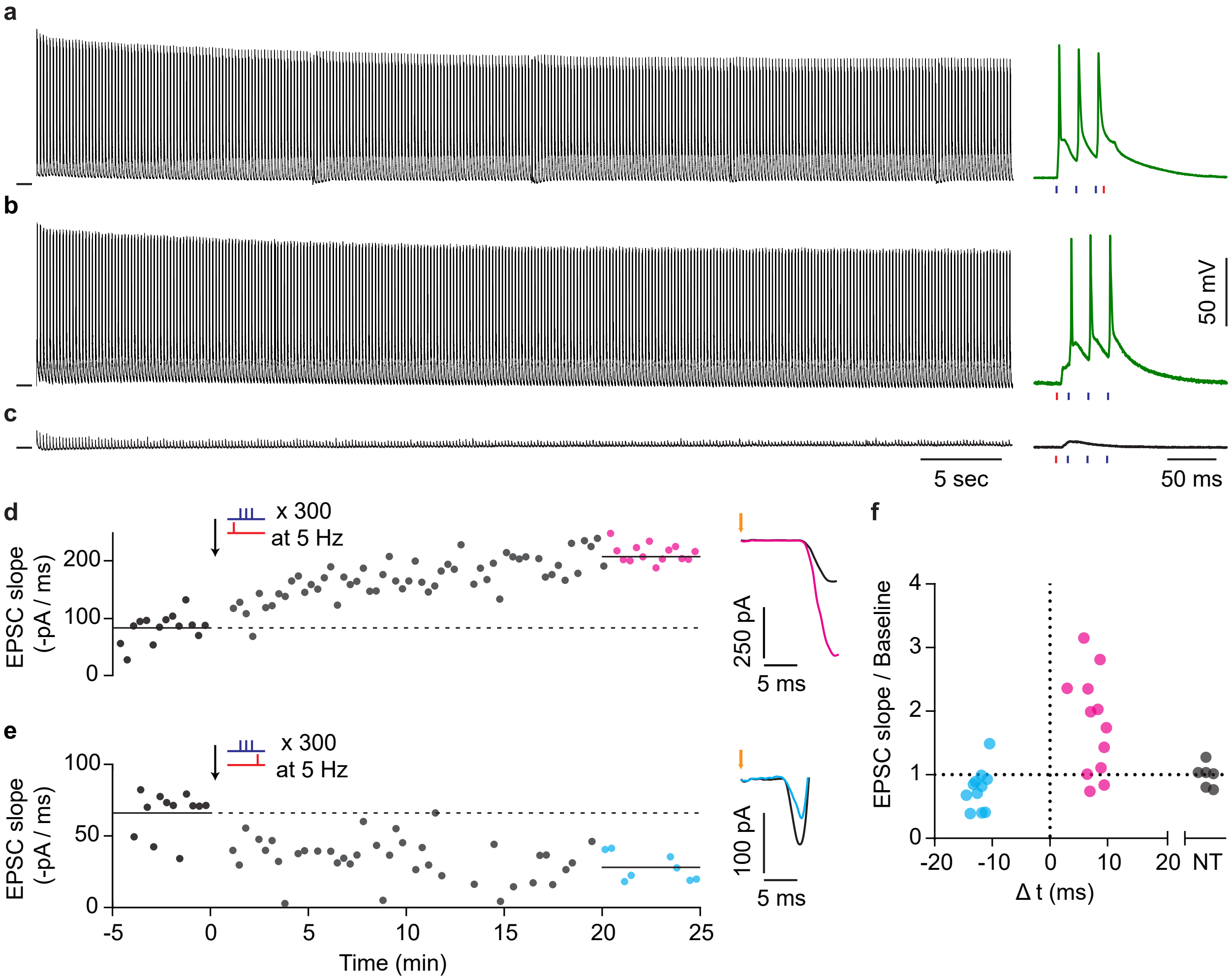

Figure 12.1: Optogenetic induction of STDP (oSTDP) while patched on the postsynaptic neuron. a-c, Membrane responses recorded from CA1 neurons during oSTDP induction: full recordings (left) and the responses to a single pairing (right). Black ticks are at −75 mV, red and violet ticks (right) indicate timing of light flashes. **a,** Firing pattern of a CheRiff-CA1 neuron during anti-causal pairing (−10 ms: 3 violet flashes at 50 Hz and 1 red flash 8 ms after, repeated 300 times at 5 Hz). Note the EPSP following three action potentials. **b,** Same as **a**, but causal pairing (+10 ms: 1 red flash and 3 violet flashes at 50 Hz 12 ms after). Note the EPSP preceding three action potentials. **c,** Membrane voltage response of a NT-CA1 neuron during causal pairing. Note the EPSP and absence of action potentials. **d and e,** The slope of excitatory postsynaptic currents (EPSCs) recorded from CheRiff-CA1 neurons in response to laser stimulation of ChrimsonR-CA3 neurons at baseline and after oSTDP induction (arrows, $t = 0$). At right are the averaged EPSCs before (black points/trace) and after (magenta or cyan points/trace) oSTDP induction. **d,** Causal stimulation induced timing dependent potentiation ($P < 0.0001$, single experiment: magenta vs black, Kolmogorov-Smirnov test). **e,** Anti-casual stimulation induced timing dependent depression ($P = 0.0003$, single experiment: cyan vs black, Kolmogorov-Smirnov test). **f,** Average EPSC slope 20 min to 25 min after oSTDP induction normalized to baseline from experiments as in **d** and **e**, Δt is the EPSP-spike-timing interval during the pairing. Hollow and filled points indicate individual experiments where EPSC slope did not or did change, respectively (Kolmogorov-Smirnov tests on raw values). NT, non-transfected neurons from slices subjected to causal light stimulation ($n = 6$).

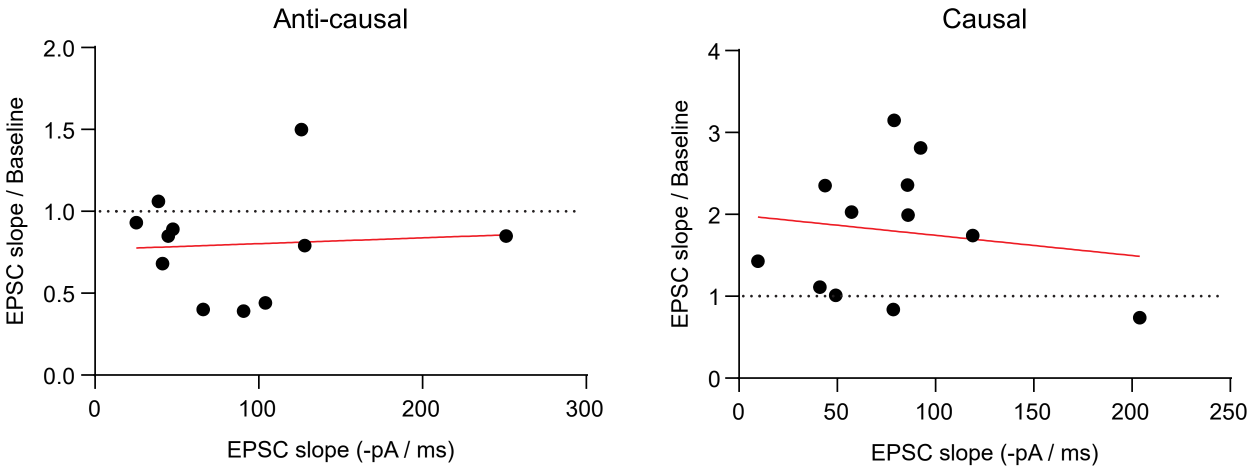

Figure 12.2: Initial EPSC slope size does not influence plasticity induction. There was no correlation between the size of the initial EPSC slope and its fold change after the oSTDP induction.

12.2 Input strength 3 days after in-incubator oSTDP induction

Having established that oSTDP induces both tLTP and tLTD during patch-clamp experiments, the illumination towers, containing independently controlled, collimated, red (630 nm) and violet (405 nm) high-power LEDs were constructed to stimulate ChrimsonR-CA3 and CheRiff-CA1 neurons in the incubator (Figure 9.3, the light stimulation parameters are listed in Table 9.3). After optimizing the number of ChrimsonR-CA3 transduced neurons and verifying with anti-cFos staining that there is no unspecific activity induced in NT-CA1 neurons during optical pairing, it was finally possible to assess the input strength from ChrimsonR-CA3 onto CheRiff-CA1 neurons 3 days after in-incubator oSTDP induction.

EPSCs evoked in CA1 neurons after ChrimsonR-CA3 light stimulation (condenser-coupled 594 nm laser beam, 1 ms durations at 0.05 Hz, Chapter 8.1) were sequentially recorded in pseudorandom order from at least one CheRiff-CA1 and two NT-CA1 neurons per OHSC. The input strength was calculated for each CheRiff-CA1 neuron as the average EPSC slope of that neuron divided by the slope of the combined average EPSC recorded from the all NT-CA1 neurons in given OHSC (see Chapter 9.8). This procedure allowed to read-out the relative (to baseline input strength in given OHSC) input strength into the CheRiff-CA1 neurons after in-incubator oSTDP induction. In slices that were not previously stimulated with light, the median input strength of CheRiff-CA1 neurons was 0.91 (Figure 12.4 a, no pairing; $\mathrm{mean} = 1.04$, $\mathrm{CV} = 0.53$). Thus, in control conditions (without paired light stimulation) CheRiff-CA1 and neighboring NT-CA1 neurons received equivalent input from the ChrimsonR-CA3 neurons.

CV - the coefficient of variation

When the input strength was assessed 3 days after in-incubator oSTDP induction, the causal pairing resulted in significant potentiation (Figure 12.4, +10 ms: median = 2.13, mean = 2.95, CV = 0.69; $P = 0.002$, Kolmogorov-Smirnov test), however somewhat surprisingly, anti-causal pairing also resulted in stronger inputs (Figure 12.4, −10 ms: median = 1.8, mean = 2.51, CV = 0.89; $P = 0.052$, Kolmogorov-Smirnov test). When OHSC were stimulated only with violet light, no late LTP was induced, meaning that coincident activity of pre- and postsynaptic neurons is an absolute requirement for oSTDP induction (Figure 12.4, post only; $P = 0.6$, Kolmogorov-Smirnov test). Also, the time interval between EPSPs and postsynaptic spikes was important, as the input strength did not change significantly when Δt was +50 ms, but showed a tendency to potentiation when the Δt was −50 ms (Figure 12.4, +50 ms: median = 0.97, mean = 2.44, CV = 1.18; $P = 0.4$; −50 ms: median = 1.78, mean = 2.38, CV = 0.66; $P = 0.13$, Kolmogorov-Smirnov test). As the stimulation was repeated every 200 ms, the tested timings covered all possible phase shifts between pre- and postsynaptic activity (Figure 12.4 c). Evidently, oSTDP induces lasting changes in relative input strength that could be read-out 3 days later.

Extra 12.1: Does virus expression level influences oSTDP outcome?

Even after very careful characterization of ChrimsonR expression after virus injection, there was no possibility to avoid a fluctuation in transduction efficiency. This fluctuation resulted in the different amount of light required to evoke sizable EPSCs in the postsynaptic neurons. At the same time, some CheRiff-CA1 neurons were highly potentiated and others had little to no change in the EPSC slope compared to their NT-CA1 neighbors (Figure 12.4, 3 days after in-incubator oSTDP induction). I reasoned, that if the ChrimsonR expression level would be involved in the difference in the amount of potentiation seen 3 days after the in-incubator oSTDP induction, then the laser power used for the read-out should correlate with the amount of recorded tLTP. However, neither in causally, nor in the anti-causally paired groups this correlation was present (Figure 12.3, $R^2_{\text{Causal}} = 0.002$, $R^2_{\text{Anti-causal}} = 0.02$, Pearson correlation coefficient). Evidently, the fluctuation in ChrimsonR expression does not influence the oSTDP induction outcome.

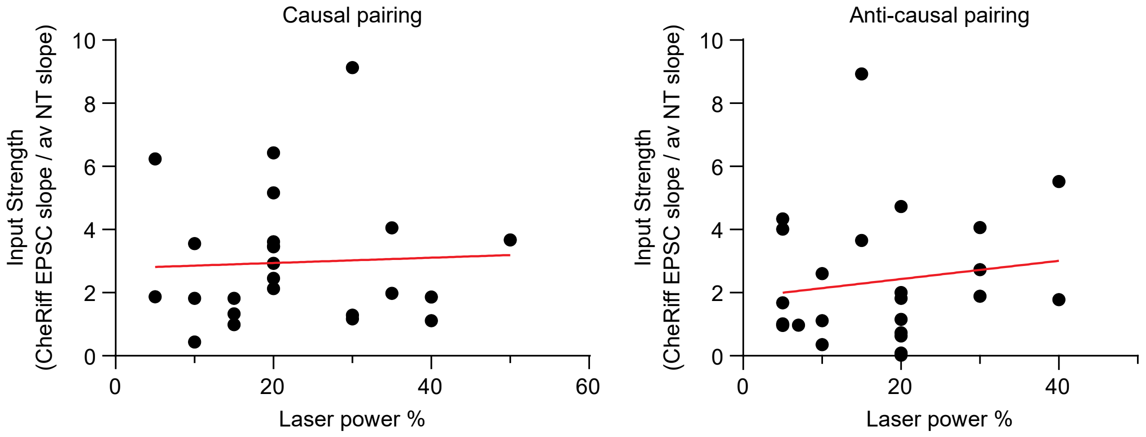

Figure 12.3: Virus expression level does not influence the in-incubator oSTDP induction outcome. There was no correlation between the laser power, used to evoke light-induced action potentials in CA3, and the input strength 3 days after in-incubator oSTDP induction.

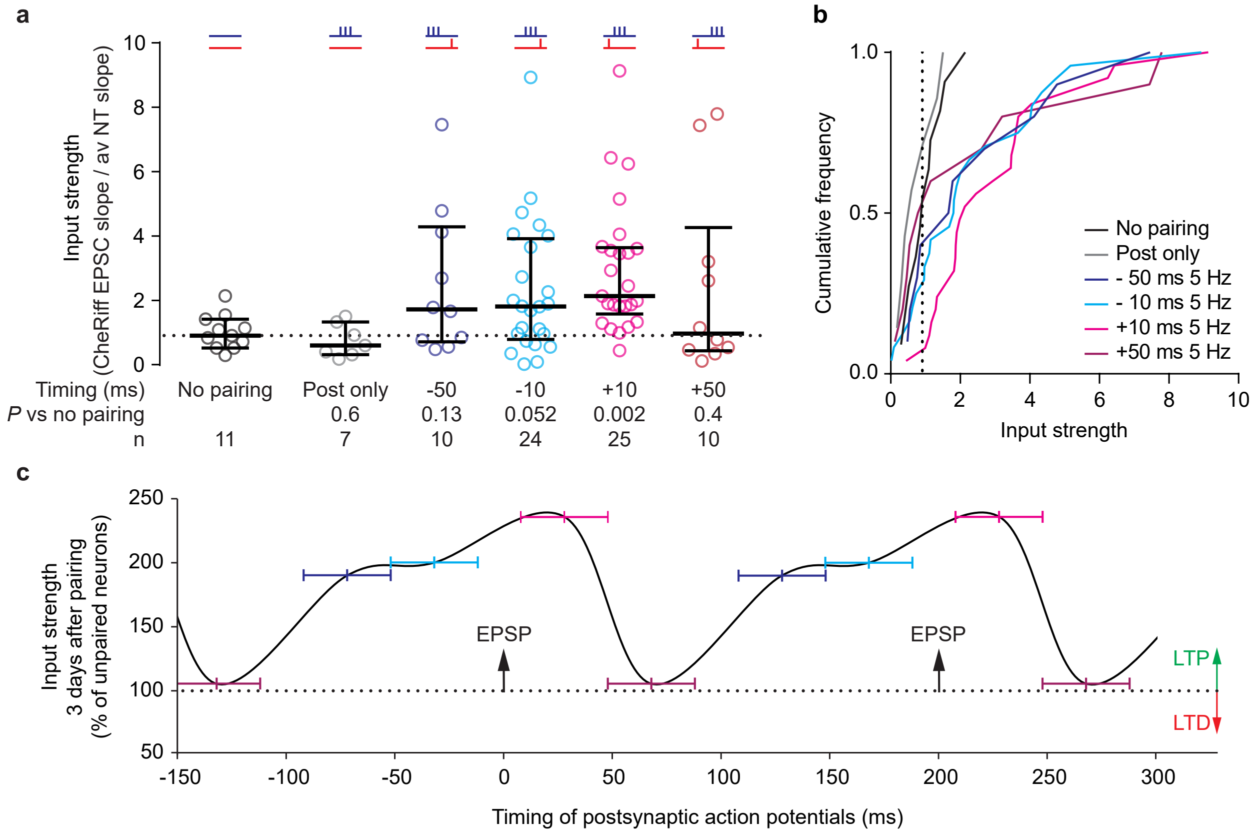

Figure 12.4: Only potentiation is evident 3 days after no-patch oSTDP. a, Normalized input strength of CheRiff-CA1 neurons recorded from slices 3 days after pairing (300 repetitions at 5 Hz). Plotted are individual data points, median and 25 % to 75 % interquartile range. The dotted line is the median input strength onto CheRiff-CA1 neurons of the non-paired slices. *'Timing'* is the target interval between start of the EPSC and the first or last postsynaptic spike. *P* values (Kolmogorov-Smirnov test) are vs 'no pairing' group. **b,** Cumulative frequency distributions of **a**. **c,** The median input strength (% *'no pairing'* median) plotted relative to the light-induced EPSPs (arrows) and action potential timings (vertical ticks on colored bars) during oSTDP pairing (data from **a**: brown +50 ms, violet −50 ms, cyan −10 ms, magenta +10 ms). Two cycles (of 300) at 5 Hz are illustrated.

12.3 NMDA and pairing frequency dependence of late LTP

In line with previous studies [34, 35, 46–48], late LTP induced 3 days after in-incubator oSTDP was abolished when NMDA receptors were blocked during and for at least 1 hour after pairing (Figure 12.5, +CPP). The pairing frequency was also important, as reducing it from 5 Hz to 0.1 Hz prevented late LTP (Figure 12.5, 0.1 Hz) [38].

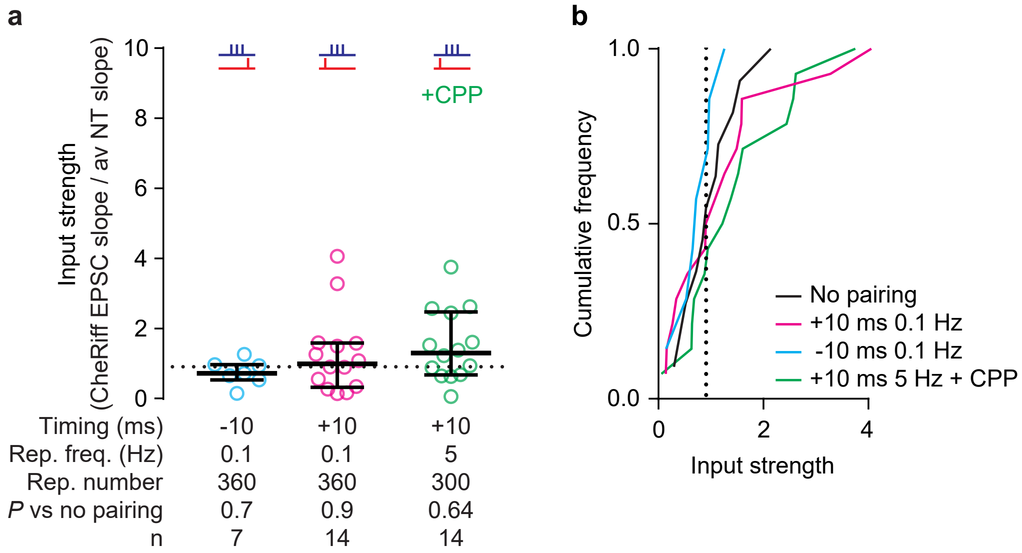

Figure 12.5: Late LTP is NMDA and frequency dependent. a, Normalized input strength of CheRiff-CA1 neurons recorded from slices where the repetition frequency was reduced to 0.1 Hz. The NMDA antagonist CPPene was in the culture medium during causal pairing (+CPP, 1 µM). Plotted are individual data points, median and 25 % to 75 % interquartile range. The dotted line is the median input strength onto CheRiff-CA1 neurons of the *'no pairing'* slices from Figure 12.4. *'Timing'* is the target interval between start of the EPSC and the first or last postsynaptic spike. *'Rep. freq.'* is the pairing repetition frequency. *'Rep. num.'* is the number of pairings. *P* values (Kolmogorov-Smirnov test) are vs *'no pairing'* group. **b,** Cumulative frequency distributions of **a**.

12.4 Absence of tLTD 3 days after in-incubator oSTDP induction

Since the short-term timing rule for patched oSTDP was similar to that of classical STDP, it was surprising that tLTD was not evident 3 days after in-incubator oSTDP induction (Figure 12.4). As discussed in [38], the LTD could be converted to LTP depending on the number of pairings. Taking this into consideration and also the fact that the synaptic input strength distribution after anti-causal pairing (−10 ms, 300 rep) looked rather binomial, I performed the anti-causal pairing at 5 Hz with a different number of repetitions to uncover the expected depression. However, while 30 pairings did not induce plasticity, all other protocols (100 to 500 repetitions) resulted in an increase of input strength (Figure 12.6).

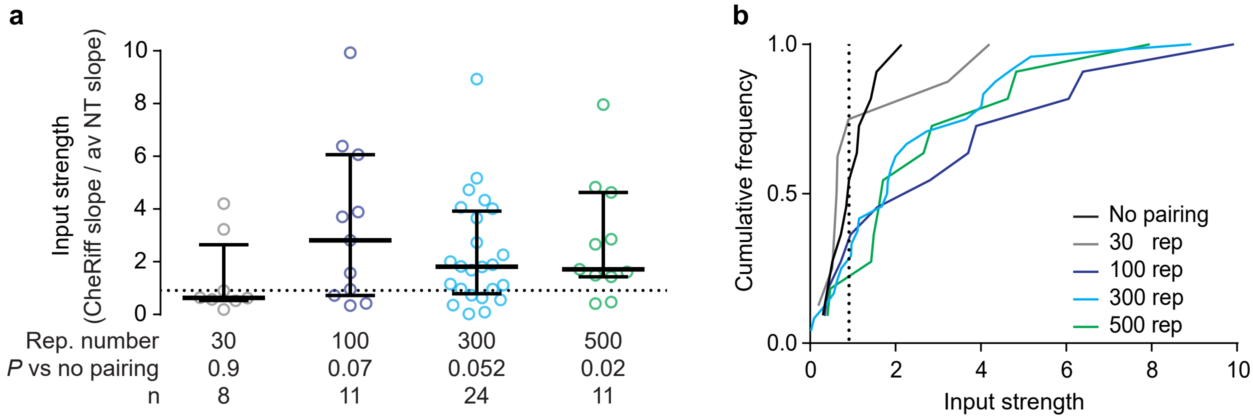

Figure 12.6: Only potentiation is evident 3 days after no-patch oSTDP. a, Normalized input strength of CheRiff-CA1 neurons recorded from slices 3 days after anti-causal pairing. The number of pairings at 5 Hz was varied as indicated (*'Rep. number'*). Plotted are individual data points, median and 25 % to 75 % interquartile range. The dotted line is the median input strength onto CheRiff-CA1 neurons of the *'no pairing'* slices from Figure 12.4. P values (Kolmogorov-Smirnov test) are vs *'no pairing'* group. **b,** Cumulative frequency distributions of **a**. *'No pairing'* and *'anti-causal 300 rep'* groups were added for reference from Figure 12.4.

12.5 Input strength 3 hours after in-incubator oSTDP induction

Since the difference in the pairing outcome between short-term (on-cell patch, 30 min) and long-term (in-incubator, 3 days) read-out time was very apparent, it was logical to assume, that some time-dependent process could be involved in converting tLTD to tLTP in days following the plasticity induction. As it takes time to settle OHSC in the recording chamber, adjust the off-axis stimulation and sequentially record from at least 4 neurons to obtain one data point, the earliest time after in-incubator oSTDP induction possible to asses was ~3 hours. Somewhat surprisingly, at this early time point input strength was not significantly changed by either causal or anti-causal spike-burst pairing, although a trend towards potentiation was apparent after causal pairing (Figure 12.7, -10 ms: $\mathrm{median} = 1.04, P = 0.2$, Kolmogorov-Smirnov test; $+10$ ms: $\mathrm{median} = 1.62, P = 0.56$, Kolmogorov-Smirnov test). Thus, tLTD was observed only immediately after oSTDP induction during patch-clamp recording, but not later, when CA1 neurons were not patched during oSTDP induction.

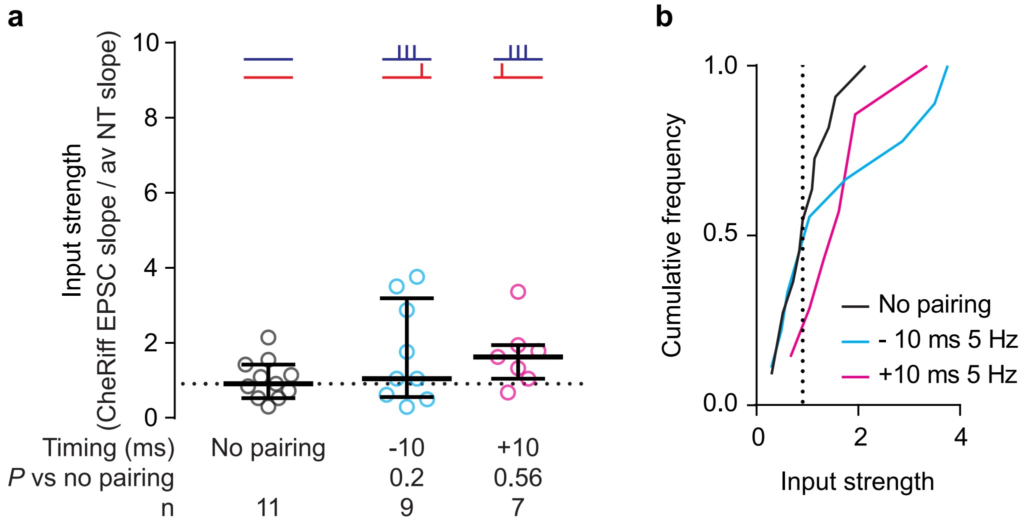

Figure 12.7: No input strength changes 3 hours after no-patch oSTDP. a, Normalized input strength of CheRiff-CA1 neurons recorded from slices ~3 hours after in-incubator oSTDP induction. Plotted are individual data points, median and 25 % to 75 % interquartile range. *'No pairing'* group is replotted from Figure 12.4. *'Timing'* is the target interval between start of the EPSC and the first or last postsynaptic spike. *P* values (Kolmogorov-Smirnov test) are vs *'no pairing'* group. **b,** Cumulative frequency distributions of **a**.

12.6 Calmodulin washout role in early tLTD

The conversion of tLTD into tLTP over time was both unexpected and intriguing. There are at least two possibilities: first, as discussed above, the tLTD converts into tLTP over days following the plasticity induction, making tLTD a transient phenomenon; second, tLTD occurs only when neurons were patched and their membrane and machinery was disrupted during it. Since varying the pairing protocol length and the read-out timing did not lead to the uncovering of the tLTD, I decided to check, whether reducing the negative effect of patching would influence the short-term oSTDP induction outcome.

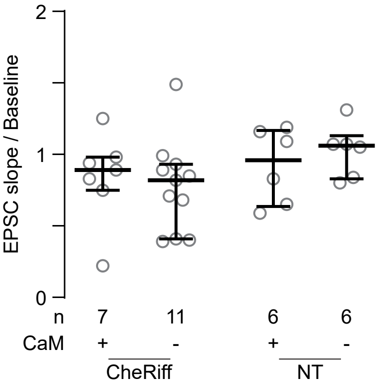

Figure 12.8: Calmodulin washout role the in early tLTD induction. Compared are anti-causal on-cell oSTDP pairing outcome in presence (CaM +) or absence (CaM -) of additional calmodulin in the patching pipette. $P_{\text{CheRiff}} = 0.7$, $P_{\text{NT}} = 0.9$, Kolmogorov-Smirnov test. *'CheRiff'* – CheRiff-expressing CA1 neurons. *'NT'* – non transfected CA1 neurons. Plotted are individual data points, median and 25 % to 75 % interquartile range.

ATP - adenosine triphosphate
GTP - guanosine triphosphate
cAMP - cyclic adenosine monophosphate
cGMP - cyclic guanosine monophosphate
EDTA - ethylenediaminetetraacetic acid

The intracellular solution used in the patching pipette already includes ATP/GTP and phosphocreatine to make sure the cells can maintain their basic energy (ATP) supply and that the important messengers cAMP and cGMP can be produced. It is also well known that the washout effect plays an important role in plasticity induction [136] and small and mobile molecules, such as Calmodulin (CaM), are the first to be diluted and washed out from the neuron during patch-clamp experiment. CaM is important for the structural plasticity and spines growth, and consequently for the LTP induction on the cellular level [137, 138]. Thus, it was reasonable to assume, that CaM washout could prevent the tLTP after anti-causal pairing, converting it to tLTD. CaM-wt (in 50 mM Tris, pH 7.5, 10 mM EDTA) was freshly diluted in intracellular solution (30 µM final concentration) and loaded in the patching pipette right before the CheRiff-CA1 or NT-CA1 neurons were patched and anti-causally paired (on-cell oSTDP, Chapter 9.4). Interestingly, having calmodulin in the patching pipette prevented early tLTD induction in CheRiff-CA1 neurons ($\mathrm{n}_{\mathrm{CaM}} = 7$, $P_{\mathrm{CaM}} = 0.2$ vs $\mathrm{n}_{\mathrm{norm}} = 11$, $P_{\mathrm{norm}} = 0.0009$; P values are after Kolmogorov-Smirnov test, *'norm'* refers to the absence of CaM in the patching pipette and Chapter 9.4) and had no effect on NT-CA1 neurons ($\mathrm{n}_{\mathrm{CaM}} = 6$, $P_{\mathrm{CaM}} = 0.8$ vs $\mathrm{n}_{\mathrm{norm}} = 6$, $P_{\mathrm{norm}} = 0.09$; P values are after Kolmogorov-Smirnov test). However, there was no statistically significant difference when the normalized EPSC slope from CheRiff-CA1 neurons from both groups were compared (Figure 12.8). Consequently, it is not possible to fully rule out neither the general washout effect nor the influence of the membrane rupture and thus, more detailed investigation is required.

12.7 Activity dependence of late LTP

The observed increase in synaptic strength days following the plasticity induction was intriguing. It is known that OHSCs are spontaneously active on their own. I reasoned that in the absence of natural inputs, the CA3-CA1 circuit is more susceptible to the "light imprinted memory" and thus tends to repeat and amplify the learned pattern, which leads to an increase in the reactivation of the paired synapses [32, 139]. To test this, I have artificially raised or lowered the activity in the OHSCs 3 hours after in-incubator oSTDP induction (see Chapter 9.6 for more details). I have chosen 3 hours since the tendency to potentiation in the causally paired group was already apparent (Figure 12.7). To lower the activity in OHSCs, paired cultures were treated with 1 µM TTX for 48 hours. Then, TTX was washed out by replacing the medium and read-out was performed 24 hours later. To increase the activity in OHSCs, the slices were extensively washed with fresh medium at the same time as for TTX treatment. In both cases, the induction of late LTP was prevented in both causally and anti-causally paired groups (Figure 12.9). These results suggest that the synaptic memory of a short episode of coincident activity was actively maintained and amplified in the cultures, pointing to a process that requires replay of activity patterns in the selected circuits.

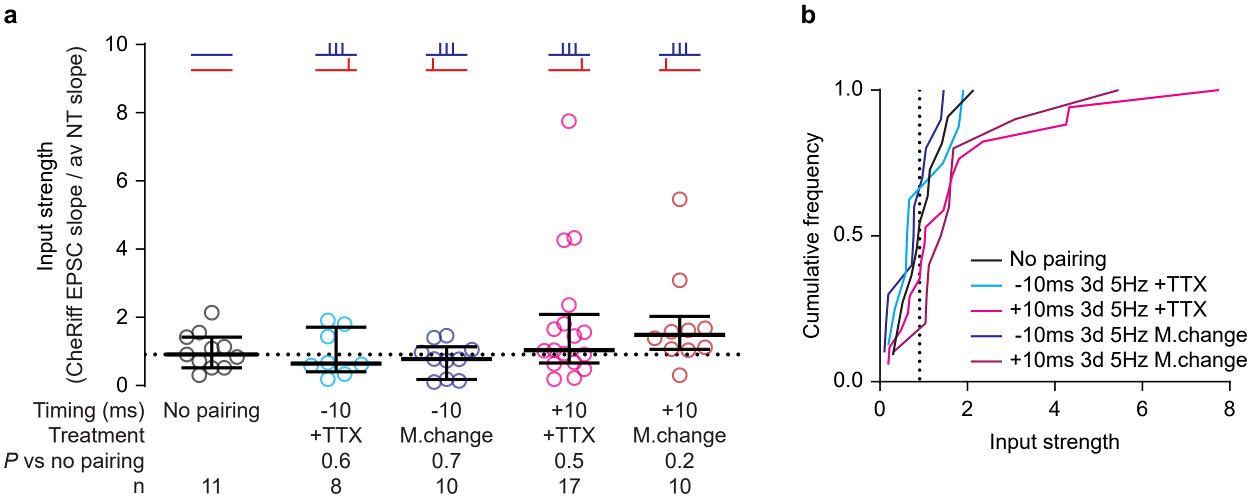

Figure 12.9: Spontaneous activity in OHSC is important for plasticity consolidation. a, Normalized input strength of CheRiff-CA1 neurons recorded from causally or anti-causally (300 repetitions at 5 Hz) paired slices 3 days later. *'No pairing'* group is reproduced from Figure 12.4. Three to four hours after oSTDP medium was changed (*'M. change'*) to increase global activity or activity was blocked with tetrodotoxin (*'+TTX'*, 1 µM). Two days later medium was changed again and TTX washed off. Plotted are individual data points, median and 25 % to 75 % interquartile range. P values (Kolmogorov-Smirnov test) are vs *'no pairing'* group. **b,** Cumulative frequency distributions of **a**.

12.8 Intrinsic excitation of postsynaptic neurons

Some studies [32, 140–143] point out an increase of excitability in postsynaptic neurons after plasticity induction, which could be a reason for late LTP in this case. However, there was no difference in active and passive cellular parameters between CheRiff-CA1 and NT-CA1 neurons (Figure 12.10). This suggests that late LTP, apparent 3 days after in-incubator oSTDP-induction, was synaptic and not due to increased postsynaptic excitability.

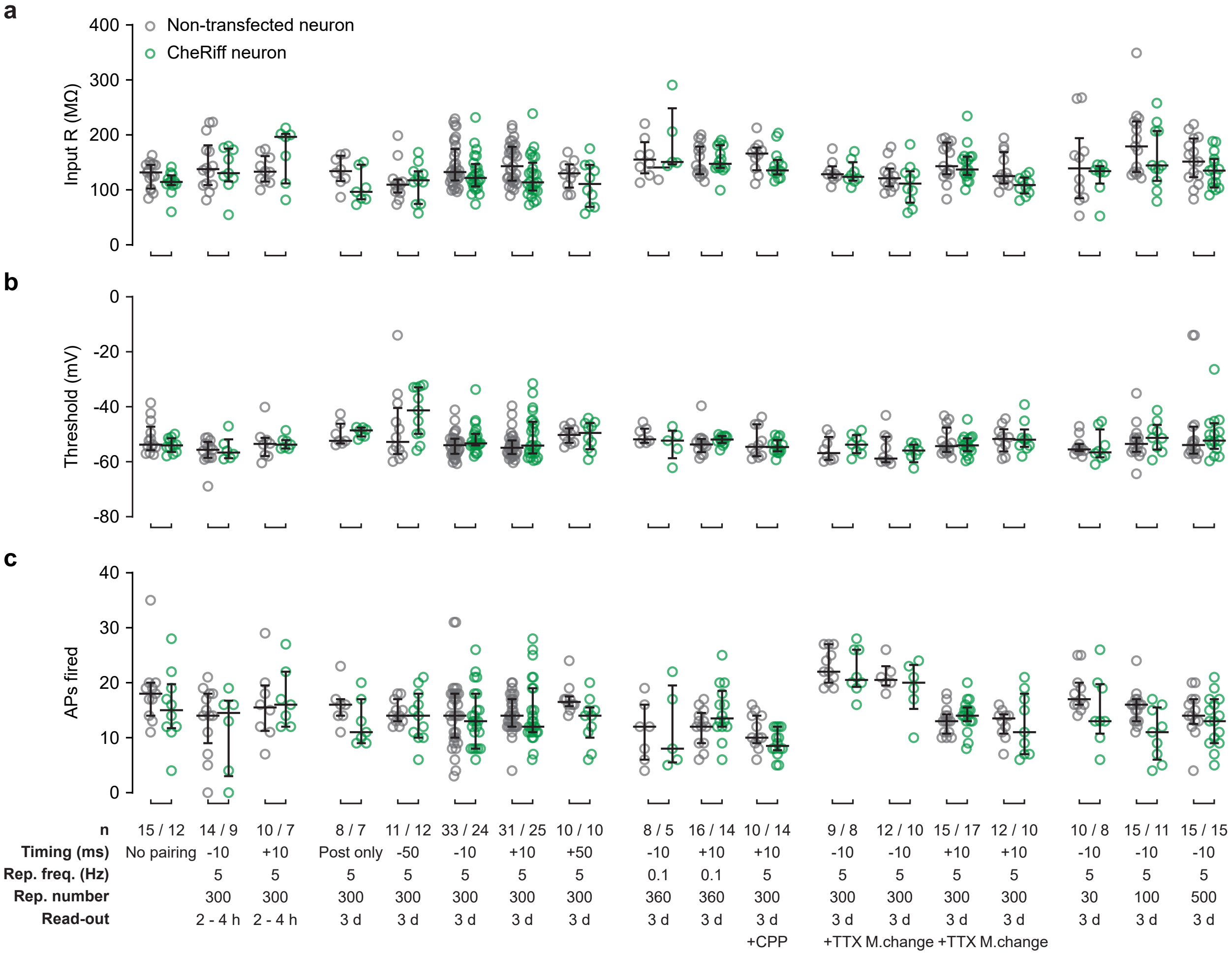

Figure 12.10: Comparison of passive and active cell parameters of CheRiff-CA1 and neighboring NT-CA1 neurons from in-incubator oSTDP experiments. a, Input resistance (R_{in}) of all CheRiff-CA1 and NT-CA1 neurons. **b,** Action potentials threshold. **c,** Numbers of action potentials fired in response to a 400 pA current step. There were no significant differences between NT-CA1 and CheRiff-CA1 neurons in any of the treatment groups (Kolmogorov-Smirnov tests). *+CPP*, 1 µM CPPene during oSTDP; *+TTX*, 1 µM tetrodotoxin 4-48 hours after oSTDP; *M. change*, medium changed 4 and 48 hours after oSTDP. *n* given as number of NT-CA1 / number of CheRiff-CA1 neurons.

12.9 Dendritic spines morphology 3 days after oSTDP induction

The strong potentiation 3 days after oSTDP induction is an interesting phenomenon, which was not possible to explain by only electrophysiology and pharmacological manipulations. Looking further into the dendritic spines could potentially help to understand the morphological changes caused by the plasticity induction and, possibly, explain the observed late LTP. It was previously shown, that dendritic spines size, shape and density change upon plasticity induction [21–23, 144–146]. It was also shown, that the spine position along the dendritic tree regarding to the synaptic-input localization is important for the STDP induction and can lead to the LTD conversion into LTP at the negative pairing window (anti-causal pairing) [50, 55–58]. Taking it together, I investigated the spine morphology and spine density in OHSC which underwent causal pairing protocol, were only stimulated with blue light (Post only: 300 repetitions at 5 Hz of miniburst) or not stimulated at all.

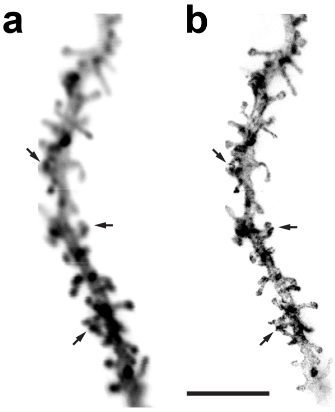

Figure 12.11: Confocal vs STED resolution power. a, A single plane confocal image of the dendritic segment. **b,** STED resolved image of the same dendritic segment as in **a**. Black arrows are showing the dendritic spines, which were too close to be detected in the confocal image. Scale bar – 5 µm.

The average dendritic spine volume of a rat CA1 pyramidal neuron is $0.06 \pm 0.08\,\mu\text{m}^3$, resulting in the dimensions right at a resolution boarder of the confocal microscopy [147, 148]. Thus, here I used stimulated emission depletion (STED) microscopy to overcome this issue (Figure 12.11). STED relays on usage of high-power depletion laser to resolve the structure and thus the specimen is prompt to photobleaching [149]. Using specially designed antibodies to enhance the original fluorescent signal is an absolute requirement in this case (Table 10.1), however, even then some small structures (like axonal boutons) would still bleach before a super-resolution image can be obtained. For this reason, it was not possible to identify the putative ChrimsonR-bouton to CheRiff-spine connections in this particular experiment, and it was decided to investigate the general spine morphology and density in three groups named above.

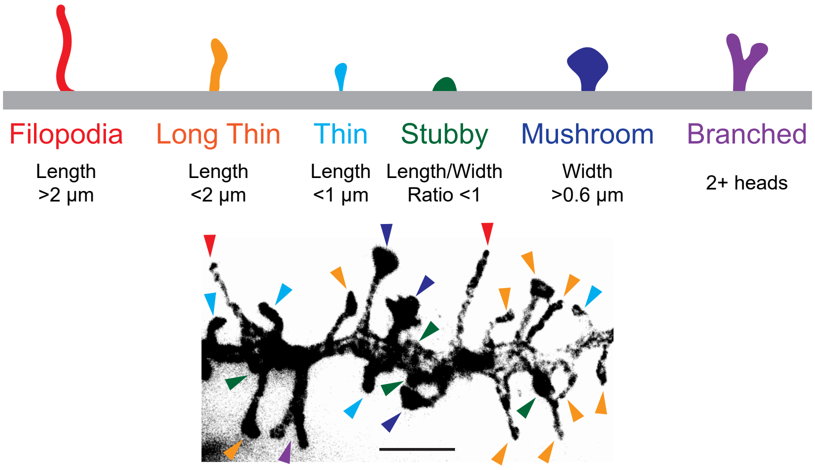

Figure 12.12: Dendritic spine classification according to their morphology. Top - a schematic representation of 6 most common dendritic spine shapes (according to [150]). **Bottom** – a STED single plane image of a dendritic segment. Triangles are color coded according to the spine morphology shown above. Scale bar – 2 µm.

One to three apical oblique dendritic segments (10 to 30 microns in length) were STED resolved per each CheRiff-CA1 neuron in OHSCs. In each segment the spines were manually classified into groups according to their morphology (Figure 12.12) [150]. Overall, there was no difference in dendritic spine density between the groups ($P = 0.57$, Kruskal-Wallis test, Figure 12.13), and median spine density in all conditions was 1.5 spines per micron (1.4 spines per micron for *'Non stimulated'*, 1.3 spines per micron for *'Causal pairing'* and 1.6 spines per micron for *'Blue light only'*), which is similar to previously reported value for OHSCs (1.3 spines per micron, two photon microscopy [22]*). The only observed difference was in the number of filopodia spines between blue light only stimulated and non-stimulated OHSCs (*'Post only'* vs *'Non stimulated'*: $P = 0.005$, Kruskal-Wallis test; Figure 12.14).

* *The slightly higher spine density is explained by the technique used to obtain the images: STED resolves spines located close together, that are otherwise counted as one spine (Figure 12.11)*

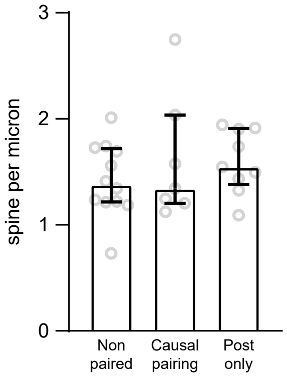

Figure 12.13: Spine density was not changed 3 days after oSTDP induction. Data is shown as an average spine density per neuron (1 to 3 dendritic segments). Plotted are individual data points, median and 25 % to 75 % interquartile range.

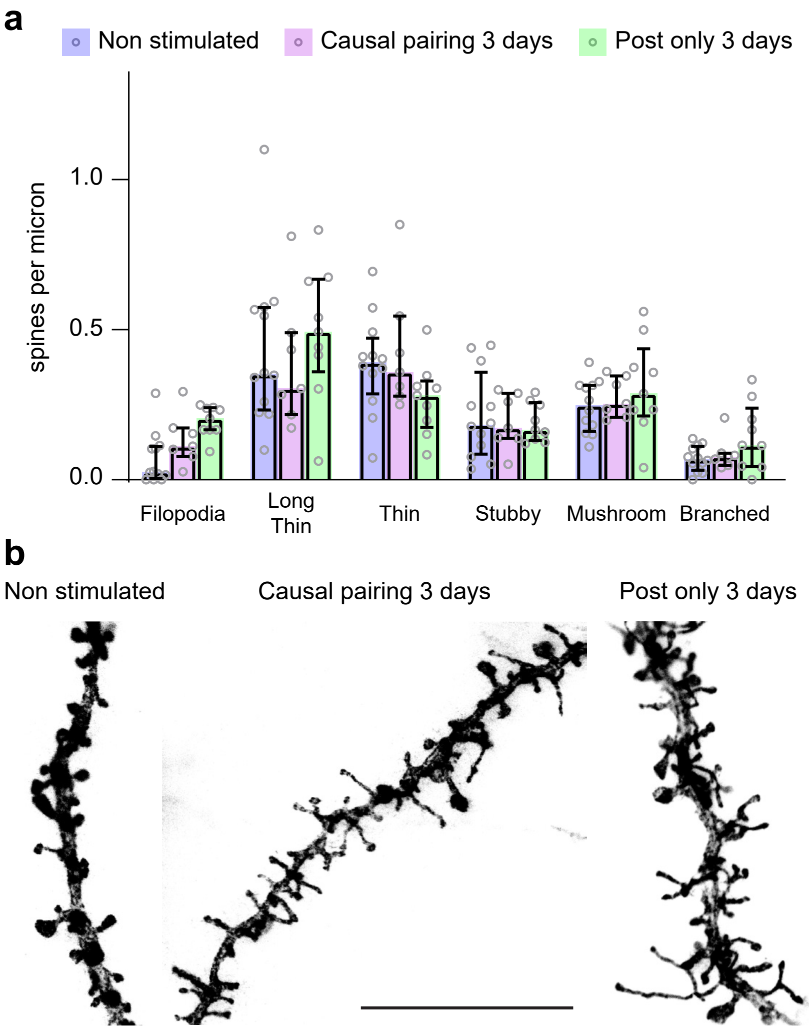

Figure 12.14: Light-induced firing in postsynaptic neurons promotes filopodia grows. a, Dendritic spine morphology after light stimulation. Plotted are individual data points, median and 25 % to 75 % interquartile range. **b,** A representative STED single plane image for every condition. Scale bar – 10 µm.

13 DISCUSSION AND PERSPECTIVES

In Part III I demonstrated that (**1**) ChrimsonR and CheRiff can be used to independently and precisely control spiking in two distinct populations of neurons, (**2**) optogenetic spike-burst pairing during patch-clamp experiments induced either tLTP (causal pairing) or tLTD (anti-causal pairing), (**3**) the long-term consequence of pairing closely apposed pre- and postsynaptic spikes is potentiation regardless of the timing sequence, (**4**) spontaneous activity in days following the plasticity induction is important for imprinted memory consolidation and (**5**) there is no difference in spine density 3 days after tLTP induction.

13.1 Short-term vs long-term consequence of oSTDP

Since oSTDP induced during patch-clamp recordings follows the same timing rules as classical STDP induced by electrical stimulation [34, 35, 37, 151, 152], using optically-induced spiking should not dramatically influence the plasticity induction outcome later on. That is why the absence of tLTD 3 days after in-incubator oSTDP induction was so unexpected and intriguing. Besides, in-incubator oSTDP is similar to the electrical-STDP in many important aspects. Late oSTDP shows strong timing dependence, as no potentiation is observed when the Δt between the EPSP and the first postsynaptic spike was 50 ms. At this time, GABA-A currents from feed-forward inhibition are strongly activated in CA1 neurons [153] and may reduce the synaptic calcium influx necessary for potentiation as has been demonstrated for back-propagating action potentials [154]. Further finding, supporting that elevated intracellular $[\mathrm{Ca}^{2+}]$ in the postsynaptic neuron is essential for late LTP, is its dependence on NMDA receptors (Figure 12.5, +CPPene), which was also well established for classical STDP [32, 46, 56]. Strong pairing frequency dependence of late oSTDP (Figure 12.5) also agrees well with classical STDP rules [38].

An attempt to find a pairing protocol which would induce the late tLTD has also failed: neither increasing nor decreasing the number of anti-causal pairing repetitions unmasked a late tLTD (Figure 12.6), nor was tLTD apparent at the earliest time window (~3 hours) feasible after in-incubator oSTDP induction (Figure 12.7). The fact that there were no statistically significant differences detected in the input strength at this early time point is consistent with a slow, activity-dependent enhancement of tLTP. It was reasonable to hypothesize that slight differences in synaptic strength or excitability, induced by the only structured activity that was ever provided in these slice cultures, were enhanced over time by an active process akin to overfitting. That the 'memory' of pairing is erased when spontaneous activity is disrupted supports this hypothesis. However, obtaining direct evidence will require the continuous monitoring of the circuit activity over several days. A promising approach would then be to use a bioluminescent $[\mathrm{Ca}^{2+}]$ sensor [155] to record the firing activity before and in following days after in-incubator oSTDP induction, since this technique can be coupled to a simple camera and does not relay on epifluorescence, although requires a supply of fresh luciferase.

Although the majority of STDP studies report both potentiation and depression, 'LTP-only' STDP windows have been observed before at human hippocampal, human and rat neocortical synapses [156–158] and in mouse hippocampus [38] and visual cortex [55], most commonly in the presence of increased dopamine [151, 156]. If presynaptic activity is paired with prolonged postsynaptic bursts (plateau potentials), the timing window for Schaffer collateral potentiation can be extended to several seconds in the causal and anti-causal direction [131]. Explanations for these discrepant outcomes of early oSTDP abound, but I speculate that if synaptic strength was assessed after several days, the outcome of repeated coincident activity may always be potentiation regardless of the exact temporal sequence. Conservation of total synaptic weight may be provided by heterosynaptic LTD or via generalized downscaling processes [159], which is supported by the fact that there was no difference in synaptic density in OHSCs 3 days after in-incubator oSTDP induction compared to control condition (Figure 12.13).

13.2 Patch-clamp associated problems in plasticity induction

Care was taken to start the oSTDP induction within 5 minutes after obtaining the whole-cell access, since it is well known, that plasticity induction is prevented by the washout of important cellular components [118, 136]. While preventing CaM washout alone seemed not to be enough to convert tLTD into tLTP (Figure 12.8), but was enough to prevent tLTD induction, trying to further understand how to minimize the patching-induced artifacts could be of a great importance for the electrophysiological studies in general. Another obvious candidate, prompt to washout by patch-clamping the neuron, is beta-actin, one of the isoforms of actin protein [118]. However, introducing actin into intracellular patching solution is a very challenging task, since actin tend to polymerize rather fast and needs to be mixed in right before use, leaving very small window for successful patch. Additional evidence against the hypothesis that early tLTD is purely due to washout are STDP studies using sharp electrodes or perforated patch recordings, that have reported both tLTD and tLTP [151, 152]. Still, it is possible that the act of patching the postsynaptic neuron compromises tLTP, and biases synapses towards depression [160].

13.3 Increase in filopodia spines number after light stimulation

Filopodia are believed to be precursors to mature synapses and potentially are used by post-synaptic neuron to detect a passing axon or local increase in glutamate concentration [161, 162]. The increase in their number in burst-firing CheRiff-CA1 neurons can be viewed as a response to the light induced postsynaptic activity, which potentially forced the neuron to search for the missing synaptic input. Since this trend was also apparent in causally paired OHSCs (Figure 12.14), it would be interesting to identify the relative position of filopodia and ChrimsonR-boutons, as well as the filopodia number in close proximity from putatively connected spines [57]. This information could help to explain the symmetrical STDP window 3 days after optical plasticity induction and broaden our understanding of Hebbian plasticity rule on behavioral relevant time scale.

Yet, it is not trivial to perform such an experiment. Either the ChrimsonR targeting to axonal boutons needs to be improved, to avoid rapid bleaching during STED image acquisition or, as an alternative, eGRASP approach [163] can help successfully identify connected synaptic partners. However, both those options require significant changes to the original constructs used in this work, and thus, cannot be used without first performing the basic control experiments to verify that there is no change caused in the oSTDP outcome.

Part IV

Characterization of activity-dependent cFos upregulation after light stimulation

CHARACTERIZATION OF ACTIVITY-DEPENDENT CFOS UPREGULATION AFTER LIGHT STIMULATION

In Part III I briefly touched the topic of immediate early gene cFos expression after light stimulation and plasticity induction. It was shown on the example of ChrimsoR-CA3 (Figure 11.5 and 11.6), that a single light-evoked action potential repeated 300 times at 5 Hz does not elevate cFos level in the neuronal nucleus, whereas a small burst (3 action potentials at 50 Hz) repeated again 300 times at 5 Hz leads to cFos expression. Since cFos is considerate to be an indicator of general activity in the cell [86–90, 95–98], it seemed important to follow up on the observed firing frequency dependence of cFos expression in hippocampus.

Thus, in Part IV I tried to answer the following questions: is cFos expression firing frequency dependent? Is there a difference in cFos expression in different hippocampal regions? How many action potentials are necessary for cFos expression?

14 CFOS UPREGULATION AFTER NEURONAL ACTIVITY

14.1 cFos protein expression window in neuronal nuclei in OHSCs

There are two ways of detecting the cFos level in the nucleus after delivered stimulation: through mRNA or protein expression. cFos mRNA production increases shortly after the stimulation (5 min to 10 min, [89, 164]) making it difficult to minimize the unwanted cFos induction during prefixation handling of the stimulated cultures. Whereas cFos protein expression is delayed by at least 30 min after the stimulation [86, 89, 164], which makes it easier to work with. In general, cFos expression window can vary depending on the brain region [86, 97], and thus it was important to verify the cFos protein expression window for different hippocampal regions. Here, I used *'High Potassium'* stimulation, which should increase cFos level in all cells [133]. OHSCs were treated two times for 2 min in HEPES buffer solution containing 50 mM Potassium and then washed three times for 2 min in normal HEPES buffer. After that, OHSC were returned to the incubator and fixed with 4 % PFA after 30 min, 60 min and 90 min. *'No stimulation'* group was used as a reference for the baseline cFos expression in pyramidal neurons in OHSCs. Evidently, the optimal read-out time for OHSCs is 60 min after the end of stimulation, since by 90 min the cFos expression level in CA3 neurons was already dramatically reduced (Figure 14.1).

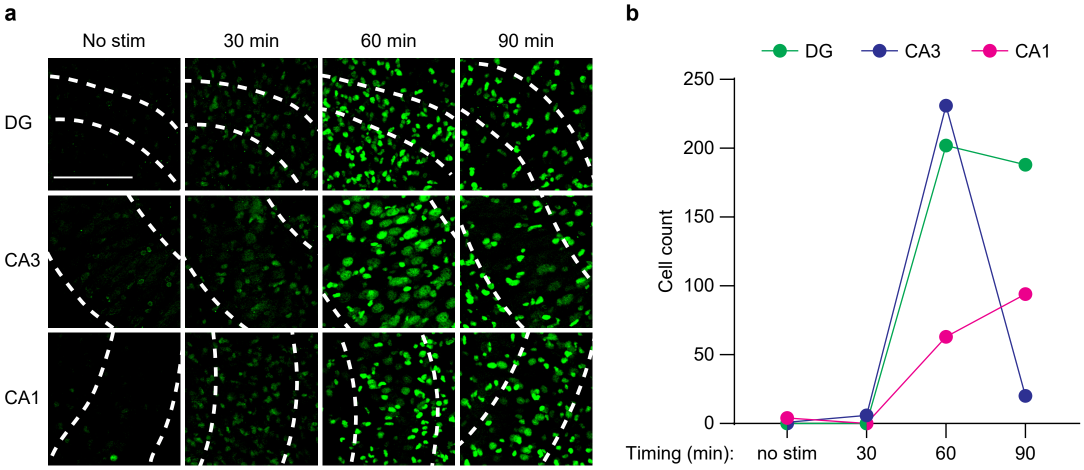

Figure 14.1: cFos induction timeline in OHSC. a, Confocal images (maximum intensity projection) of cFos expression in DG, CA3 and CA1 area of OHSC 30 min, 60 min and 90 min after *'High Potassium'* stimulation. *'No stim.'* – non-stimulated control. Note high cFos expression in small glial cells. Dotted lines show approximately the border of pyramidal (granule) cell layer. Scale bar – 100 µm. **b,** cFos positive pyramidal neurons count in each region at different time point. Plotted are individual data points.

14.2 Viral expression of opsins over extended period of time leads to cFos expression

Some optogenetic tools delivered to the neurons in form of the viral-vector can be toxic and lead to the neuronal death, if expressed for an extended period of time. To gather information about different hippocampal regions, the uniform opsin expression in majority of the pyramidal neurons was essential. To achieve this high level of transduction, I expressed AAV$_{\mathrm{Rh10}}$-syn-ChrimsonR-TdT with virus drop technique (Figure 14.2, Chapter 7.3). Since in this case the opsin expresses slower compared to the virus injection timeline*, I first checked the ChrimsonR toxicity over 3 weeks by investigating the cFos protein expression in transduced pyramidal neurons. I was expecting to see minuscule amount of cFos positive pyramidal neurons (spontaneously active neurons) if ChrimsonR expression was not toxic, and rather large number otherwise. Indeed, when ChrimsonR was expressed in OHSCs for longer than two weeks, cFos level was elevated in many pyramidal neurons (Figure 14.3). Accordingly, all following experiments were performed on day 7 after virus transduction to avoid virus-induced cFos expression.

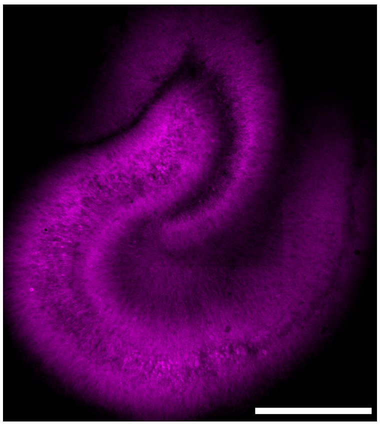

Figure 14.2: Homogeneous expression of ChrimsonR in OHSC. Confocal image (median intensity projection) of the slice expressing ChrimsonR after virus drop. Scale bar - 500 µm.

* ***Why there is a difference in expression time?*** *With local injection more copies of the virus are tightly delivered inside the tissue, whereas with virus drop the virus particles concentration is higher on the surface of the OHSC and fewer copies will be available for individual neurons, slowing down the tool-expression process.*

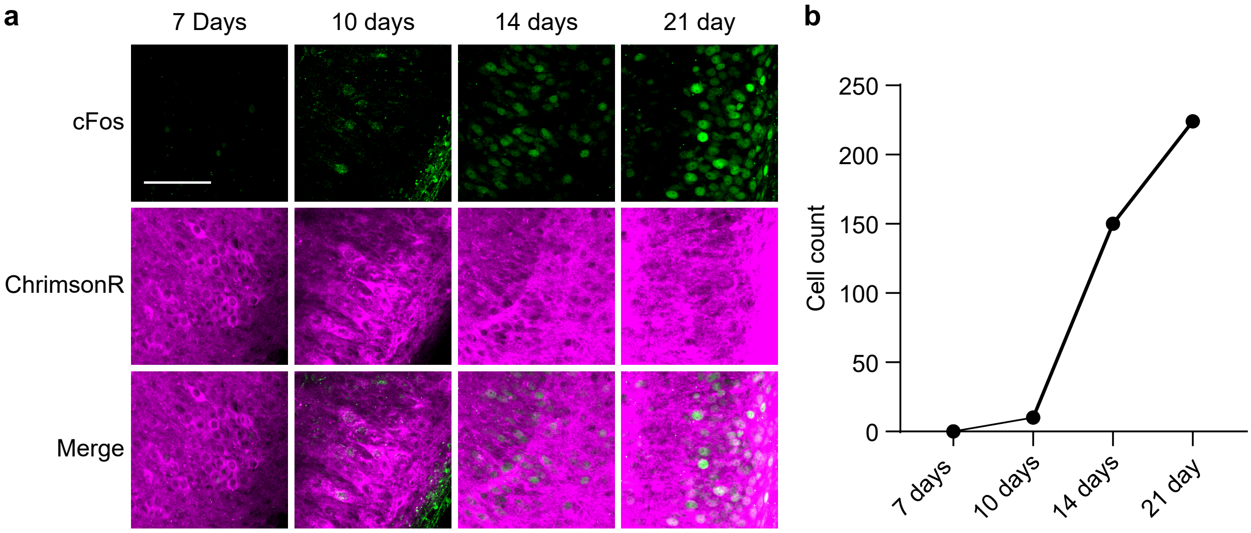

Figure 14.3: ChrimsonR-induced cFos expression. a, Confocal images (maximum intensity projection) of cFos and ChrimsonR-virus expression in CA3 pyramidal neurons 7, 10, 14 and 21 days after virus drop of AAV$_{\mathrm{Rh10}}$-ChrimsonR-TdT. Note the difference in virus expression. Scale bar – 100 µm. **b,** cFos positive pyramidal neurons count from **a**. Plotted are individual data points.

14.3 Optimal light stimulation protocol for ChrimsonR transduced pyramidal neurons

After establishing that 7 days of ChrimsonR virus expression does not elevate the cFos level in pyramidal neurons, I verified the light induced firing threshold in CA3 and CA1 neurons. I recorded from a number of pyramidal neurons in both areas in cell-attached mode in recording medium with fast synaptic transmission blockers (CPPene, NBQX, picrotoxin, Table 9.1, Chapter 9.2). The soma of each neuron was first stimulated every 10 s with 1 ms of 625 nm light flash at different intensities to determine the firing threshold (Figure 14.4). The majority of pyramidal neurons fired an action potential in a response to the light stimulation with intensity of 7 mW/mm^2 or below, which is in good agreement with the data shown earlier (Chapter 11.1). Then, a train of ten 1 ms flashes at 5 Hz, 10 Hz and 50 Hz was given at 20 s intervals with the intensity of 7 mW/mm^2 and 11 mW/mm^2 to determine, how well ChrimsonR-neurons can follow the stimulation pattern at selected intensities (Figure 14.5) [80]. Clearly, the majority of CA1 and CA3 neurons were perfectly following the presented pattern when given at 7 mW/mm^2, whereas a number of CA3 neurons were burst-firing when the pattern was given at 11 mW/mm^2. Therefore, the stimulation for the in-incubator tower was set to 1 ms at 7 mW/mm^2 (630 nm) as a most reliable (Table 9.3).

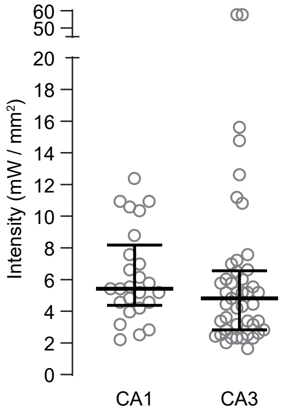

Figure 14.4: Light-induced firing threshold of ChrimsonR neurons. Shown data for ChrimsonR-CA3 and ChrimsonR-CA1 neurons ($n_{CA3} = 45$; $n_{CA1} = 25$; $P = 0.27$ Kolmogorov-Smirnov test). Plotted are individual data points, median and 25 % to 75 % interquartile range.

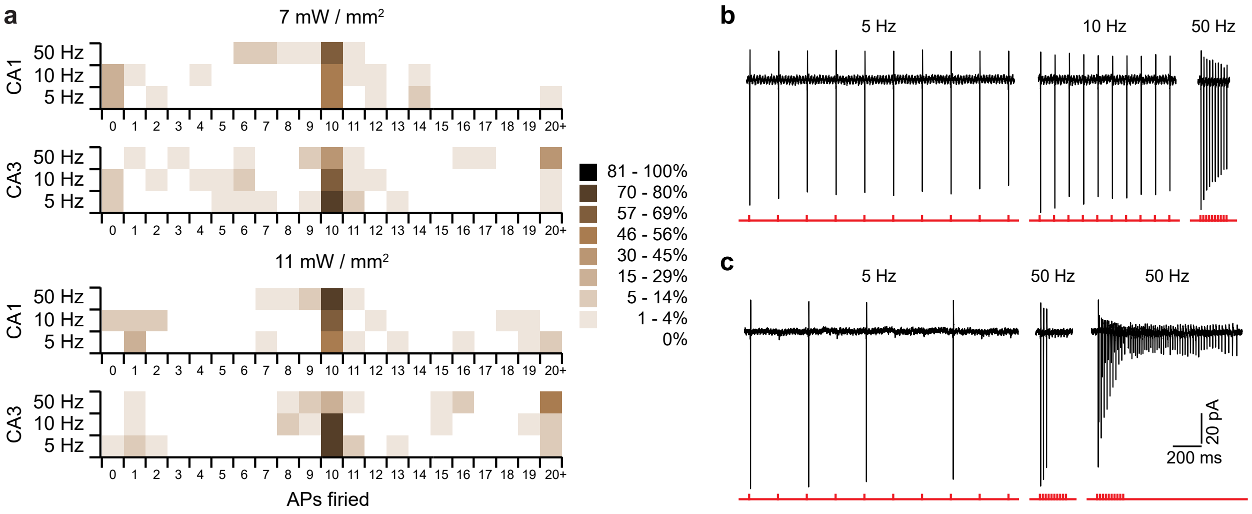

Figure 14.5: Pattern following of ChrimsonR neurons. a, Number of light-induced action potentials fired in response to ten 1 ms red light flashes at different frequencies for neurons from Figure 14.4. Color scheme indicates the percentage of all CA3 or CA1 neurons recorded. **b and c,** Cell-attached spikes recorded from ChrimsonR-CA3 neurons in response to 1 ms, 7 mW/mm^2 flashes at 5 Hz, 10 Hz and 50 Hz. The cell in **b** follows perfectly the stimulation. **c,** Examples of cells firing fewer or more action potentials than light flashes.

In the end of each recording the whole-cell configuration was obtained to verify the cell type and parameters (Figure 14.6).

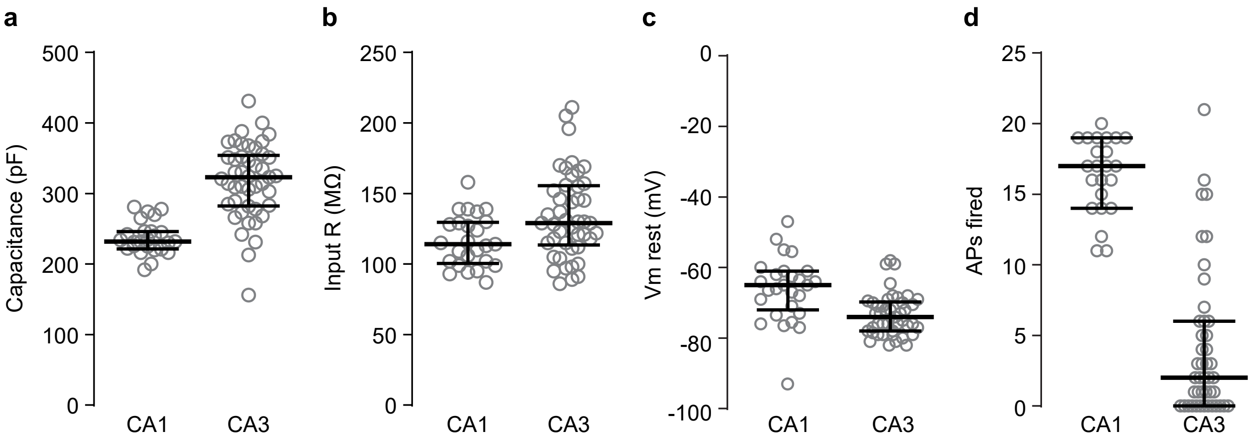

Figure 14.6: Cell parameters of ChrimsonR expressing neurons from the Figure 14.4. **a,** Capacitance ($n_{CA3} = 45$; $n_{CA1} = 25$; $P < 0.0001$). **b,** Input resistance ($n_{CA3} = 45$; $n_{CA1} = 25$; $P = 0.05$). **c,** Resting membrane potential ($n_{CA3} = 45$; $n_{CA1} = 25$; $P < 0.0001$). **d,** Number of action potentials fired in response to 400 pA current injection step ($n_{CA3} = 44$; $n_{CA1} = 25$; $P < 0.0001$). All P values are given after Kolmogorov-Smirnov test. Plotted are individual data points, median and 25 % to 75 % interquartile range.

14.4 cFos expression depends on the firing frequency.

It was reported that cFos upregulation depends on the activity history of the cell [90, 95, 97, 98], however there was no consistent study linking the number of action potentials and firing frequency to the expression level of cFos so far. Here, I show the cFos upregulation dependence on firing frequency of pyramidal neurons.

OHSCs were treated with synaptic transmission blockers (CPPene, NBQX, picrotoxin, Table 9.1) and transferred to the dark incubator overnight. A single experiment contained several groups of 1 to 3 OHSCs which were stimulated in the in-incubator stimulation tower (Figure 9.3). After stimulation, OHSCs were letter-coded and moved back to the dark incubator. An hour after the end of stimulation, slices were fixed in 4 % PFA and stained against cFos as described in Chapter 10. Each experiment also contained 1 to 4 OHSCs which were either treated with *'High Potassium'* HEPES buffer (50 mM) for 2 min 2 times (no synaptic transmission blockers, positive control) or not stimulated in anyway (synaptic transmission blockers, negative control). Those control OHSCs were used to decide whether to keep or discard the experiment: when cFos expression was high in negative control or not detected in the positive control, the whole experiment was discarded*.

To investigate how cFos upregulation depends on firing frequency, the ChrimsonR-transduced OHSCs were stimulated 300 times at 0.1 Hz,

* ***Why discard the whole experiment?*** *The positive and negative control groups were used for two-point normalization (see Extra 14.1, Figures 14.11 and 14.12). If there is no difference between the groups, the normalization cannot be performed. Also, it could be an indicator that something went wrong during the preparation phase and thus other groups could be compromised as well.*

1 Hz, 5 Hz, 10 Hz and 50 Hz. For each OHSC the number of cFos positive neurons in pyramidal (or granular) cell layer was counted per field of view (FOV: 635 x 635 μm). Also, the median intensity of each cFos positive nucleus was measured (Chapter 10.4). As expected from previously collected data (oSTDP, Figure 11.5 and 11.6), the cFos expression after 5 Hz stimulation was low (Figures 14.7, 14.8 and 14.11; Figures A.1 and A.2), while 300 action potentials fired at 50 Hz induced cFos in all hippocampal regions. Somewhat surprisingly, stimulation at low frequency (0.1 Hz) also induced cFos, while there was almost no cFos upregulation at the intermediate frequencies. When the pairing frequency was further reduced to 0.005 Hz (300 repetitions, total stimulation time 16 h 40 min), there was no longer strong cFos expression evident. Interestingly, while there was a clear U-shaped frequency dependency for the number of neurons expressing cFos, there was no overall difference in median intensity of positive nuclei between the conditions (Figure 14.7).

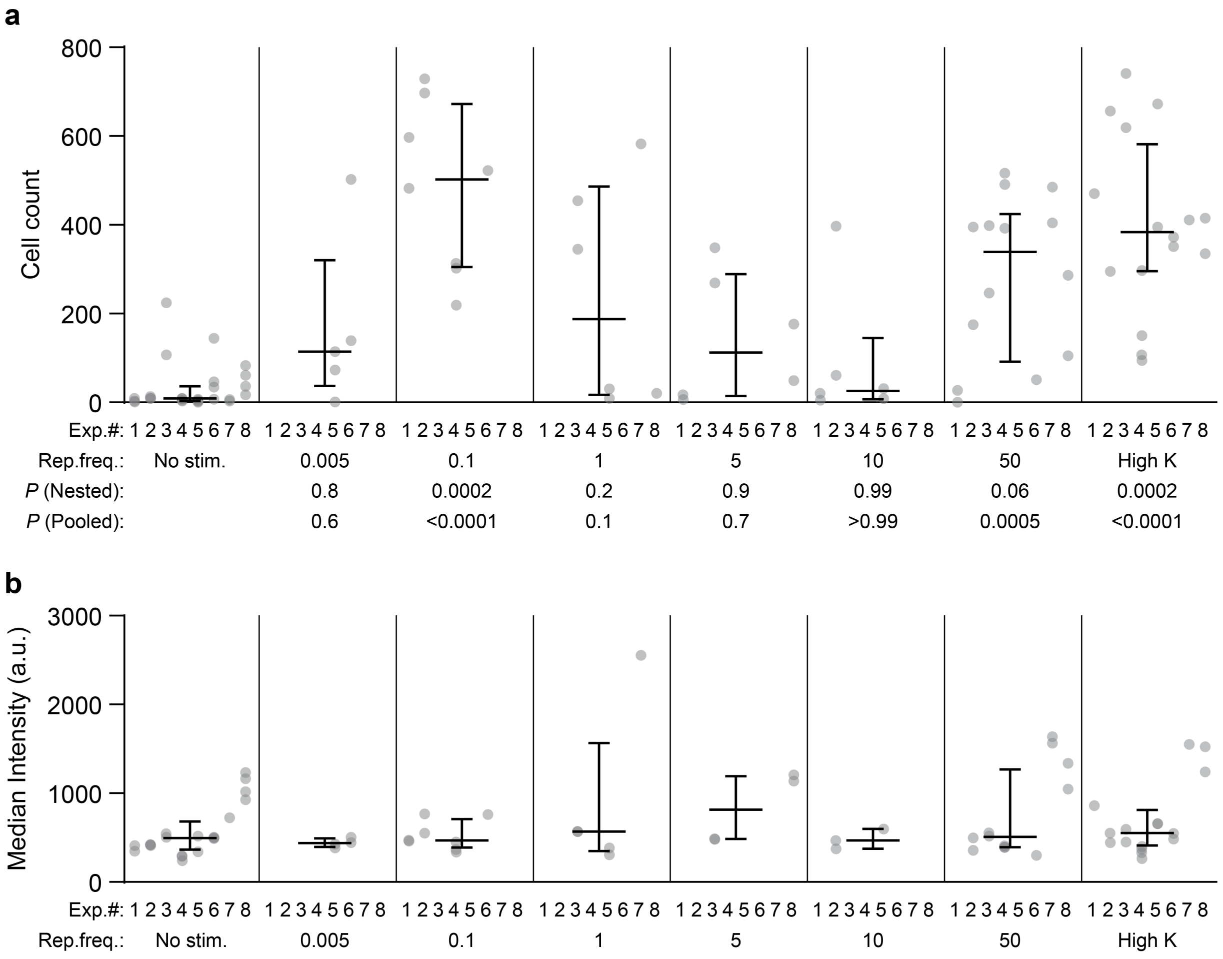

Figure 14.7: cFos expression depends on firing frequency. a, cFos positive neurons count in OHSCs per experiment. Each dot represents analysis of 3 FOVs (DG, CA3 and CA1; 635 x 635 μm). Plotted are individual data points, median and 25 % to 75 % interquartile range. *P* (*Nested*) – One-way Anova on Nested data. *P* (*Pooled*) – Kruskal-Wallis test on pooled data. **b,** Median intensity of cFos positive pyramidal neurons from **a**. Note, that only intensity of cFos positive neurons were considered. All *P* values are given vs *'No stim.'* group. *'Rep.freq.'* - frequency at which 300 of 1 ms light stimuli were repeated.

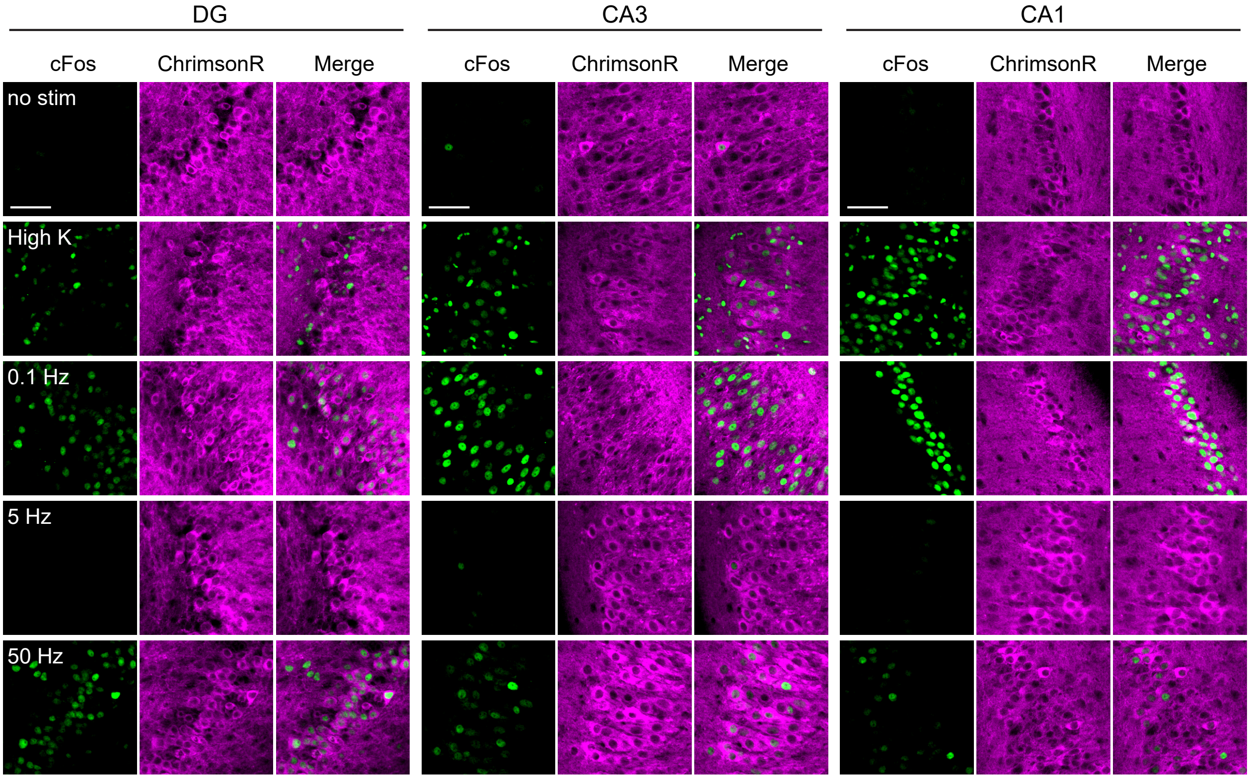
DG
CA3
CA1
cFos
ChrimsonR
Merge
no stim
High K
0.1 Hz
5 Hz
50 Hz

Figure 14.8: cFos expression in OHSCs after 300 stimulations at different frequencies. Confocal images (single plane) of cFos expression pattern 60 min after light stimulation at different frequencies in 3 regions. Scale bars – 50 µm.

14.5 cFos expression depends on the number of spikes

During oSTDP, mini bursts (3 spikes at 50 Hz) were repeated at 5 Hz, and this was sufficient to induce cFos expression in CheRiff-CA1 neurons. As shown in Chapter 14.4, 300 action potentials at 50 Hz also induce cFos expression. Since it was not obvious how many action potentials are required for cFos expression in different hippocampal regions, OHSCs were stimulated at 50 Hz 3, 10 and 30 times in addition to the previous groups (Figures 14.9, 14.10 and 14.12; Figures B.1 and B.2). Interestingly, 3 light-induced action potentials were enough to induce cFos expression in CA1 neurons but less sufficient in case of CA3 or DG, whereas 10 action potentials were not sufficient to induce cFos expression in any region. 30 and 300 repetitions at 50 Hz resulted in similar cFos expression pattern across the OHSC.

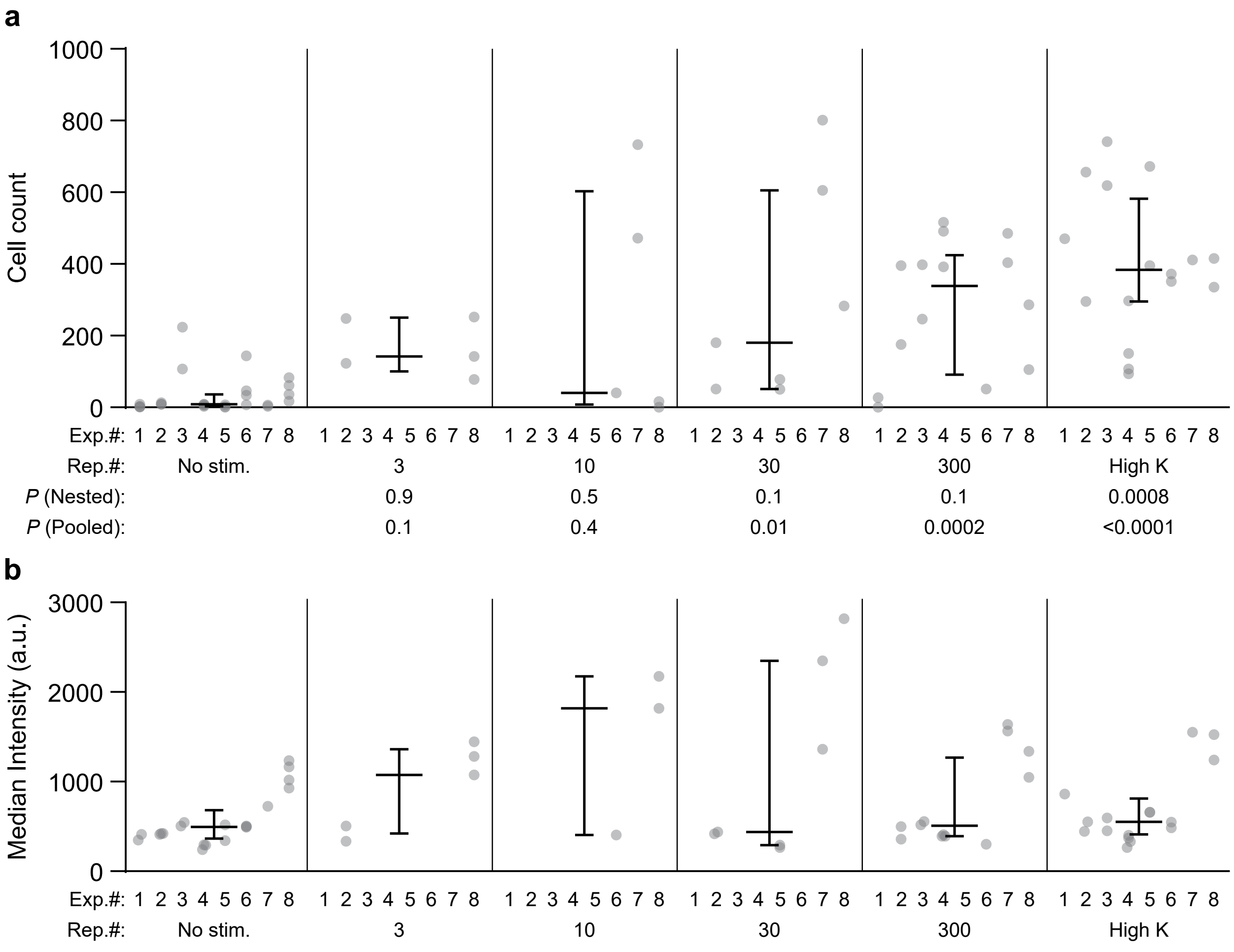

Figure 14.9: cFos expression depends on number of spike. a, cFos positive neurons count in OHSCs per experiment. Each dot represents analysis of 3 FOVs (DG, CA3 and CA1; 635 x 635 µm). Plotted are individual data points, median and 25 % to 75 % interquartile range. *P* (*Nested*) – One-way Anova on Nested data. *P* (*Pooled*) – Kruskal-Wallis test on pooled data. **b,** Median intensity of cFos positive pyramidal neurons from **a**. Note, that only intensity of cFos positive neurons were considered. All *P* values are given vs *'No stim.'* group. *'Rep.#'* - number of 1 ms light stimuli given at 50 Hz. *'300 rep.'* group is replotted from Figure 14.7 (50 Hz).

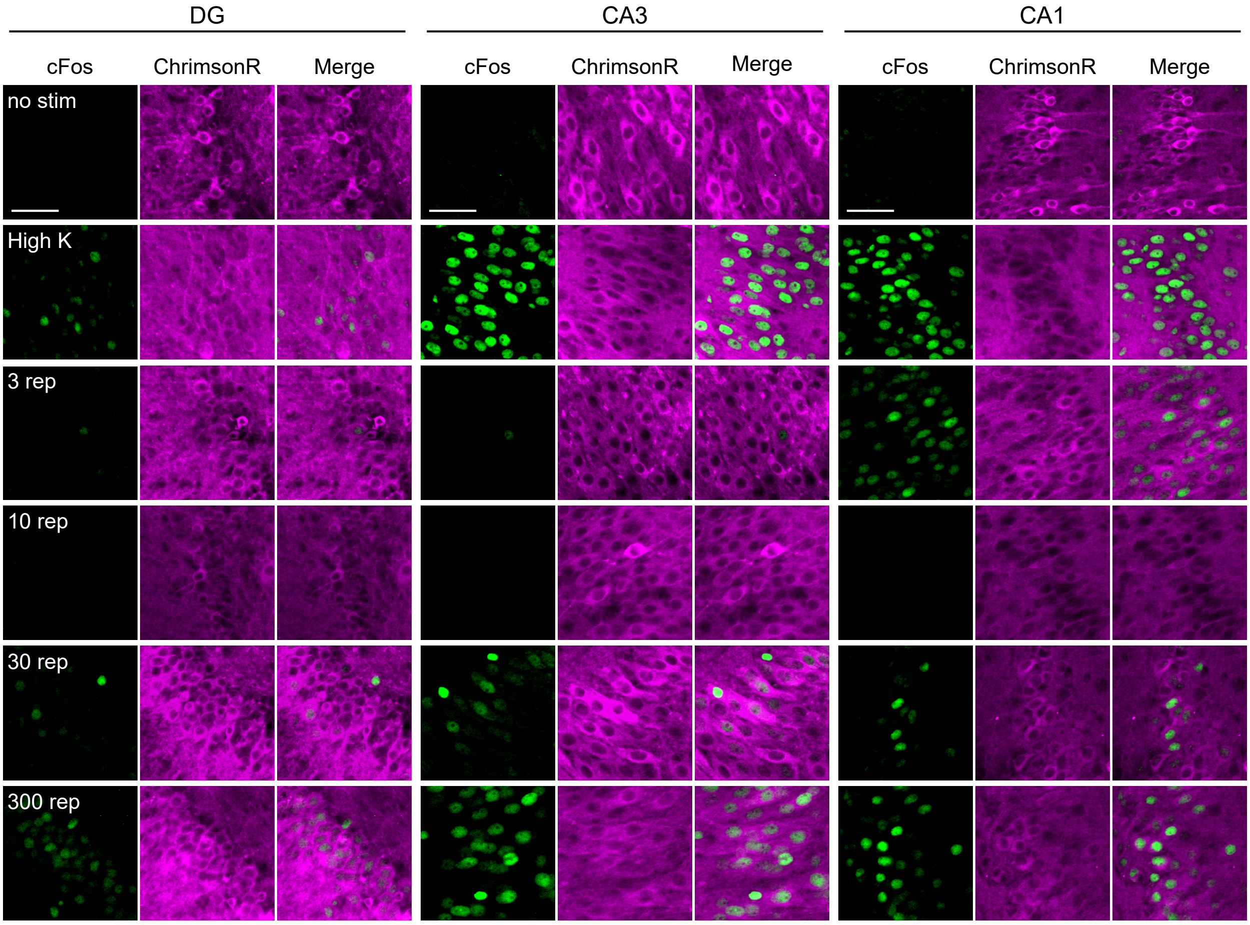
DG
CA3
CA1
cFos
ChrimsonR
Merge
no stim
High K
3 rep
10 rep
30 rep
300 rep

Figure 14.10: cFos expression in OHSCs after stimulations at 50 Hz with different number of spikes. Confocal images (single plane) of cFos expression pattern 60 min after light stimulation at 50 Hz with different number of spikes in 3 regions. Scale bars – 50 µm.

Extra 14.1: Two-point normalization

Since the data was collected over 18 months, two-point normalization was used to pool it together:

$$z_i = \frac{x_i - \min(x)}{\max(x) - \min(x)} \tag{14.1}$$

Where $x = (x_1, ..., x_i)$ – the cFos positive nucleus count in the selected group per FOV or per OHSC in the selected experiment; $\min(x)$ – the median of the *'No stimulation'* group in the selected experiment; $\max(x)$ – the median of the *'High Potassium'* group in the selected experiment; z_i – the normalized value, scaled between minimum $(\min = 0)$ and maximum $(\max = 1)$ cFos count in the selected experiment. Minimum ranged between 0 and 70 cFos positive nucleus per FOV in a selected experiment and maximum ranged between 26.5 and 237. Note, that due to spontaneous activity in the OHSCs z_i could be lower than 0, and that light stimulation could induce higher upregulation in cFos level than pharmacological manipulation (here *'High Potassium'* stimulation), and thus z_i could be higher than 1. The result of the two-point normalization is shown in Figure 14.11 and Figure 14.12.

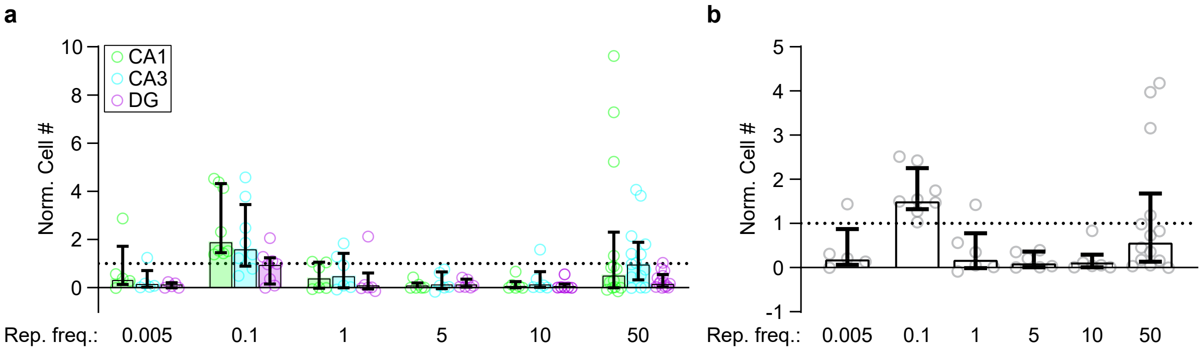

Figure 14.11: Two-point normalization of cell count data from Figure 14.7. a, Normalized cFos-positive cell counts per FOV (635 x 635 µm). **b,** Same as **a**, but for the whole OHSC. Dotted line at 1 is maximum of two-point normalization (median of *'High K'* group for each experiment), 0 – minimum of two-point normalization (median of *'No stim.'* group for each experiment). Plotted are individual data points, median and 25 % to 75 % interquartile range.

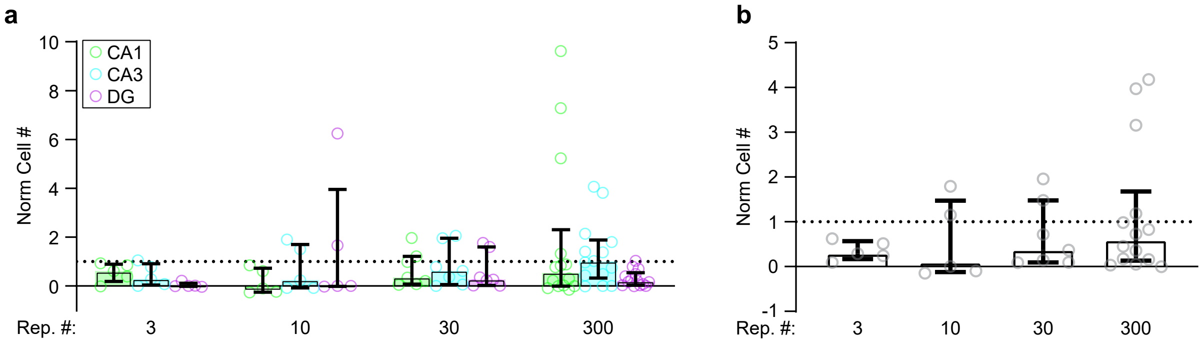

Figure 14.12: Two-point normalization of cell count data from Figure 14.9. a, Normalized cFos-positive cell counts per FOV (635 x 635 µm). **b,** Same as **a**, but for the whole OHSC. Dotted line at 1 is maximum of two-point normalization (median of *'High K'* group for each experiment), 0 – minimum of two-point normalization (median of *'No stim.'* group for each experiment). Plotted are individual data points, median and 25 % to 75 % interquartile range. *'300 rep.'* group is replotted from Figure 14.11 (50 Hz).

14.6 cFos expression in PCP4-CA2 neurons

The CA2 region of the hippocampus is rather unique compared to the other regions. It is not only significantly smaller in size, but also different in protein expression pattern [165]. CA2 neurons highly express RGS14 and PCP4 [165–167] and thus can be identified after fixation by staining against either of those proteins. Here, I used anti-PCP4 staining to investigate the cFos expression pattern in CA2 pyramidal neurons after light stimulation.

RGS14 - regulator of G protein signaling 14
PCP4 - Purkinje cell protein 4

Around 20 % of PCP4 positive neurons (PCP4-CA2) either were not transduced with the virus or were expressing it weakly (Figures 14.13 and 14.14). Therefore, care was taken during analysis to exclude the virus negative PCP4-CA2 neurons, since they were not sensitive to the light during stimulation.

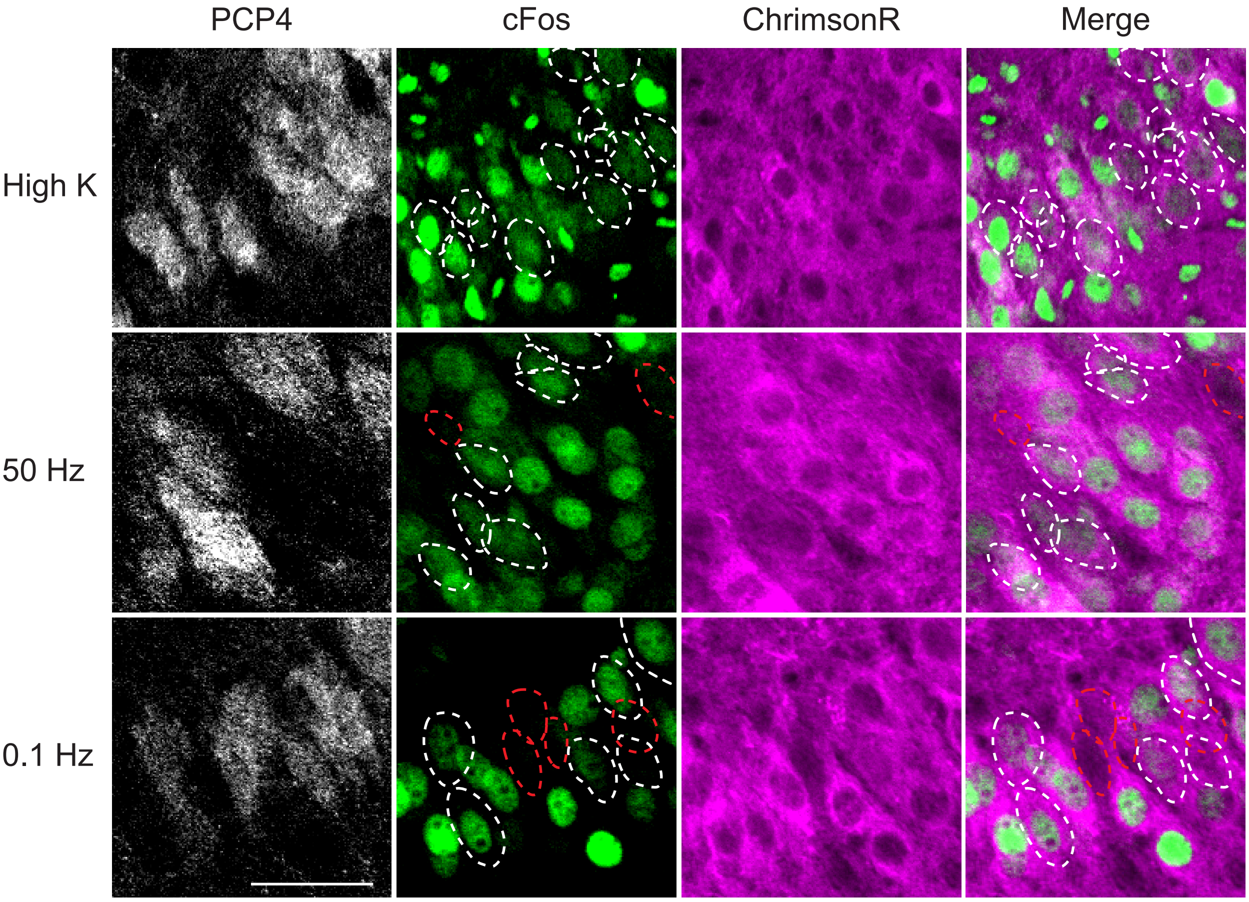

Figure 14.13: cFos expression in CA2 area after stimulation. Confocal images (single plane) of cFos expression pattern in PCP4 positive and negative neurons in CA2 area of OHSC after stimulation. Dotted outlines – PCP4 positive neurons. White dotted outline – ChrimsonR positive neurons; red dotted outline – ChrimsonR negative neurons. Scale bar – 50 µm.

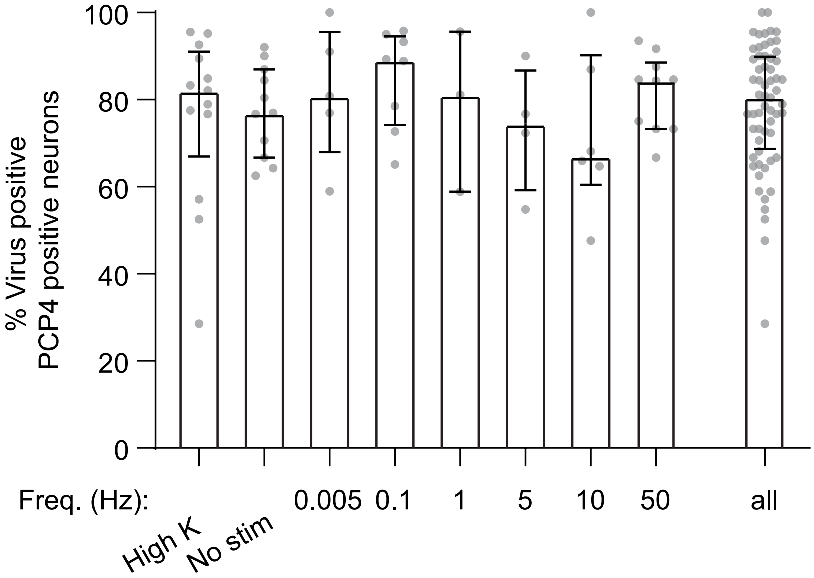

Figure 14.14: ChrimsonR expression in PCP4-CA2 neurons. Percent of PCP4 positive neurons in CA2 that express ChrimsonR. *'All'* – pooled data from all groups. Plotted are individual data points, median and 25 % to 75 % interquartile range.

I compared the cFos expression in PCP4-CA2 neurons to their closest PCP4-negative neighbors. There was a clear trend showing that PCP4-CA2 neurons in general had less cFos expression that their neighbors (Figure 14.15 a). The most significant difference was observed in case of *'High Potassium'* stimulation and light stimulation at 50 Hz. Light stimulation at 0.1 Hz and 5 Hz showed a similar tendency, however the difference was not statistically significant.

Interestingly, there was no difference in the median intensity of cFos expression level neither for *'High Potassium'* nor for the 50 Hz group, however the median intensity of cFos expression in PCP4-CA2 neurons after 300 light stimuli at 0.1 Hz was significantly lower than in their PCP4-negative neighbors (Figure 14.15 b). This difference between 0.1 Hz and 50 Hz groups yet again suggest that there are possibly two different mechanisms involved in cFos induction.

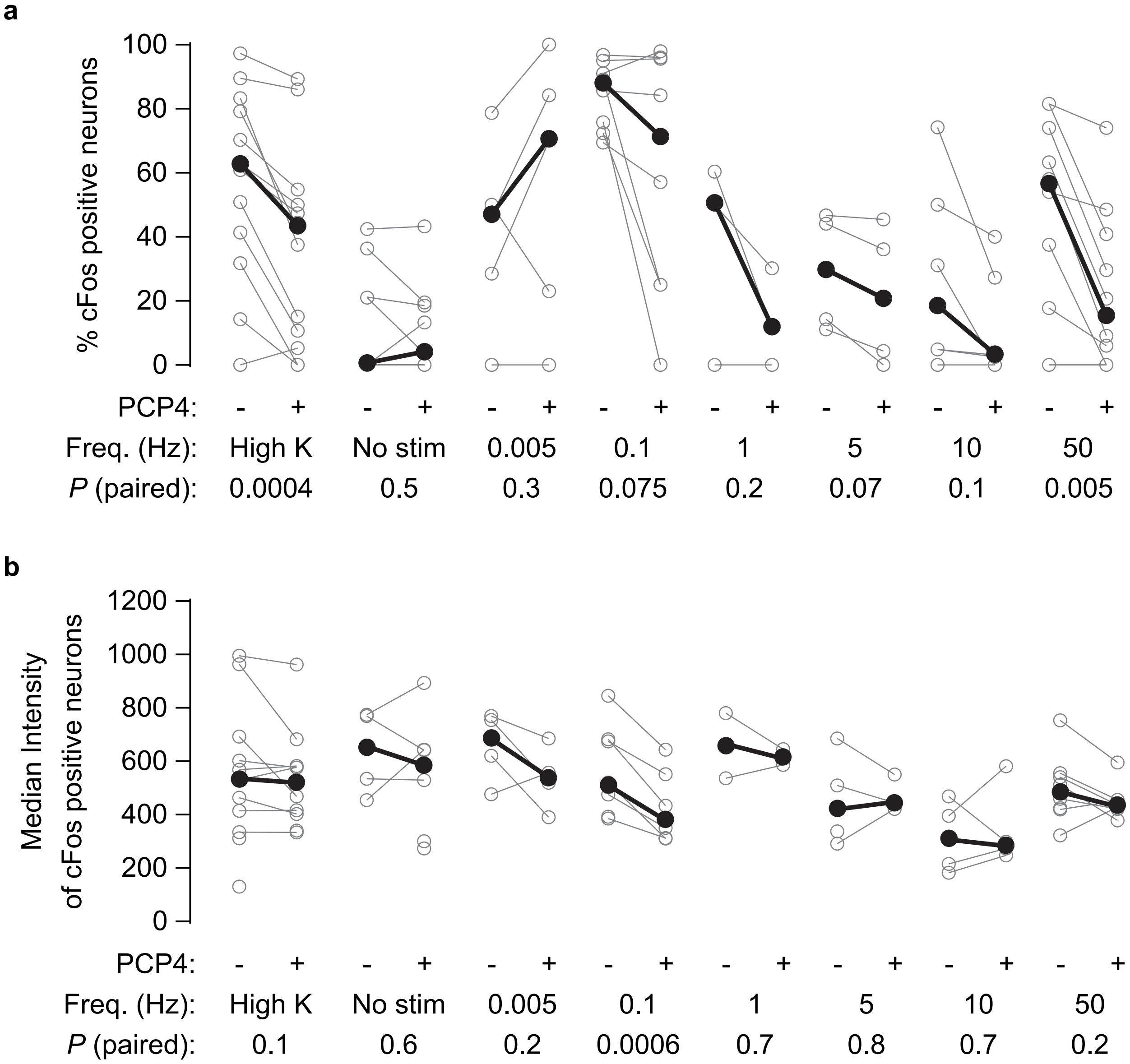

Figure 14.15: cFos expression in PCP4 positive and PCP4 negative ChrimsonR-CA2 neurons. a, Percent of ChrimsonR positive neurons in CA2 area that express cFos. Number of light stimuli – 300 per group. **b,** Median intensity of cFos positive pyramidal neurons from **a**. Note, that all experiments with no cFos expression were removed. *P* (*paired*) – Paired t-test. Plotted are individual data points.

15 DISCUSSION AND PERSPECTIVES

In Part IV I have shown that (1) the cFos expression in the hippocampus depends on a neuronal firing frequency, (2) the number of action potentials and also (3) on the hippocampal region.

Although, the cFos expression dependence on neuronal activity was previously shown for DRG [90, 95, 98] and cortical neurons [97], the clear U shape of firing frequency dependence in cFos expression in hippocampal neurons is rather intriguing and should be investigated further. It is also important to understand the mechanism behind the cFos expression after neuronal firing at 0.1 Hz, since this frequency is usually used in various plasticity protocols as a baseline stimulation [168–170]. As was shown on Figure 5.1, the cFos expression depends on the CREB phosphorylation through various signaling pathways. Fast and slow pathways could potentially regulate cFos expression after stimulation at 0.1 Hz and 50 Hz. Preliminary data has however shown, that inhibiting slow MAPK pathway leads to no cFos expression in neurons after light stimulation at both 0.1 Hz and 50 Hz (Figures 15.1, C.1, C.2 and C.3). To further understand if the cFos expression mechanism after stimulation at 0.1 Hz and 50 Hz is different, more finely tuned pharmacological experiments are required.

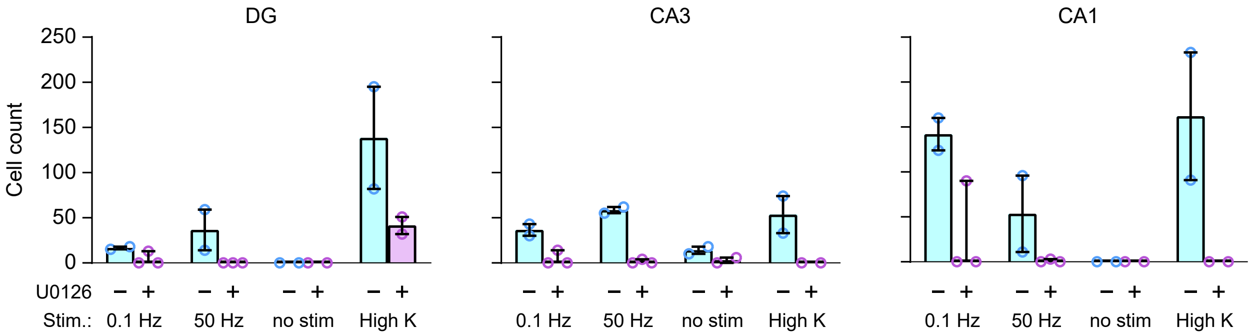

Figure 15.1: cFos expression depends on the MAPK signalling pathway (Preliminary data). cFos positive neurons count in OHSCs treated with U0126 (MAPK signaling pathway blocker, Table 9.1) and untreated OHSCs. Each dot represents analysis of a FOV (635 x 635 µm). *'Stim.'* - frequency at which 300 of 1 ms light stimuli were repeated. Plotted are individual data points, median and 25 % to 75 % interquartile range.

It is reasonable to expect that rapid elevation in intracellular [Ca^{2+}] level should play more significant role in cFos expression after high frequency stimulation, where as CaMKII may be involved in the signal integration at lower frequencies [90, 98, 171]. As was shown for DRG neurons [95, 98], the single action potential does not elevate the intracellular calcium level significantly, however the stimulation at 0.1 Hz leads to a significant cFos upregulation, indeed suggesting that in this case change in intracellular [Ca^{2+}] level does not play a major role.

Another interesting finding in regard to the [Ca^{2+}]-dependent signaling pathway is shown in Chapter 14.6. CA2 pyramidal neurons have more complex molecular composition than the pyramidal neurons in other hippocampal regions [2, 165, 172], particularly STEP, PCP4 and RGS14 are known to be enriched in this area. It is also known that RGS14 plays a critical role in inhibiting synaptic plasticity in CA2 through inhibiting of postsynaptic calcium signaling and participates in MAPK signaling pathway [173, 174]. A dramatic reduction of cFos expression after 50 Hz stimulation in PCP4-CA2 compared to their PCP4-negative neighbors and only a tendency in case of 0.1 Hz stimulation supports the hypothesis that calcium plays an important role for cFos expression after high frequency stimulation but to a lesser degree after low frequency stimulation.

STEP - striatum-enriched protein-tyrosine phosphatase

According to the literature, the majority of PCP4-CA2 neurons are also expressing RGS14 [166, 167, 172].

The data shown in Chapter 14.5 suggests that [Ca^{2+}]-dependent signaling pathway in CA1 may be more sensitive than in the CA3 neurons, since 3 action potentials fired at high frequency led to cFos upregulation only in CA1 region. However still the absence of cFos expression after 10 action potentials fired at 50 Hz point out the complexity of the primary and secondary messengers involved in the cFos signaling pathway in hippocampal pyramidal neurons. To further understand how action potential firing is related to cFos expression one could use FRET/FLIM sensors [175] to monitor the CaMKII activity [171] or CREB phosphorylation [176] before, during and after the stimulation.

FRET - Förster resonance energy transfer

FLIM - fluorescence lifetime imaging microscopy

Overall, it is important to understand and characterize the activity-dependent expression of IEG cFos in hippocampus and in the brain in general. Many studies in neuroscience use the cFos expression pattern to explain the behavior results or on cFos promoter to express optogenetic tools in activity-dependent manner [177–182]. The lack of knowledge on the firing frequency dependence of cFos expression can and will lead to the misinterpretation of the behavior tasks results and could potentially slow the neuroscience field in general.

CONCLUSION

In present work I induced STDP using a two-color all-optical protocol and read-out the effects on synaptic strength three days later. I showed that it is possible to independently control the firing of presynaptic CA3 and postsynaptic CA1 neurons in hippocampal slice cultures using the channelrhodopsins ChrimsonR and CheRiff. However, it is important to point out, that this independent control is only achievable when the light pulses are short (1 ms to 2 ms), when low power (~1 mW/mm^2) 400 nm light is used to activate CheRiff-CA1 and moderate power (~8 mW/mm^2) light with the wavelength above 550 nm is used to activate ChrimsonR-CA3 neurons. I demonstrated that light-evoked spike-burst pairing induces STDP which follows classical rules when synaptic strength assessed shortly after: causal pre before post pairing causes potentiation and anti-causal post before pre pairing causes depression. However surprisingly, 3 days after oSTDP induction only potentiation was apparent when the timing interval was 10 ms for both causal and anti-causal pairing and the repetition frequency was 5 Hz. I showed that this late-potentiation is spike-timing sensitive, NMDAR and pairing frequency dependent and relays on the ongoing activity in OHSC in the days following the all-optical plasticity induction. I conclude that the late effects of STDP are potentiation when the pre and postsynaptic activity is closely spaced in time in a contrast to early effects of STDP, where both tLTP and tLTD were present.

There is still a very important question left to answer: can it be that tLTD is a recording artefact and that is why only apparent during patch-clamp recordings? I tried to address this question with preventing the wash-out during the on-cell plasticity induction, however, the question is still persisting and further pharmacological experiments are required. Also, it is reasonable to assume that ongoing replay of activity strengthens the potentiation and is required for the conversion of LTD into LTP over time. This hypothesis, however, also needs further experiments for verification.

Structural synaptic plasticity in days following all-optical STDP induction was briefly discussed in this study. Further investigation of morphological changes in dendritic spines and the general rewiring of the circuit after oSTDP could help to understand memory consolidation mechanisms and also provide valuable information of STDP-induced spine dynamics. This information can be potentially used to track the already mentioned hypothetical conversion of LTD into LTP.

In the second part of this work I introduced the results of basic activity-dependent (or action potential-dependent) expression of IEG cFos in OHSCs. I showed that cFos expression has a pronounced U-shaped dependence on firing frequency and that the number of action potentials fired by the neuron required for the cFos upregulation depends on the hippocampal region. Special attention was given to the activity-dependent cFos expression pattern in CA2 neurons. I have shown that PCP4-CA2 neurons differ from their PCP4-negative close neighbors. A preliminary attempt was made to identify the cFos signaling pathway, however further detailed pharmacological experiments are required to draw conclusions.

In general, taken together the findings presented in this work should make us, first, to think more about the long-term consequences of the STDP and other plasticity mechanisms and potentially adjust the memory consolidation theory for behavior-relevant timescale. And second, we should be more careful with interpreting results or using the neuroscientific-tools based on IEGs expression in the various types of neurons in the brain. Without the careful characterization of activity-dependent expression, as was demonstrated here for cFos, the wrong conclusions could be drawn. In the long run, it is also essential to transfer the findings *in vivo* and further investigate their mechanisms and relevance for experience-driven plasticity in the living animals.

Part V

APPENDIX

APPENDIX A:

cFos expression depends on the firing frequency: data per hippocampal region

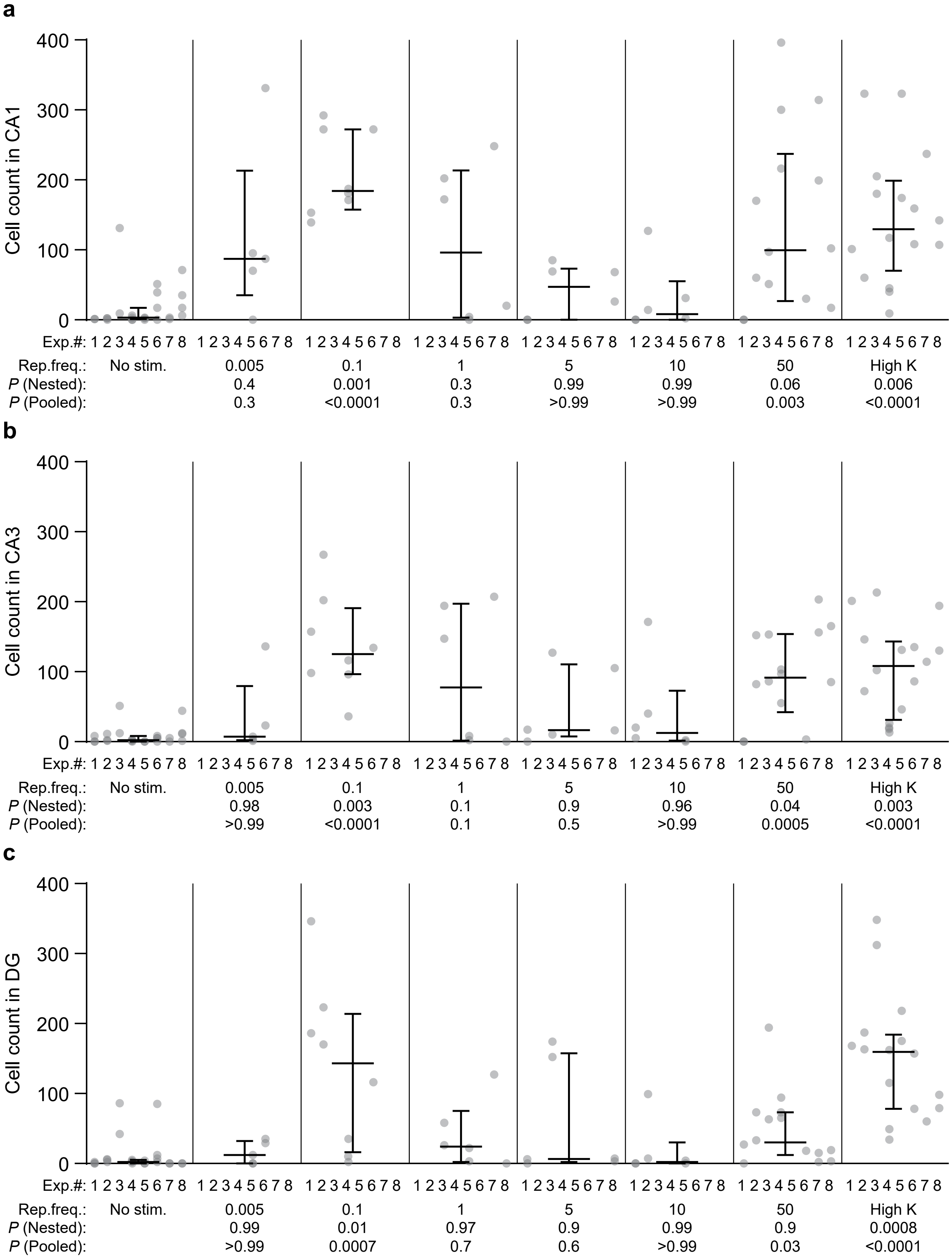

Figure A.1: Additional information to Figure 14.7 a. cFos positive neurons count in OHSCs per experiment. Each dot represents analysis of a FOV (635 x 635 μm). Plotted are individual data points, median and 25 % to 75 % interquartile range. *P* (*Nested*) – One-way Anova on Nested data. *P* (*Pooled*) – Kruskal-Wallis test on pooled data. All *P* values are given vs *'No stim.'* group. **a,** CA1. **b,** CA3. **c,** DG. *'Rep.freq.'* - frequency at which 300 of 1 ms light stimuli were repeated.

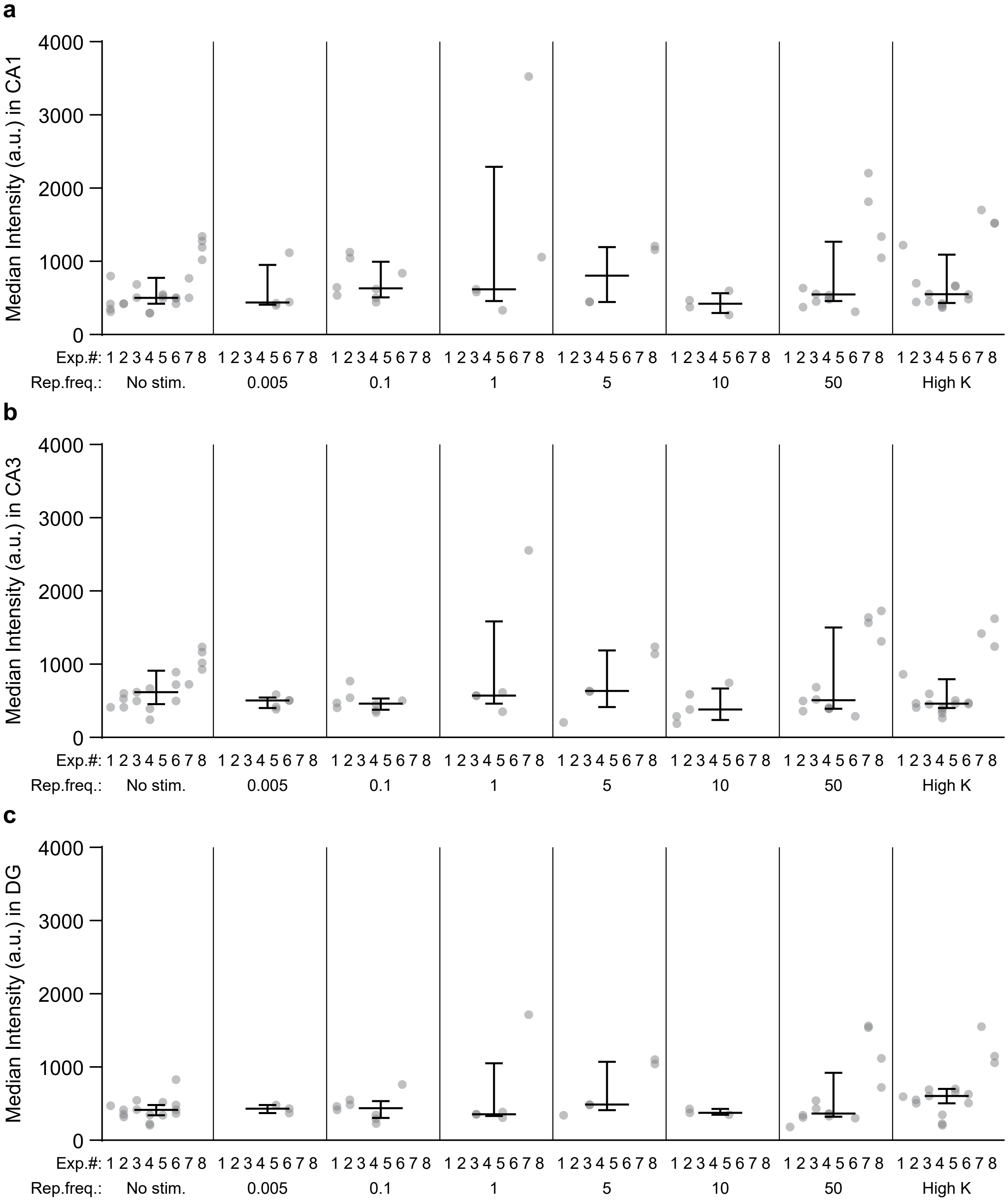

Figure A.2: Additional information to Figure 14.7 b. Median intensity of cFos positive pyramidal neurons. Note, that only intensity of cFos positive neurons were considered. Each dot represents analysis of a FOV (635 x 635 µm). Plotted are individual data points, median and 25 % to 75 % interquartile range. **a,** CA1. **b,** CA3. **c,** DG.

APPENDIX B:

cFos expression depends on the number of spikes: data per hippocampal region

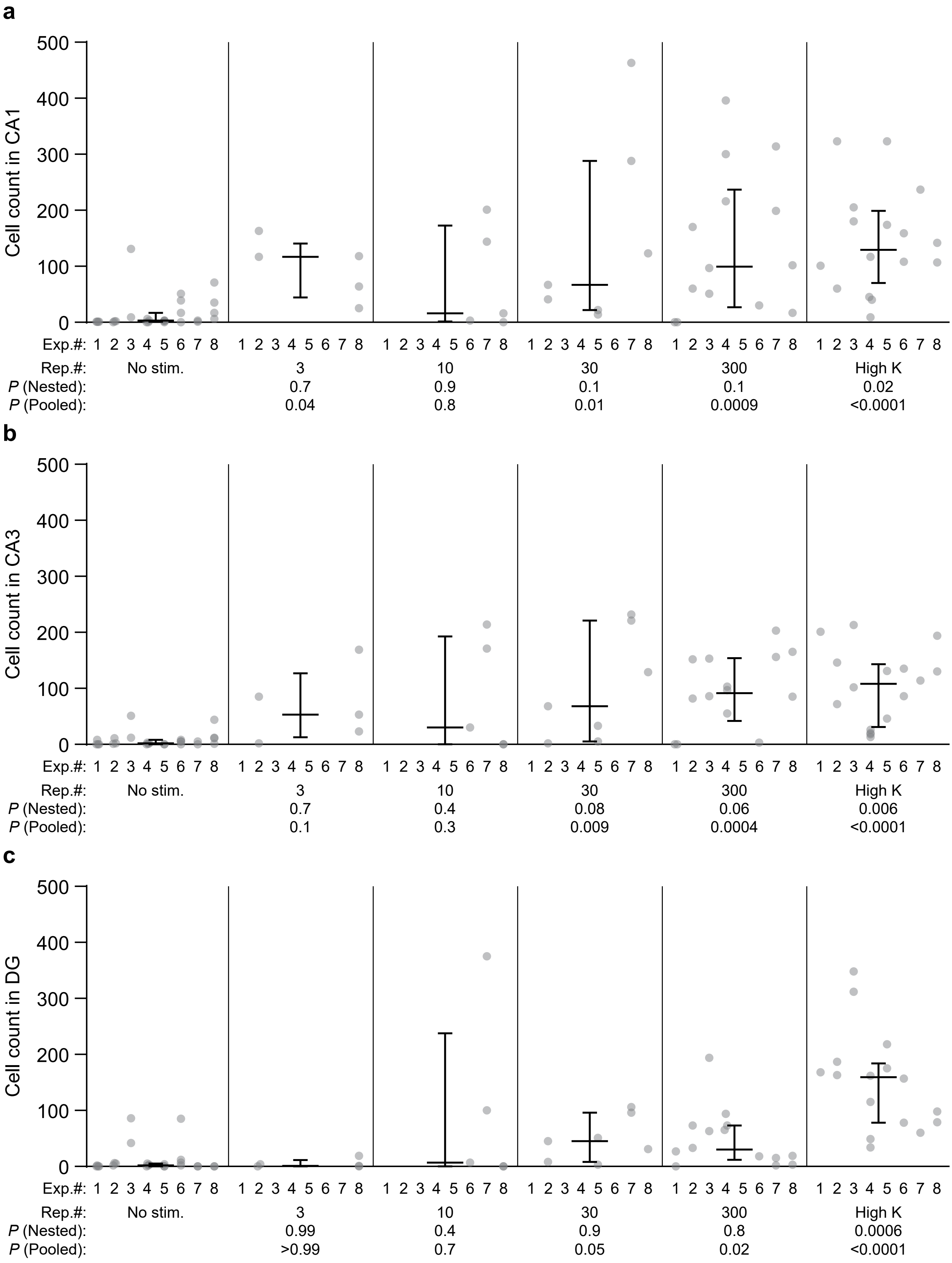

Figure B.1: Additional information to Figure 14.9 a. cFos positive neurons count in OHSC per experiment. Each dot represents analysis of a FOV (635 x 635 µm). Plotted are individual data points, median and 25 % to 75 % interquartile range. *P* (*Nested*) – One-way Anova on Nested data. *P* (*Pooled*) – Kruskal-Wallis test on pooled data. All *P* values are given vs *'No stim.'* group. **a,** CA1. **b,** CA3. **c,** DG. *'Rep.#'* - number of 1 ms light stimuli given at 50 Hz. *'300 rep.'* group is replotted from the Figure A.1

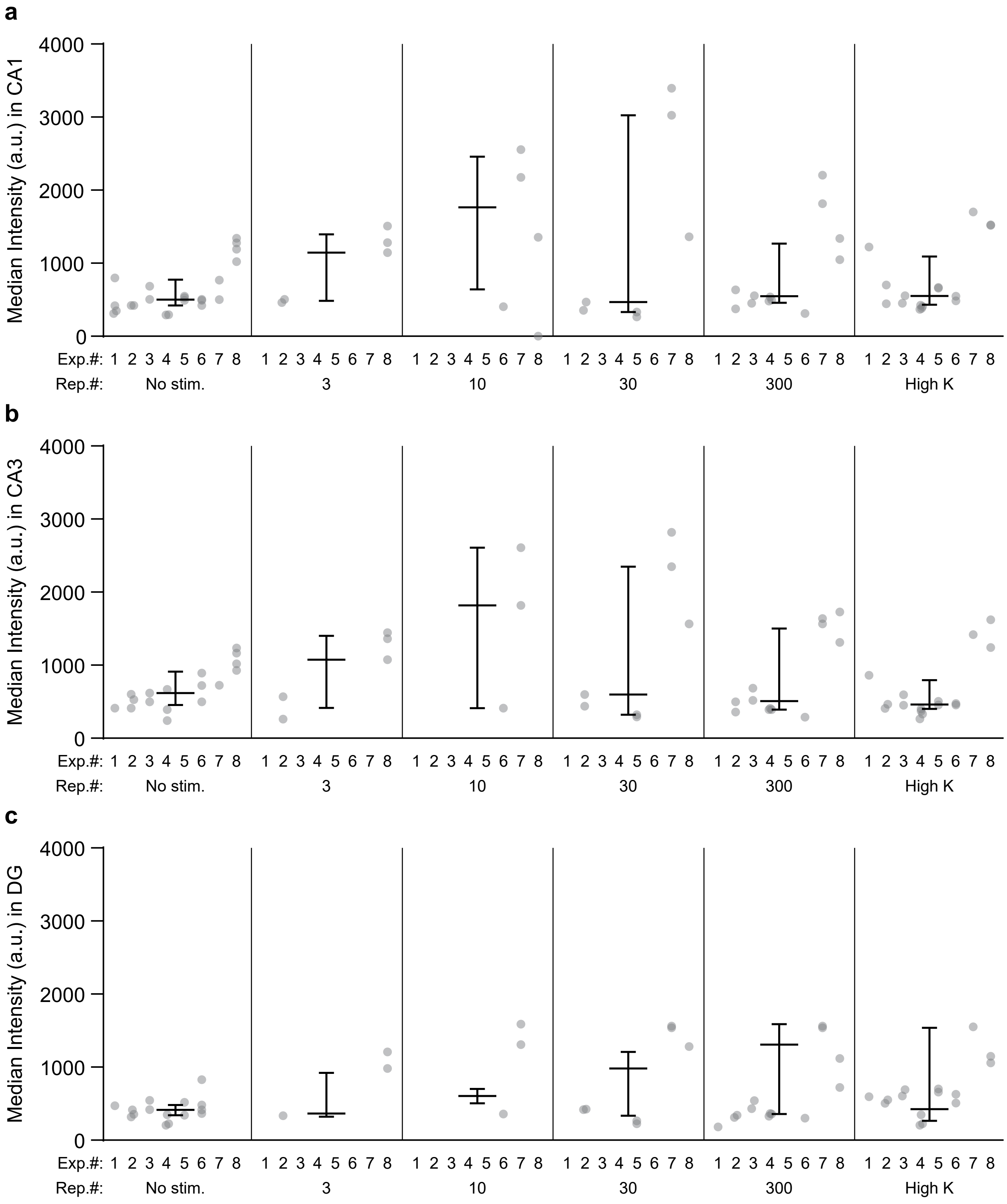

Figure B.2: Additional information to Figure 14.9 b. Median intensity of cFos positive pyramidal neurons. Note, that only intensity of cFos positive neurons were considered. Each dot represents analysis of a FOV (635 x 635 µm). Plotted are individual data points, median and 25 % to 75 % interquartile range. **a,** CA1. **b,** CA3. **c,** DG. *'Rep.#'* - number of 1 ms light stimuli given at 50 Hz. *'300 rep.'* group is replotted from the Figure A.2

APPENDIX C:
cFos expression depends on the MAPK signaling pathway

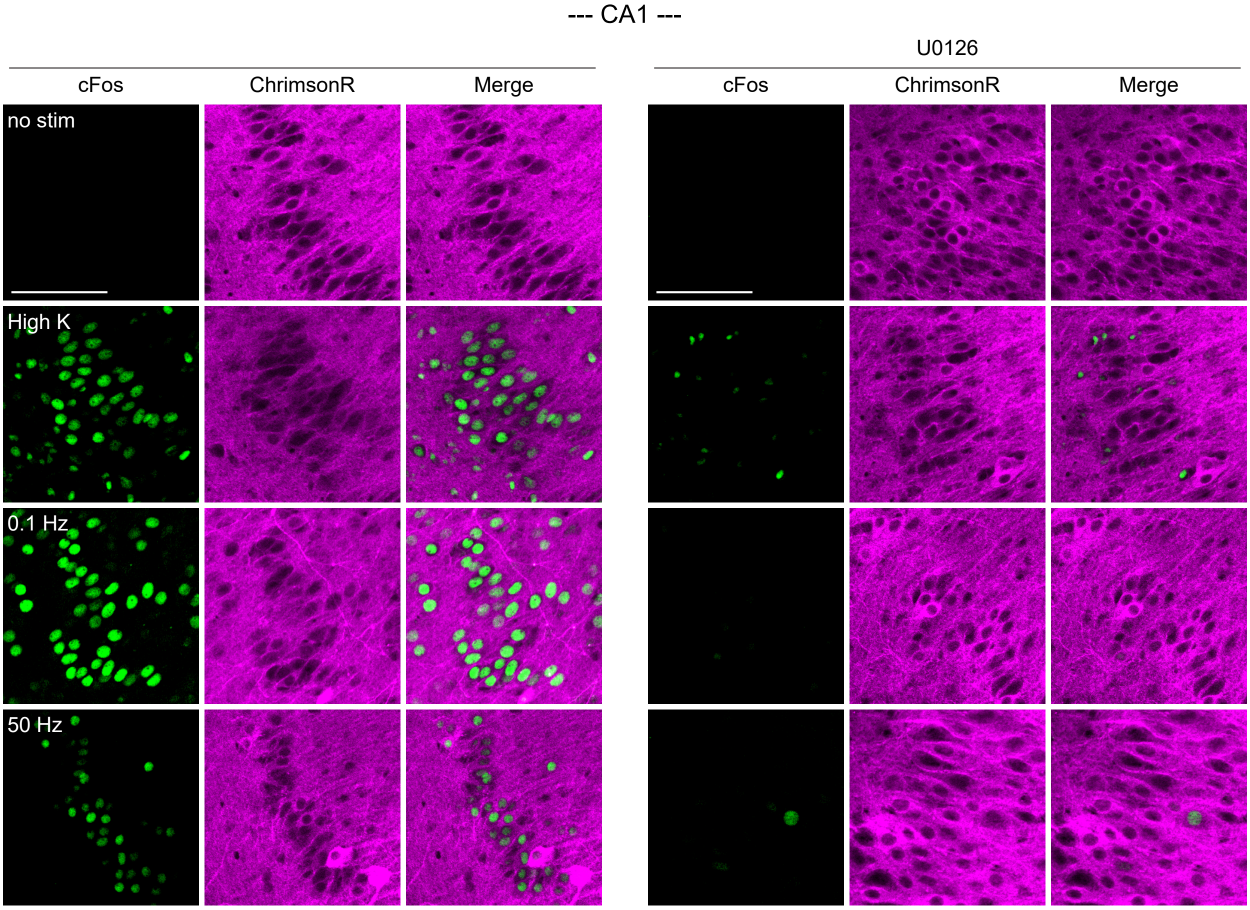
--- CA1 ---
U0126
cFos
ChrimsonR
Merge
cFos
ChrimsonR
Merge
no stim
High K
0.1 Hz
50 Hz

Figure C.1: Additional information to Figure 15.1 CA1. Confocal images (single plane) of OHSCs treated overnight with U0126 (MAPK signaling pathway blocker, Table 9.1). Shown is FOV in CA1. Scale bars - 100 µm.

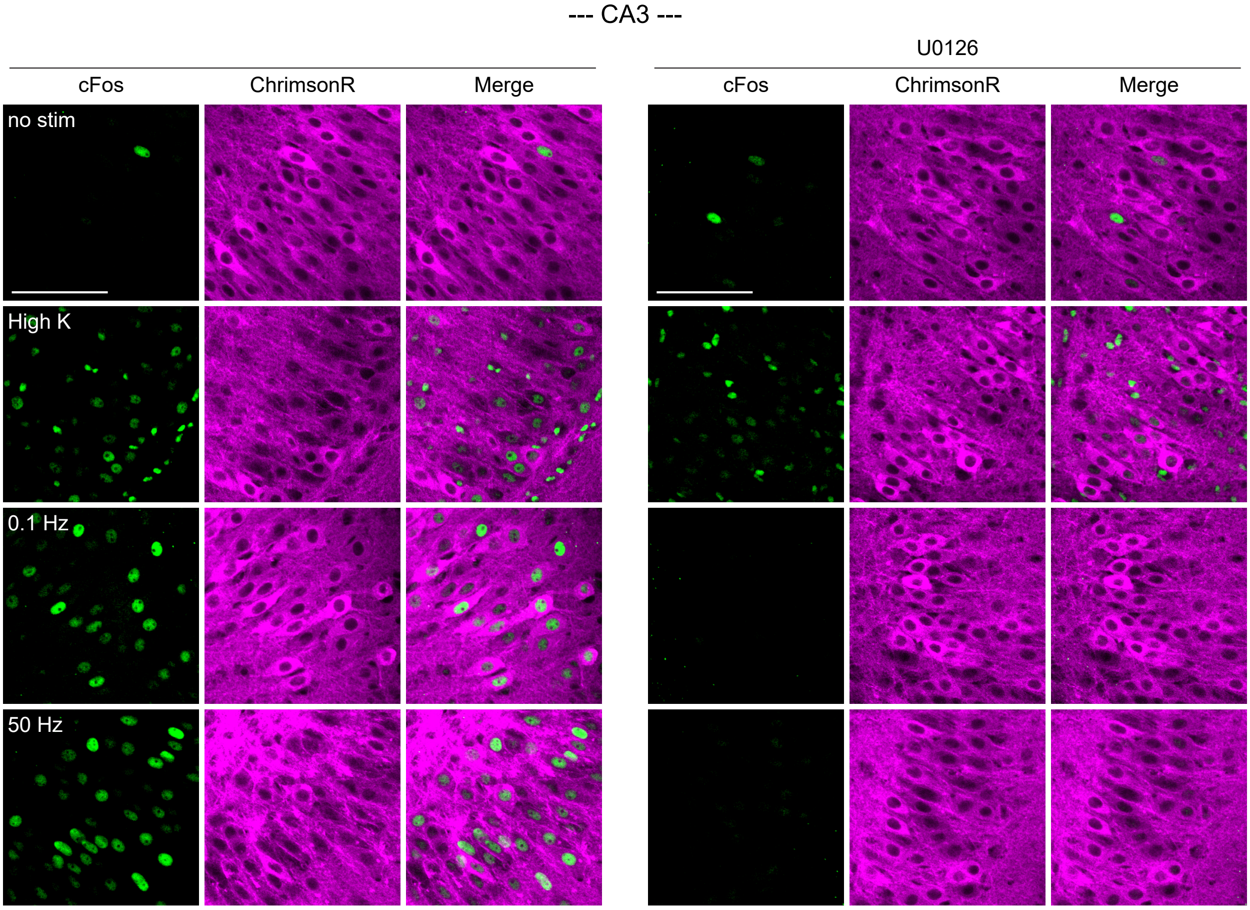
--- CA3 ---
U0126
cFos
ChrimsonR
Merge
cFos
ChrimsonR
Merge
no stim
High K
0.1 Hz
50 Hz

Figure C.2: Additional information to Figure 15.1 CA3. Confocal images (single plane) of OHSCs treated overnight with U0126 (MAPK signaling pathway blocker, Table 9.1). Shown is FOV in CA3. Scale bars - 100 µm.

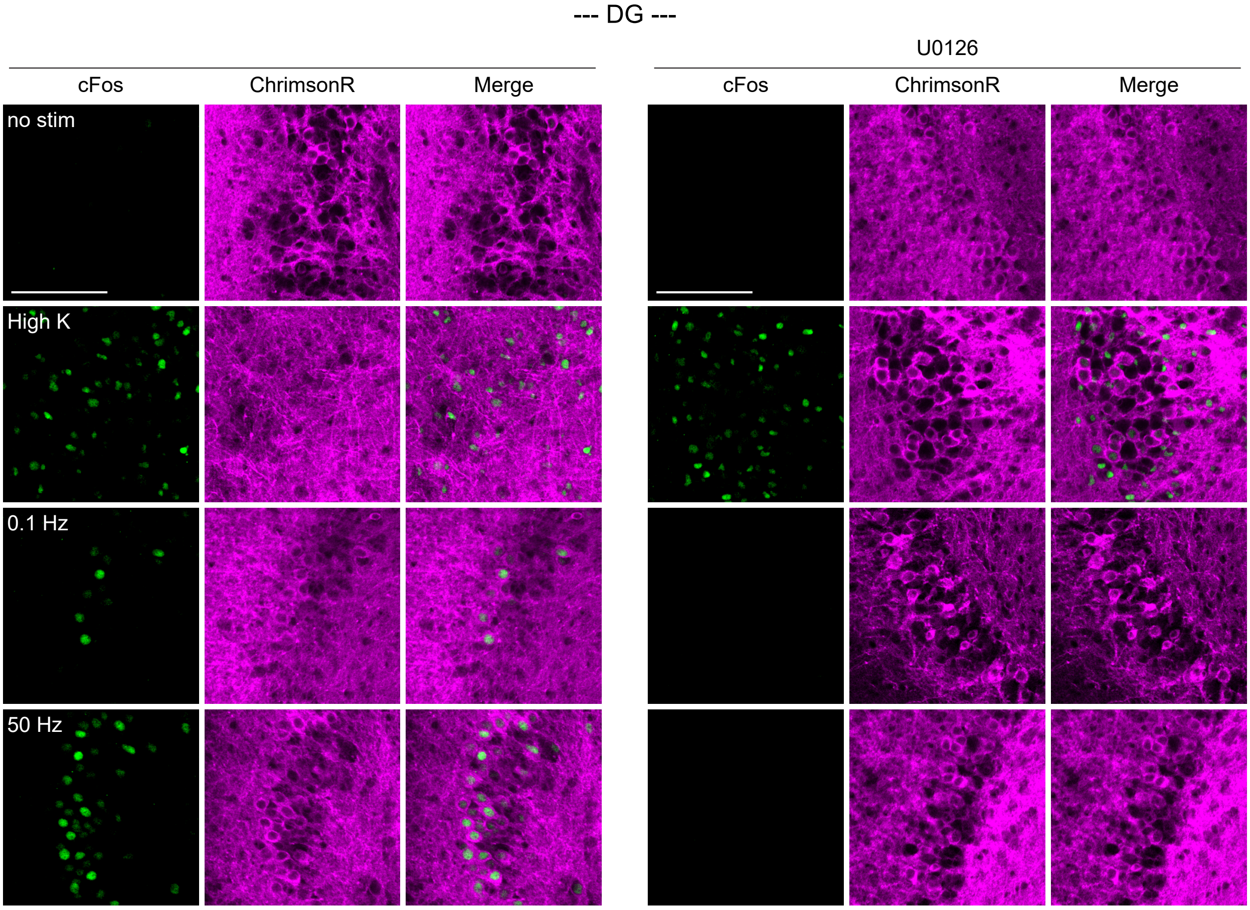
--- DG ---
U0126
cFos
ChrimsonR
Merge
cFos
ChrimsonR
Merge
no stim
High K
0.1 Hz
50 Hz

Figure C.3: Additional information to Figure 15.1 DG. Confocal images (single plane) of OHSCs treated overnight with U0126 (MAPK signaling pathway blocker, Table 9.1). Shown is FOV in DG. Scale bars - 100 µm.

LIST OF FIGURES

1.1 Trisynaptic circuit. 4
2.1 NMDAR-dependent LTP and LTD at hippocampal CA1 synapses. 6
2.2 Model of AMPAR trafficking during LTP and LTD. 7
3.1 Diversity of temporal windows for STDP induction. 10
4.1 Novel channelrhodopsin spectral classes discovered through algal transcriptome sequencing. 11
4.2 Phylogenetic analysis of known and putative channelrhodopsins. 12
5.1 A schematic representation of activity-dependent activation of cFos signaling pathway. 13
7.1 DNA expression in organotypic hippocampal slice culture by viral vector transduction. 20
8.1 Electrophysiology setup. 24
8.2 Field of view of 40x objective during patch-clamp experiments. 24
8.3 Patch-clamp measurement configurations. 24
8.4 Electrical equivalent circuits of patch-clamp measurement configurations. 25
8.5 Patch-clamp process as an ERC-circuit. 25
8.6 How to calculate cell parameters from a test pulse. 26
9.1 Light induced spiking threshold of ChrimsonR-CA3 neurons. 30
9.2 Causal and anti-causal pairing. 31
9.3 In-incubator stimulation tower. 32
9.4 Typical set of recorded EPSCs in a given OHSC. 33
9.5 Multipeak EPSC in a responce to the presynaptic light stimulation. 34
9.6 Peak and slope detection example. 34
9.7 Currents and potentials in voltage- and current-clamp mode. 35
11.1 ChrimsonR and CheRiff expression in OHSC. 45
11.2 Light induced spiking of ChrimsonR and CheRiff expressing neurons. 45
11.3 CheRiff and ChrimsonR functional characterization. 46
11.4 Light vs electrically induced action potentials in CheRiff-CA1 neuron. 47
11.5 cFos expression pattern after causal pairing vs number of ChrimsonR-CA3 neurons. 48
11.6 CA3 neurons express cFos after burst firing. 49
12.1 Optogenetic induction of STDP (oSTDP) while patched on the postsynaptic neuron. 52
12.2 Initial EPSC slope size does not influence plasticity induction. 53
12.3 Virus expression level does not influence the in-incubator oSTDP induction outcome. 54
12.4 Only potentiation is evident 3 days after no-patch oSTDP. 55
12.5 Late LTP is NMDA and frequency dependent. 56
12.6 Only potentiation is evident 3 days after no-patch oSTDP. 57
12.7 No input strength changes 3 hours after no-patch oSTDP. 58
12.8 Calmodulin washout role the in early tLTD induction. 58
12.9 Spontaneous activity in OHSC is important for plasticity consolidation. 60
12.10 Comparison of passive and active cell parameters of CheRiff-CA1 and neighboring NT-CA1 neurons from in-incubator oSTDP experiments. 61
12.11 Confocal vs STED resolution power. 62
12.12 Dendritic spine classification according to their morphology. 62
12.13 Spine density was not changed 3 days after oSTDP induction. 63
12.14 Light-induced firing in postsynaptic neurons promotes filopodia grows. 63
14.1 Fos induction timeline in OHSC. 73
14.2 Homogeneous expression of ChrimsonR in OHSC. 74

14.3 ChrimsonR-induced cFos expression. 74
14.4 Light-induced firing threshold of ChrimsonR neurons. 75
14.5 Pattern following of ChrimsonR neurons. 75
14.6 Cell parameters of ChrimsonR expressing neurons from the Figure 14.4. 76
14.7 cFos expression depends on firing frequency. 77
14.8 cFos expression in OHSCs after 300 stimulations at different frequencies. 78
14.9 cFos expression depends on number of spike. 79
14.10 cFos expression in OHSCs after stimulations at 50 Hz with different number of spikes. 80
14.11 Two-point normalization of cell count data from Figure 14.7. 81
14.12 Two-point normalization of cell count data from Figure 14.9. 81
14.13 cFos expression in CA2 area after stimulation. 82
14.14 ChrimsonR expression in PCP4-CA2 neurons. 83
14.15 cFos expression in PCP4 positive and PCP4 negative ChrimsonR-CA2 neurons. 84
15.1 cFos expression depends on the MAPK signalling pathway (Preliminary data). 85
A.1 Additional information to Figure 14.7 a 92
A.2 Additional information to Figure 14.7 b 93
B.1 Additional information to Figure 14.9 a 95
B.2 Additional information to Figure 14.9 b 96
C.1 Additional information to Figure 15.1 CA1. 98
C.2 Additional information to Figure 15.1 CA3. 99
C.3 Additional information to Figure 15.1 DG. 100

LIST OF TABLES

7.1 List of viral vectors 22
7.2 List of plasmids 22
9.1 List of drugs for pharmacological manipulation 29
9.2 oSTDP pairing parameters 30
9.3 In-ncubator tower LEDs parameters 32
10.1 List of antibodies 37
10.2 Confocal excitation/emission settings 38

ACRONYMS

A

AAV - Adeno-associated viruse
ACSF - Artificial cerebrospinal fluid
AMPAR - α-amino-3-hydroxy-5-methyl-4-isoxazolepropionic acid receptor
AP - Action potential
ATP - Adenosine triphosphate

C

CA1 - *Cornu Ammonis* region 1
CA2 - *Cornu Ammonis* region 2
CA3 - *Cornu Ammonis* region 3
CaM - Calmodulin
CaMK - Calcium/calmodulin-dependent kinase
Cm - Membrane capacitance
CPPene - Midafotel
CREB - Cyclic adenosine monophosphate response element-binding protein
CV - The coefficient of variation

D

DG - Dentate gyrus
DIV - Day *in vitro*

E

EDTA - Ethylenediaminetetraacetic acid
eGFP - Enhanced green fluorescent protein
EGTA - Ethylene glycol-bis(β-aminoethyl ether)-N,N,N′,N′-tetraacetic acid
EPSC - Excitatory postsynaptic current
EPSP - Excitatory postsynaptic potential

F

fEPSP - Field excitatory postsynaptic potential
FOV - Field of view

G

GABA - Gamma aminobutyric acid
GFP - Green fluorescent protein

H

HEPES - 4-(2-hydroxyethyl)-1-piperazineethanesulfonic acid
HFS - High frequency stimulation

I

IEG - Immediate Early Gene
IPSC - Inhibitory postsynaptic current
IPSP - Inhibitory postsynaptic potential

L

LFS - Low frequency stimulation
LJP - Liquid junction potential
LTD - Long-term depression
LTP - Long-term potentiation

M

MAPK - Mitogen-activated protein kinase

N

NBQX - 2,3-dihydroxy-6-nitro-7-sulfamoyl-benzo[f]quinoxaline
NMDAR - N-methyl-D-aspartate receptor
NT - Non transfected pyramidal neuron

O

OHSC - Organotypic hippocampal slice culture
oSTDP - Optogenetically induced spike timing dependent plasticity

P

PBS - Phosphate buffered solution
PCP4 - Purkinje cell protein 4
PFA - Paraformaldehyde

R

RGS14 - Regulator of G protein signaling 14
Rin - Input resistance
Rm - Membrane resistance
Rs - Series resistance

S

STDP - Spike timing dependent plasticity
STED - Stimulated emission depletion

T

tLTD - Timing-dependent long term depression
tLTP - Timing-dependent long term potentiation
TTX - Tetrodotoxin

U

UKE - University Medical Center Hamburg-Eppendorf

V

Vm - Membrane potential

BIBLIOGRAPHY

[1] W. B. Scoville and B. Milner: *Loss of recent memory after bilateral hippocampal lesions*, "Journal of neurology, neurosurgery, and psychiatry" vol. 20, no. 1, 11 (1957) (cited on page 3).

[2] P. Andersen, R. Morris, D. Amaral, T. Bliss, and J. O'Keefe: *The hippocampus book*, Oxford university press 2006 (cited on pages 3, 33, 86).

[3] H. Van Praag, A. F. Schinder, B. R. Christie, N. Toni, T. D. Palmer, and F. H. Gage: *Functional neurogenesis in the adult hippocampus*, "Nature" vol. 415, no. 6875, 1030–1034 (2002) (cited on page 3).

[4] S. R. Cajal et al.: *Histology of the nervous system of man and vertebrates*, "History of Neuroscience (Oxford Univ Press, New York)", no. 6 (1995) (cited on page 3).

[5] L. Stoppini, P.-A. Buchs, and D. Muller: *A simple method for organotypic cultures of nervous tissue*, "Journal of neuroscience methods" vol. 37, no. 2, 173–182 (1991) (cited on pages 4, 19).

[6] A. De Simoni, C. B. Griesinger, and F. A. Edwards: *Development of rat CA1 neurones in acute versus organotypic slices: role of experience in synaptic morphology and activity*, "The Journal of physiology" vol. 550, no. 1, 135–147 (2003) (cited on page 4).

[7] S. J. Martin, P. D. Grimwood, and R. G. Morris: *Synaptic plasticity and memory: an evaluation of the hypothesis*, "Annual review of neuroscience" vol. 23, no. 1, 649–711 (2000) (cited on page 5).

[8] A. Citri and R. C. Malenka: *Synaptic plasticity: multiple forms, functions, and mechanisms*, "Neuropsychopharmacology" vol. 33, no. 1, 18–41 (2008) (cited on pages 5–7).

[9] R. S. Zucker and W. G. Regehr: *Short-term synaptic plasticity*, "Annual review of physiology" vol. 64, no. 1, 355–405 (2002) (cited on page 5).

[10] T. V. Bliss and T. Lømo: *Long-lasting potentiation of synaptic transmission in the dentate area of the anaesthetized rabbit following stimulation of the perforant path*, "The Journal of physiology" vol. 232, no. 2, 331–356 (1973) (cited on page 5).

[11] T. V. Bliss and A. R. Gardner-Medwin: *Long-lasting potentiation of synaptic transmission in the dentate area of the unanaesthetized rabbit following stimulation of the perforant path.* "The Journal of physiology" vol. 232, no. 2, 357–374 (1973) (cited on page 5).

[12] T. V. Bliss and G. L. Collingridge: *A synaptic model of memory: long-term potentiation in the hippocampus*, "Nature" vol. 361, no. 6407, 31–39 (1993) (cited on page 5).

[13] Y. Dan and M.-M. Poo: *Spike timing-dependent plasticity: from synapse to perception*, "Physiological reviews" vol. 86, no. 3, 1033–1048 (2006) (cited on pages 5, 9).

[14] M. L. Mayer, G. L. Westbrook, and P. B. Guthrie: *Voltage-dependent block by Mg 2+ of NMDA responses in spinal cord neurones*, “Nature” vol. 309, no. 5965, 261–263 (1984) (cited on page 6).

[15] L. Nowak, P. Bregestovski, P. Ascher, A. Herbet, and A. Prochiantz: *Magnesium gates glutamate-activated channels in mouse central neurones*, “Nature” vol. 307, no. 5950, 462–465 (1984) (cited on page 6).

[16] B. M. Kampa, J. Clements, P. Jonas, and G. J. Stuart: *Kinetics of Mg2+ unblock of NMDA receptors: implications for spike-timing dependent synaptic plasticity*, “The Journal of physiology” vol. 556, no. 2, 337–345 (2004) (cited on page 6).

[17] R. C. Malenka and M. F. Bear: *LTP and LTD: an embarrassment of riches*, “Neuron” vol. 44, no. 1, 5–21 (2004) (cited on pages 6, 7).

[18] V. A. Derkach, M. C. Oh, E. S. Guire, and T. R. Soderling: *Regulatory mechanisms of AMPA receptors in synaptic plasticity*, “Nature Reviews Neuroscience” vol. 8, no. 2, 101–113 (2007) (cited on page 6).

[19] D. V. Lissin, S. N. Gomperts, R. C. Carroll, C. W. Christine, D. Kalman, M. Kitamura, S. Hardy, R. A. Nicoll, R. C. Malenka, and M. Von Zastrow: *Activity differentially regulates the surface expression of synaptic AMPA and NMDA glutamate receptors*, “Proceedings of the National Academy of Sciences” vol. 95, no. 12, 7097–7102 (1998) (cited on pages 6, 7).

[20] M. Park, E. C. Penick, J. G. Edwards, J. A. Kauer, and M. D. Ehlers: *Recycling endosomes supply AMPA receptors for LTP*, “Science” vol. 305, no. 5692, 1972–1975 (2004) (cited on page 6).

[21] M. Bosch and Y. Hayashi: *Structural plasticity of dendritic spines*, “Current opinion in neurobiology” vol. 22, no. 3, 383–388 (2012) (cited on pages 7, 62).

[22] Y. Oe, K. Tominaga-Yoshino, S. Hasegawa, and A. Ogura: *Dendritic spine dynamics in synaptogenesis after repeated LTP inductions: dependence on pre-existing spine density*, “Scientific reports” vol. 3, 1957 (2013) (cited on pages 7, 62, 63).

[23] J. S. Wiegert, M. Pulin, C. E. Gee, and T. G. Oertner: *The fate of hippocampal synapses depends on the sequence of plasticity-inducing events*, “Elife” vol. 7, e39151 (2018) (cited on pages 7, 62).

[24] S. M. Dudek and M. F. Bear: *Homosynaptic long-term depression in area CA1 of hippocampus and effects of N-methyl-D-aspartate receptor blockade*, in *How We Learn; How We Remember: Toward An Understanding Of Brain And Neural Systems: Selected Papers of Leon N Cooper*, World Scientific 1995, pp. 200–204 (cited on page 7).

[25] U. V. Nägerl, N. Eberhorn, S. B. Cambridge, and T. Bonhoeffer: *Bidirectional activity-dependent morphological plasticity in hippocampal neurons*, “Neuron” vol. 44, no. 5, 759–767 (2004) (cited on page 7).

[26] Q. Zhou, K. J. Homma, and M.-m. Poo: *Shrinkage of dendritic spines associated with long-term depression of hippocampal synapses*, “Neuron” vol. 44, no. 5, 749–757 (2004) (cited on page 7).

[27] H. Hsieh, J. Boehm, C. Sato, T. Iwatsubo, T. Tomita, S. Sisodia, and R. Malinow: *AMPAR removal underlies Aβ-induced synaptic depression and dendritic spine loss*, "Neuron" vol. 52, no. 5, 831–843 (2006) (cited on page 7).

[28] N. Caporale and Y. Dan: *Spike timing–dependent plasticity: a Hebbian learning rule*, "Annu. Rev. Neurosci." vol. 31, 25–46 (2008) (cited on pages 9, 10).

[29] J. J. Letzkus, B. M. Kampa, and G. J. Stuart: *Does spike timing-dependent synaptic plasticity underlie memory formation?*, "Clinical and Experimental Pharmacology and Physiology" vol. 34, no. 10, 1070–1076 (2007) (cited on page 9).

[30] K. Buchanan and J. Mellor: *The activity requirements for spike timing-dependent plasticity in the hippocampus*, "Frontiers in synaptic neuroscience" vol. 2, 11 (2010) (cited on page 9).

[31] A. Suvrathan, H. L. Payne, and J. L. Raymond: *Timing rules for synaptic plasticity matched to behavioral function*, "Neuron" vol. 92, no. 5, 959–967 (2016) (cited on page 9).

[32] D. Debanne, Y. Inglebert, and M. Russier: *Plasticity of intrinsic neuronal excitability*, "Current opinion in neurobiology" vol. 54, 73–82 (2019) (cited on pages 9, 59, 61, 65).

[33] D. Hebb: *The organization of behavior*, Wiley & Sons: New York, USA 1949 (cited on page 9).

[34] G.-q. Bi and M.-m. Poo: *Synaptic modifications in cultured hippocampal neurons: dependence on spike timing, synaptic strength, and postsynaptic cell type*, "Journal of neuroscience" vol. 18, no. 24, 10464–10472 (1998) (cited on pages 9, 51, 56, 65).

[35] D. Debanne, B. H. Gähwiler, and S. M. Thompson: *Long-term synaptic plasticity between pairs of individual CA3 pyramidal cells in rat hippocampal slice cultures*, "The Journal of Physiology" vol. 507, no. 1, 237–247 (1998) (cited on pages 9, 51, 56, 65).

[36] B. Sakmann: *Regulation of Synaptic Efficacy by Coincidence of Postsynaptic APs and EPSPs*, "J. Neurophysiol" vol. 76, 3460 (1996) (cited on page 9).

[37] H. Markram, J. Lübke, M. Frotscher, and B. Sakmann: *Regulation of synaptic efficacy by coincidence of postsynaptic APs and EPSPs*, "Science" vol. 275, no. 5297, 213–215 (1997) (cited on pages 9, 65).

[38] G. M. Wittenberg and S. S.-H. Wang: *Malleability of spike-timing-dependent plasticity at the CA3–CA1 synapse*, "Journal of Neuroscience" vol. 26, no. 24, 6610–6617 (2006) (cited on pages 9, 51, 56, 65, 66).

[39] M. Nishiyama, K. Hong, K. Mikoshiba, M.-M. Poo, and K. Kato: *Calcium stores regulate the polarity and input specificity of synaptic modification*, "Nature" vol. 408, no. 6812, 584–588 (2000) (cited on page 9).

[40] C. C. Bell, V. Z. Han, Y. Sugawara, and K. Grant: *Synaptic plasticity in a cerebellum-like structure depends on temporal order*, "Nature" vol. 387, no. 6630, 278–281 (1997) (cited on page 9).

[41] T. Tzounopoulos, Y. Kim, D. Oertel, and L. O. Trussell: *Cell-specific, spike timing–dependent plasticities in the dorsal cochlear nucleus*, "Nature neuroscience" vol. 7, no. 7, 719–725 (2004) (cited on page 9).

[42] T. Tzounopoulos, M. E. Rubio, J. E. Keen, and L. O. Trussell: *Coactivation of pre-and postsynaptic signaling mechanisms determines cell-specific spike-timing-dependent plasticity*, "Neuron" vol. 54, no. 2, 291–301 (2007) (cited on page 9).

[43] C. D. Holmgren and Y. Zilberter: *Coincident spiking activity induces long-term changes in inhibition of neocortical pyramidal cells*, "Journal of Neuroscience" vol. 21, no. 20, 8270–8277 (2001) (cited on page 9).

[44] M. A. Woodin, K. Ganguly, and M.-m. Poo: *Coincident pre-and postsynaptic activity modifies GABAergic synapses by postsynaptic changes in Cl- transporter activity*, "Neuron" vol. 39, no. 5, 807–820 (2003) (cited on page 9).

[45] J. S. Haas, T. Nowotny, and H. D. Abarbanel: *Spike-timing-dependent plasticity of inhibitory synapses in the entorhinal cortex*, "Journal of neurophysiology" vol. 96, no. 6, 3305–3313 (2006) (cited on page 9).

[46] T. Nevian and B. Sakmann: *Spine Ca2+ signaling in spike-timing-dependent plasticity*, "Journal of Neuroscience" vol. 26, no. 43, 11001–11013 (2006) (cited on pages 9, 47, 51, 56, 65).

[47] C. M. Tigaret, V. Olivo, J. H. Sadowski, M. C. Ashby, and J. R. Mellor: *Coordinated activation of distinct Ca 2+ sources and metabotropic glutamate receptors encodes Hebbian synaptic plasticity*, "Nature communications" vol. 7, no. 1, 1–14 (2016) (cited on pages 9, 47, 51, 56).

[48] E. Edelmann, E. Cepeda-Prado, M. Franck, P. Lichtenecker, T. Brigadski, and V. Leßmann: *Theta burst firing recruits BDNF release and signaling in postsynaptic CA1 neurons in spike-timing-dependent LTP*, "Neuron" vol. 86, no. 4, 1041–1054 (2015) (cited on pages 9, 51, 56).

[49] J. C. Magee and D. Johnston: *A synaptically controlled, associative signal for Hebbian plasticity in hippocampal neurons*, "Science" vol. 275, no. 5297, 209–213 (1997) (cited on page 9).

[50] R. C. Froemke, J. J. Letzkus, B. Kampa, G. B. Hang, and G. Stuart: *Dendritic synapse location and neocortical spike-timing-dependent plasticity*, "Frontiers in synaptic neuroscience" vol. 2, 29 (2010) (cited on pages 9, 62).

[51] H.-X. Wang, R. C. Gerkin, D. W. Nauen, and G.-Q. Bi: *Coactivation and timing-dependent integration of synaptic potentiation and depression*, "Nature neuroscience" vol. 8, no. 2, 187–193 (2005) (cited on page 9).

[52] F. G. Pike, R. M. Meredith, A. W. Olding, and O. Paulsen: *Postsynaptic bursting is essential for 'Hebbian'induction of associative long-term potentiation at excitatory synapses in rat hippocampus*, "The Journal of physiology" vol. 518, no. 2, 571–576 (1999) (cited on page 9).

[53] B. M. Kampa, J. J. Letzkus, and G. J. Stuart: *Requirement of dendritic calcium spikes for induction of spike-timing-dependent synaptic plasticity*, "The Journal of physiology" vol. 574, no. 1, 283–290 (2006) (cited on page 9).

[54] P. J. Sjöström and M. Häusser: *A cooperative switch determines the sign of synaptic plasticity in distal dendrites of neocortical pyramidal neurons*, "Neuron" vol. 51, no. 2, 227–238 (2006) (cited on page 9).

[55] S. Tazerart, D. E. Mitchell, S. Miranda-Rottmann, and R. Araya: *A spike timing-dependent plasticity rule for single, clustered and distributed dendritic spines*, "bioRxiv", 397323 (2018) (cited on pages 9, 62, 66).

[56] J. J. Letzkus, B. M. Kampa, and G. J. Stuart: *Learning rules for spike timing-dependent plasticity depend on dendritic synapse location*, "Journal of Neuroscience" vol. 26, no. 41, 10420–10429 (2006) (cited on pages 9, 62, 65).

[57] K. F. Lee, C. Soares, J.-P. Thivierge, and J.-C. Béïque: *Correlated synaptic inputs drive dendritic calcium amplification and cooperative plasticity during clustered synapse development*, "Neuron" vol. 89, no. 4, 784–799 (2016) (cited on pages 9, 62, 67).

[58] E. Edelmann, E. Cepeda-Prado, and V. Leßmann: *Coexistence of multiple types of synaptic plasticity in individual hippocampal CA1 pyramidal neurons*, "Frontiers in synaptic neuroscience" vol. 9, 7 (2017) (cited on pages 9, 62).

[59] N. L. Golding, N. P. Staff, and N. Spruston: *Dendritic spikes as a mechanism for cooperative long-term potentiation*, "Nature" vol. 418, no. 6895, 326–331 (2002) (cited on page 9).

[60] G. Nagel, D. Ollig, M. Fuhrmann, S. Kateriya, A. M. Musti, E. Bamberg, and P. Hegemann: *Channelrhodopsin-1: a light-gated proton channel in green algae*, "Science" vol. 296, no. 5577, 2395–2398 (2002) (cited on page 11).

[61] G. Nagel, T. Szellas, W. Huhn, S. Kateriya, N. Adeishvili, P. Berthold, D. Ollig, P. Hegemann, and E. Bamberg: *Channelrhodopsin-2, a directly light-gated cation-selective membrane channel*, "Proceedings of the National Academy of Sciences" vol. 100, no. 24, 13940–13945 (2003) (cited on page 11).

[62] E. S. Boyden, F. Zhang, E. Bamberg, G. Nagel, and K. Deisseroth: *Millisecond-timescale, genetically targeted optical control of neural activity*, "Nature neuroscience" vol. 8, no. 9, 1263–1268 (2005) (cited on page 11).

[63] T. Ishizuka, M. Kakuda, R. Araki, and H. Yawo: *Kinetic evaluation of photosensitivity in genetically engineered neurons expressing green algae light-gated channels*, "Neuroscience research" vol. 54, no. 2, 85–94 (2006) (cited on page 11).

[64] G. Nagel, M. Brauner, J. F. Liewald, N. Adeishvili, E. Bamberg, and A. Gottschalk: *Light activation of channelrhodopsin-2 in excitable cells of Caenorhabditis elegans triggers rapid behavioral responses*, "Current Biology" vol. 15, no. 24, 2279–2284 (2005) (cited on page 11).

[65] X. Li, D. V. Gutierrez, M. G. Hanson, J. Han, M. D. Mark, H. Chiel, P. Hegemann, L. T. Landmesser, and S. Herlitze: *Fast noninvasive activation and inhibition of neural and network activity by vertebrate rhodopsin and green algae channelrhodopsin*, "Proceedings of the National Academy of Sciences" vol. 102, no. 49, 17816–17821 (2005) (cited on page 11).

[66] A. Kianianmomeni: *Optogenetics: Methods and protocols*, Humana Press 2016 (cited on page 11).

[67] H. Yawo, H. Kandori, and A. Koizumi: *Optogenetics: light-sensing proteins and their applications*, Springer 2015 (cited on page 11).

[68] O. P. Ernst, D. T. Lodowski, M. Elstner, P. Hegemann, L. S. Brown, and H. Kandori: *Microbial and animal rhodopsins: structures, functions, and molecular mechanisms*, "Chemical reviews" vol. 114, no. 1, 126–163 (2014) (cited on page 11).

[69] A. Berndt, O. Yizhar, L. A. Gunaydin, P. Hegemann, and K. Deisseroth: *Bi-stable neural state switches*, "Nature neuroscience" vol. 12, no. 2, 229 (2009) (cited on page 11).

[70] J. Wietek, R. Beltramo, M. Scanziani, P. Hegemann, T. G. Oertner, and J. S. Wiegert: *An improved chloride-conducting channelrhodopsin for light-induced inhibition of neuronal activity in vivo*, "Scientific reports" vol. 5, 14807 (2015) (cited on page 11).

[71] J. Wietek, S. Rodriguez-Rozada, J. Tutas, F. Tenedini, C. Grimm, T. G. Oertner, P. Soba, P. Hegemann, and J. S. Wiegert: *Anion-conducting channelrhodopsins with tuned spectra and modified kinetics engineered for optogenetic manipulation of behavior*, "Scientific reports" vol. 7, no. 1, 1–18 (2017) (cited on page 11).

[72] J. S. Wiegert, M. Mahn, M. Prigge, Y. Printz, and O. Yizhar: *Silencing neurons: tools, applications, and experimental constraints*, "Neuron" vol. 95, no. 3, 504–529 (2017) (cited on page 11).

[73] H. E. Kato, Y. S. Kim, J. M. Paggi, K. E. Evans, W. E. Allen, C. Richardson, K. Inoue, S. Ito, C. Ramakrishnan, L. E. Fenno, et al.: *Structural mechanisms of selectivity and gating in anion channelrhodopsins*, "Nature" vol. 561, no. 7723, 349–354 (2018) (cited on page 11).

[74] J. Oppermann, P. Fischer, A. Silapetere, B. Liepe, S. Rodriguez-Rozada, J. Flores-Uribe, E. Peter, A. Keidel, J. Vierock, J. Kaufmann, et al.: *MerMAIDs: a family of metagenomically discovered marine anion-conducting and intensely desensitizing channelrhodopsins*, "Nature communications" vol. 10, no. 1, 1–13 (2019) (cited on page 11).

[75] M. Rappleye and A. Berndt: *Structural basis for ion selectivity and engineering in channelrhodopsins*, "Current opinion in structural biology" vol. 57, 176–184 (2019) (cited on page 11).

[76] A. Berndt, P. Schoenenberger, J. Mattis, K. M. Tye, K. Deisseroth, P. Hegemann, and T. G. Oertner: *High-efficiency channelrhodopsins for fast neuronal stimulation at low light levels*, "Proceedings of the National Academy of Sciences" vol. 108, no. 18, 7595–7600 (2011) (cited on page 11).

[77] L. A. Gunaydin, O. Yizhar, A. Berndt, V. S. Sohal, K. Deisseroth, and P. Hegemann: *Ultrafast optogenetic control*, "Nature neuroscience" vol. 13, no. 3, 387 (2010) (cited on page 11).

[78] S. Kleinlogel, K. Feldbauer, R. E. Dempski, H. Fotis, P. G. Wood, C. Bamann, and E. Bamberg: *Ultra light-sensitive and fast neuronal activation with the [Ca 2+]-permeable channelrhodopsin CatCh*, "Nature neuroscience" vol. 14, no. 4, 513–518 (2011) (cited on page 11).

[79] O. Yizhar, L. E. Fenno, M. Prigge, F. Schneider, T. J. Davidson, D. J. O'shea, V. S. Sohal, I. Goshen, J. Finkelstein, J. T. Paz, et al.: *Neocortical excitation/inhibition balance in information processing and social dysfunction*, "Nature" vol. 477, no. 7363, 171–178 (2011) (cited on page 11).

[80] N. C. Klapoetke, Y. Murata, S. S. Kim, S. R. Pulver, A. Birdsey-Benson, Y. K. Cho, T. K. Morimoto, A. S. Chuong, E. J. Carpenter, Z. Tian, et al.: *Independent optical excitation of distinct neural populations*, "Nature methods" vol. 11, no. 3, 338 (2014) (cited on pages 11, 45, 75).

[81] D. R. Hochbaum, Y. Zhao, S. L. Farhi, N. Klapoetke, C. A. Werley, V. Kapoor, P. Zou, J. M. Kralj, D. Maclaurin, N. Smedemark-Margulies, et al.: *All-optical electrophysiology in mammalian neurons using engineered microbial rhodopsins*, "Nature methods" vol. 11, no. 8, 825 (2014) (cited on pages 11, 45).

[82] L. Wen, H. Wang, S. Tanimoto, R. Egawa, Y. Matsuzaka, H. Mushiake, T. Ishizuka, and H. Yawo: *Opto-current-clamp actuation of cortical neurons using a strategically designed channelrhodopsin*, "PloS one" vol. 5, no. 9 (2010) (cited on page 11).

[83] A. Rozenberg, J. Oppermann, J. Wietek, R. G. F. Lahore, R.-A. Sandaa, G. Bratbak, P. Hegemann, and O. Béjà: *Lateral gene transfer of anion-conducting channelrhodopsins between green algae and giant viruses*, "bioRxiv" (2020) (cited on pages 11, 12).

[84] S.-Y. Hou, E. G. Govorunova, M. Ntefidou, C. E. Lane, E. N. Spudich, O. A. Sineshchekov, and J. L. Spudich: *Diversity of Chlamydomonas channelrhodopsins*, "Photochemistry and photobiology" vol. 88, no. 1, 119–128 (2012) (cited on page 11).

[85] M. Karasuyama, K. Inoue, R. Nakamura, H. Kandori, and I. Takeuchi: *Understanding Colour Tuning Rules and Predicting Absorption Wavelengths of Microbial Rhodopsins by Data-Driven Machine-Learning Approach*, "Scientific reports" vol. 8, no. 1, 1–11 (2018) (cited on page 11).

[86] D. N. Barry and S. Commins: *Temporal dynamics of immediate early gene expression during cellular consolidation of spatial memory*, "Behavioural brain research" vol. 327, 44–53 (2017) (cited on pages 13, 71, 73).

[87] K. Minatohara, M. Akiyoshi, and H. Okuno: *Role of immediate-early genes in synaptic plasticity and neuronal ensembles underlying the memory trace*, "Frontiers in molecular neuroscience" vol. 8, 78 (2016) (cited on pages 13, 71).

[88] D. Mahringer, A. V. Petersen, A. Fiser, H. Okuno, H. Bito, J.-F. Perrier, and G. B. Keller: *Expression of c-Fos and Arc in hippocampal region CA1 marks neurons that exhibit learning-related activity changes*, "bioRxiv", 644526 (2019) (cited on pages 13, 71).

[89] G. E. Hoffman, M. S. Smith, and J. G. Verbalis: *c-Fos and related immediate early gene products as markers of activity in neuroendocrine systems*, "Frontiers in neuroendocrinology" vol. 14, no. 3, 173–213 (1993) (cited on pages 13, 71, 73).

[90] R. D. Fields, F. Eshete, B. Stevens, and K. Itoh: *Action potential-dependent regulation of gene expression: temporal specificity in Ca2+, cAMP-responsive element binding proteins, and mitogen-activated protein kinase signaling*, "Journal of Neuroscience" vol. 17, no. 19, 7252–7266 (1997) (cited on pages 13, 14, 71, 76, 85, 86).

[91] P. F. Worley, R. V. Bhat, J. M. Baraban, C. A. Erickson, B. L. McNaughton, and C. A. Barnes: *Thresholds for synaptic activation of transcription factors in hippocampus: correlation with long-term enhancement*, "Journal of Neuroscience" vol. 13, no. 11, 4776–4786 (1993) (cited on page 13).

[92] J. I. Morgan and T. Curran: *Stimulus-transcription coupling in the nervous system: involvement of the inducible proto-oncogenes fos and jun*, "Annual review of neuroscience" vol. 14, no. 1, 421–451 (1991) (cited on page 13).

[93] P. Hughes and M. Dragunow: *Induction of immediate-early genes and the control of neurotransmitter-regulated gene expression within the nervous system.* "Pharmacological reviews" vol. 47, no. 1, 133–178 (1995) (cited on page 13).

[94] F. N. Velazquez, C. G. Prucca, O. Etienne, D. S. D'Astolfo, D. C. Silvestre, F. D. Boussin, and B. L. Caputto: *Brain development is impaired in c-fos-/- mice*, "Oncotarget" vol. 6, no. 19, 16883 (2015) (cited on page 13).

[95] H. Sheng, R. Fields, and P. Nelson: *Specific regulation of immediate early genes by patterned neuronal activity*, "Journal of neuroscience research" vol. 35, no. 5, 459–467 (1993) (cited on pages 13, 14, 71, 76, 85, 86).

[96] J.-Y. Joo, K. Schaukowitch, L. Farbiak, G. Kilaru, and T.-K. Kim: *Stimulus-specific combinatorial functionality of neuronal c-fos enhancers*, "Nature neuroscience" vol. 19, no. 1, 75 (2016) (cited on pages 13, 71).

[97] K. M. Tyssowski, N. R. DeStefino, J.-H. Cho, C. J. Dunn, R. G. Poston, C. E. Carty, R. D. Jones, S. M. Chang, P. Romeo, M. K. Wurzelmann, et al.: *Different neuronal activity patterns induce different gene expression programs*, "Neuron" vol. 98, no. 3, 530–546 (2018) (cited on pages 13, 14, 71, 73, 76, 85).

[98] R. D. Fields: *Signaling from neural impulses to genes*, "The Neuroscientist" vol. 2, no. 6, 315–325 (1996) (cited on pages 13, 14, 71, 76, 85, 86).

[99] T. Kawashima, H. Okuno, and H. Bito: *A new era for functional labeling of neurons: activity-dependent promoters have come of age*, "Frontiers in neural circuits" vol. 8, 37 (2014) (cited on page 13).

[100] F. C. Cruz, F. J. Rubio, and B. T. Hope: *Using c-fos to study neuronal ensembles in corticostriatal circuitry of addiction*, "Brain research" vol. 1628, 157–173 (2015) (cited on pages 13, 14).

[101] A. R. Garner, D. C. Rowland, S. Y. Hwang, K. Baumgaertel, B. L. Roth, C. Kentros, and M. Mayford: *Generation of a synthetic memory trace*, "Science" vol. 335, no. 6075, 1513–1516 (2012) (cited on page 13).

[102] L. Xie, Y. Liu, Y. Hu, B. Wang, Z. Zhu, Y. Jiang, Y. Suo, M. Hu, J. Gao, R. Ullah, et al.: *Neonatal sevoflurane exposure induces impulsive behavioral deficit through disrupting excitatory neurons in the medial prefrontal cortex in mice*, "Translational Psychiatry" vol. 10, no. 1, 1–11 (2020) (cited on page 13).

[103] X. Zhang, J. Kim, and S. Tonegawa: *Amygdala reward neurons form and store fear extinction memory*, "Neuron" (2020) (cited on page 13).

[104] G.-Y. Wu, K. Deisseroth, and R. W. Tsien: *Activity-dependent CREB phosphorylation: convergence of a fast, sensitive calmodulin kinase pathway and a slow, less sensitive mitogen-activated protein kinase pathway*, "Proceedings of the National Academy of Sciences" vol. 98, no. 5, 2808–2813 (2001) (cited on page 13).

[105] S. Cohen and M. E. Greenberg: *Communication between the synapse and the nucleus in neuronal development, plasticity, and disease*, "Annual review of cell and developmental biology" vol. 24, 183–209 (2008) (cited on page 13).

[106] D. Gandolfi, S. Cerri, J. Mapelli, M. Polimeni, S. Tritto, M.-T. Fuzzati-Armentero, A. Bigiani, F. Blandini, L. Mapelli, and E. D'Angelo: *Activation of the CREB/c-fos pathway during long-term synaptic plasticity in the cerebellum granular layer*, "Frontiers in cellular neuroscience" vol. 11, 184 (2017) (cited on page 14).

[107] A. Rajadhyaksha, A. Barczak, W. Macıas, J.-C. Leveque, S. E. Lewis, and C. Konradi: *L-type Ca2+ channels are essential for glutamate-mediated CREB phosphorylation and c-fos gene expression in striatal neurons*, "Journal of Neuroscience" vol. 19, no. 15, 6348–6359 (1999) (cited on page 14).

[108] G. M. Thomas and R. L. Huganir: *MAPK cascade signalling and synaptic plasticity*, "Nature Reviews Neuroscience" vol. 5, no. 3, 173–183 (2004) (cited on page 14).

[109] J. Xing, D. D. Ginty, and M. E. Greenberg: *Coupling of the RAS-MAPK pathway to gene activation by RSK2, a growth factor-regulated CREB kinase*, "Science" vol. 273, no. 5277, 959–963 (1996) (cited on page 14).

[110] C. E. Gee, I. Ohmert, J. S. Wiegert, and T. G. Oertner: *Preparation of slice cultures from rodent hippocampus*, "Cold Spring Harbor Protocols" vol. 2017, no. 2, pdb–prot094888 (2017) (cited on page 19).

[111] J. Dyhrfjeld-Johnsen, Y. Berdichevsky, W. Swiercz, H. Sabolek, and K. Staley: *Interictal spikes precede ictal discharges in an organotypic hippocampal slice culture model of epileptogenesis*, "Journal of clinical neurophysiology: official publication of the American Electroencephalographic Society" vol. 27, no. 6, 418 (2010) (cited on page 19).

[112] J. S. Wiegert, C. E. Gee, and T. G. Oertner: *Viral vector-based transduction of slice cultures*, "Cold Spring Harbor Protocols" vol. 2017, no. 2, pdb–prot094896 (2017) (cited on pages 21, 45).

[113] J. S. Wiegert, C. E. Gee, and T. G. Oertner: *Single-cell electroporation of neurons*, "Cold Spring Harbor protocols" vol. 2017, no. 2, pdb–prot094904 (2017) (cited on pages 21, 45).

[114] J. S. Wiegert, C. E. Gee, and T. G. Oertner: *Stimulating neurons with heterologously expressed light-gated ion channels*, "Cold Spring Harbor Protocols" vol. 2017, no. 2, pdb–top089714 (2017) (cited on page 23).

[115] B. A. Suter, T. O'Connor, V. Iyer, L. Petreanu, B. M. Hooks, T. Kiritani, K. Svoboda, and G. M. Shepherd: *Ephus: multipurpose data acquisition software for neuroscience experiments*, "Frontiers in neural circuits" vol. 4, 100 (2010) (cited on pages 24, 29).

[116] M. D. Binder, N. Hirokawa, and U. Windhorst: *Encyclopedia of neuroscience*, Springer Berlin, Germany 2009 (cited on pages 24, 35).

[117] L. J. DeFelice: *Electrical properties of cells*, "Trends in neuroscience" vol. 21, 312–312 (1998) (cited on pages 24, 25).

[118] J.-i. Tanaka, Y. Horiike, M. Matsuzaki, T. Miyazaki, G. C. Ellis-Davies, and H. Kasai: *Protein synthesis and neurotrophin-dependent structural plasticity of single dendritic spines*, "Science" vol. 319, no. 5870, 1683–1687 (2008) (cited on pages 24, 66).

[119] D. L. Ypey and L. J. DeFelice: *The patch-clamp technique explained and exercised with the use of simple electrical equivalent circuits*, "Electrical Properties of Cells; Springer: Boston, MA, USA", 7 (2000) (cited on page 25).

[120] A. J. Sherman, A. Shrier, and E. Cooper: *Series resistance compensation for whole-cell patch-clamp studies using a membrane state estimator*, "Biophysical journal" vol. 77, no. 5, 2590–2601 (1999) (cited on page 25).

[121] W. Walz, A. A. Boulton, and G. B. Baker: *Patch-clamp analysis: advanced techniques*, 35, Springer Science & Business Media 2002 (cited on page 26).

[122] Y. Okada: *Patch clamp techniques*, Springer 2012 (cited on page 26).

[123] P. H. Barry and J. W. Lynch: *Liquid junction potentials and small cell effects in patch-clamp analysis*, "The Journal of membrane biology" vol. 121, no. 2, 101–117 (1991) (cited on page 27).

[124] E. Neher: *Correction for liquid junction potentials in patch clamp experiments*, "Methods in enzymology" vol. 207, 123–131 (1992) (cited on page 27).

[125] L. Squire, D. Berg, F. E. Bloom, S. Du Lac, A. Ghosh, and N. C. Spitzer: *Fundamental neuroscience*, Academic Press 2008 (cited on page 35).

[126]J. Schindelin, I. Arganda-Carreras, E. Frise, V. Kaynig, M. Longair, T. Pietzsch, S. Preibisch, C. Rueden, S. Saalfeld, B. Schmid, et al.: *Fiji: an open-source platform for biological-image analysis*, “Nature methods” vol. 9, no. 7, 676–682 (2012) (cited on page 38).

[127]S. Song, K. D. Miller, and L. F. Abbott: *Competitive Hebbian learning through spike-timing-dependent synaptic plasticity*, “Nature neuroscience” vol. 3, no. 9, 919–926 (2000) (cited on page 43).

[128]W. Gerstner, R. Kempter, J. L. Van Hemmen, and H. Wagner: *A neuronal learning rule for sub-millisecond temporal coding*, “Nature” vol. 383, 76–81 (1996) (cited on page 43).

[129]R. P. Costa, R. C. Froemke, P. J. Sjöström, and M. C. van Rossum: *Unified pre-and postsynaptic long-term plasticity enables reliable and flexible learning*, “Elife” vol. 4, e09457 (2015) (cited on page 43).

[130]M. C. Van Rossum, G. Q. Bi, and G. G. Turrigiano: *Stable Hebbian learning from spike timing-dependent plasticity*, “Journal of neuroscience” vol. 20, no. 23, 8812–8821 (2000) (cited on page 43).

[131]K. C. Bittner, A. D. Milstein, C. Grienberger, S. Romani, and J. C. Magee: *Behavioral time scale synaptic plasticity underlies CA1 place fields*, “Science” vol. 357, no. 6355, 1033–1036 (2017) (cited on pages 43, 66).

[132]Y.-P. Zhang and T. G. Oertner: *Optical induction of synaptic plasticity using a light-sensitive channel*, “Nature methods” vol. 4, no. 2, 139–141 (2007) (cited on page 47).

[133]P. Schoenenberger, D. Gerosa, and T. G. Oertner: *Temporal control of immediate early gene induction by light*, “PloS one” vol. 4, no. 12 (2009) (cited on pages 47, 73).

[134]J. Jaworski, K. Kalita, and E. Knapska: *c-Fos and neuronal plasticity: the aftermath of Kaczmarek's theory*, “Acta Neurobiol Exp” vol. 78, 287–296 (2018) (cited on page 47).

[135]N. Holbro, Å. Grunditz, J. S. Wiegert, and T. G. Oertner: *AMPA receptors gate spine Ca2+ transients and spike-timing-dependent potentiation*, “Proceedings of the National Academy of Sciences” vol. 107, no. 36, 15975–15980 (2010) (cited on page 51).

[136]R. Malinow and R. W. Tsien: *Presynaptic enhancement shown by whole-cell recordings of long-term potentiation in hippocampal slices*, “Nature” vol. 346, no. 6280, 177–180 (1990) (cited on pages 58, 66).

[137]M. Matsuzaki, N. Honkura, G. C. Ellis-Davies, and H. Kasai: *Structural basis of long-term potentiation in single dendritic spines*, “Nature” vol. 429, no. 6993, 761–766 (2004) (cited on page 58).

[138]Q. Wang, M. Chen, N. P. Schafer, C. Bueno, S. S. Song, A. Hudmon, P. G. Wolynes, M. N. Waxham, and M. S. Cheung: *Assemblies of calcium/calmodulin-dependent kinase II with actin and their dynamic regulation by calmodulin in dendritic spines*, “Proceedings of the National Academy of Sciences” vol. 116, no. 38, 18937–18942 (2019) (cited on page 58).

[139] J. H. Sadowski, M. W. Jones, and J. R. Mellor: *Sharp-wave ripples orchestrate the induction of synaptic plasticity during reactivation of place cell firing patterns in the hippocampus*, "Cell reports" vol. 14, no. 8, 1916–1929 (2016) (cited on page 59).

[140] J. Xu, N. Kang, L. Jiang, M. Nedergaard, and J. Kang: *Activity-dependent long-term potentiation of intrinsic excitability in hippocampal CA1 pyramidal neurons*, "Journal of Neuroscience" vol. 25, no. 7, 1750–1760 (2005) (cited on page 61).

[141] D. A. Coulter, J. Lo Turco, M. Kubota, J. F. Disterhoft, J. W. Moore, and D. L. Alkon: *Classical conditioning reduces amplitude and duration of calcium-dependent afterhyperpolarization in rabbit hippocampal pyramidal cells*, "Journal of neurophysiology" vol. 61, no. 5, 971–981 (1989) (cited on page 61).

[142] A. Frick, J. Magee, and D. Johnston: *LTP is accompanied by an enhanced local excitability of pyramidal neuron dendrites*, "Nature neuroscience" vol. 7, no. 2, 126–135 (2004) (cited on page 61).

[143] D. Debanne and M.-M. Poo: *Spike-timing dependent plasticity beyond synapse-pre-and post-synaptic plasticity of intrinsic neuronal excitability*, "Frontiers in synaptic neuroscience" vol. 2, 21 (2010) (cited on page 61).

[144] M. Trommald, G. Hulleberg, and P. Andersen: *Long-term potentiation is associated with new excitatory spine synapses on rat dentate granule cells.* "Learning & Memory" vol. 3, no. 2-3, 218–228 (1996) (cited on page 62).

[145] M. De Roo, P. Klauser, and D. Muller: *LTP promotes a selective long-term stabilization and clustering of dendritic spines*, "PLoS biology" vol. 6, no. 9 (2008) (cited on page 62).

[146] R. Araya, T. P. Vogels, and R. Yuste: *Activity-dependent dendritic spine neck changes are correlated with synaptic strength*, "Proceedings of the National Academy of Sciences" vol. 111, no. 28, E2895–E2904 (2014) (cited on page 62).

[147] K. M. Harris and J. K. Stevens: *Dendritic spines of CA 1 pyramidal cells in the rat hippocampus: serial electron microscopy with reference to their biophysical characteristics*, "Journal of Neuroscience" vol. 9, no. 8, 2982–2997 (1989) (cited on page 62).

[148] R. Yuste: *Dendritic spines*, MIT press 2010 (cited on page 62).

[149] G. Vicidomini, P. Bianchini, and A. Diaspro: *STED super-resolved microscopy*, "Nature methods" vol. 15, no. 3, 173 (2018) (cited on page 62).

[150] W. C. Risher, T. Ustunkaya, J. S. Alvarado, and C. Eroglu: *Rapid Golgi analysis method for efficient and unbiased classification of dendritic spines*, "PloS one" vol. 9, no. 9 (2014) (cited on pages 62, 63).

[151] J.-C. Zhang, P.-M. Lau, and G.-Q. Bi: *Gain in sensitivity and loss in temporal contrast of STDP by dopaminergic modulation at hippocampal synapses*, "Proceedings of the National Academy of Sciences" vol. 106, no. 31, 13028–13033 (2009) (cited on pages 65, 66).

[152] R. M. Meredith, A. M. Floyer-Lea, and O. Paulsen: *Maturation of long-term potentiation induction rules in rodent hippocampus: role of GABAergic inhibition*, “Journal of Neuroscience” vol. 23, no. 35, 11142–11146 (2003) (cited on pages 65, 66).

[153] D. D. Samulack, S. Williams, and J.-C. Lacaille: *Hyperpolarizing synaptic potentials evoked in CA1 pyramidal cells by glutamate stimulation of interneurons from the oriens/alveus border of rat hippocampal slices. I. Electrophysiological response properties*, “Hippocampus” vol. 3, no. 3, 331–344 (1993) (cited on page 65).

[154] J. J. Marlin and A. G. Carter: *GABA-A receptor inhibition of local calcium signaling in spines and dendrites*, “Journal of Neuroscience” vol. 34, no. 48, 15898–15911 (2014) (cited on page 65).

[155] J. Yang, D. Cumberbatch, S. Centanni, S.-q. Shi, D. Winder, D. Webb, and C. H. Johnson: *Coupling optogenetic stimulation with NanoLuc-based luminescence (BRET) Ca++ sensing*, “Nature communications” vol. 7, no. 1, 1–10 (2016) (cited on page 66).

[156] Z. Brzosko, W. Schultz, and O. Paulsen: *Retroactive modulation of spike timing-dependent plasticity by dopamine*, “Elife” vol. 4, e09685 (2015) (cited on page 66).

[157] G. T. Silva, M. B. Verhoog, N. B. Goriounova, A. Loebel, J. Hjorth, J. C. Baayen, C. P. De Kock, and H. D. Mansvelder: *Human synapses show a wide temporal window for spike-timing-dependent plasticity*, “Frontiers in synaptic neuroscience” vol. 2, 12 (2010) (cited on page 66).

[158] M. B. Verhoog, N. A. Goriounova, J. Obermayer, J. Stroeder, J. J. Hjorth, G. Testa-Silva, J. C. Baayen, C. P. de Kock, R. M. Meredith, and H. D. Mansvelder: *Mechanisms underlying the rules for associative plasticity at adult human neocortical synapses*, “Journal of Neuroscience” vol. 33, no. 43, 17197–17208 (2013) (cited on page 66).

[159] G. G. Turrigiano: *The dialectic of Hebb and homeostasis*, “Philosophical Transactions of the Royal Society B: Biological Sciences” vol. 372, no. 1715, 20160258 (2017) (cited on page 66).

[160] P. J. Sjöström, G. G. Turrigiano, and S. B. Nelson: *Rate, timing, and cooperativity jointly determine cortical synaptic plasticity*, “Neuron” vol. 32, no. 6, 1149–1164 (2001) (cited on page 66).

[161] S. Cohen-Cory: *The developing synapse: construction and modulation of synaptic structures and circuits*, “Science” vol. 298, no. 5594, 770–776 (2002) (cited on page 67).

[162] A. S. Ozcan: *Filopodia: a rapid structural plasticity substrate for fast learning*, “Frontiers in synaptic neuroscience” vol. 9, 12 (2017) (cited on page 67).

[163] J.-H. Choi, S.-E. Sim, J.-i. Kim, D. I. Choi, J. Oh, S. Ye, J. Lee, T. Kim, H.-G. Ko, C.-S. Lim, et al.: *Interregional synaptic maps among engram cells underlie memory formation*, “Science” vol. 360, no. 6387, 430–435 (2018) (cited on page 67).

[164] S. Craner, G. Hoffman, J. Lund, A. Humphrey, and R. Lund: *cFos labeling in rat superior colliculus: activation by normal retinal pathways and pathways from intracranial retinal transplants*, "Experimental neurology" vol. 117, no. 3, 219–229 (1992) (cited on page 73).

[165] S. M. Dudek, G. M. Alexander, and S. Farris: *Rediscovering area CA2: unique properties and functions*, "Nature Reviews Neuroscience" vol. 17, no. 2, 89 (2016) (cited on pages 82, 86).

[166] F. Leroy, J. Park, A. Asok, D. H. Brann, T. Meira, L. M. Boyle, E. W. Buss, E. R. Kandel, and S. A. Siegelbaum: *A circuit from hippocampal CA2 to lateral septum disinhibits social aggression*, "Nature" vol. 564, no. 7735, 213–218 (2018) (cited on pages 82, 86).

[167] K. Kohara, M. Pignatelli, A. J. Rivest, H.-Y. Jung, T. Kitamura, J. Suh, D. Frank, K. Kajikawa, N. Mise, Y. Obata, et al.: *Cell type–specific genetic and optogenetic tools reveal hippocampal CA2 circuits*, "Nature neuroscience" vol. 17, no. 2, 269 (2014) (cited on pages 82, 86).

[168] E. Campanac and D. Debanne: *Spike timing-dependent plasticity: a learning rule for dendritic integration in rat CA1 pyramidal neurons*, "The Journal of physiology" vol. 586, no. 3, 779–793 (2008) (cited on page 85).

[169] K. A. Buchanan and J. R. Mellor: *The development of synaptic plasticity induction rules and the requirement for postsynaptic spikes in rat hippocampal CA1 pyramidal neurones*, "The Journal of Physiology" vol. 585, no. 2, 429–445 (2007) (cited on page 85).

[170] R. M. Meredith, C. D. Holmgren, M. Weidum, N. Burnashev, and H. D. Mansvelder: *Increased threshold for spike-timing-dependent plasticity is caused by unreliable calcium signaling in mice lacking fragile X gene FMR1*, "Neuron" vol. 54, no. 4, 627–638 (2007) (cited on page 85).

[171] J.-Y. Chang, Y. Nakahata, Y. Hayano, and R. Yasuda: *Mechanisms of Ca 2+/calmodulin-dependent kinase II activation in single dendritic spines*, "Nature communications" vol. 10, no. 1, 1–12 (2019) (cited on page 86).

[172] V. Chevaleyre and R. A. Piskorowski: *Hippocampal area CA2: an overlooked but promising therapeutic target*, "Trends in molecular medicine" vol. 22, no. 8, 645–655 (2016) (cited on page 86).

[173] P. R. Evans, P. Parra-Bueno, M. S. Smirnov, D. J. Lustberg, S. M. Dudek, J. R. Hepler, and R. Yasuda: *RGS14 restricts plasticity in hippocampal CA2 by limiting postsynaptic calcium signaling*, "eneuro" vol. 5, no. 3 (2018) (cited on page 86).

[174] P. R. Evans, K. J. Gerber, E. B. Dammer, D. M. Duong, D. Goswami, D. J. Lustberg, J. Zou, J. J. Yang, S. M. Dudek, P. R. Griffin, et al.: *Interactome analysis reveals regulator of G protein signaling 14 (RGS14) is a novel calcium/calmodulin (Ca2+/CaM) and CaM kinase II (CaMKII) binding partner*, "Journal of proteome research" vol. 17, no. 4, 1700–1711 (2018) (cited on page 86).

[175]C. P. O'Banion and R. Yasuda: *Fluorescent sensors for neuronal signaling*, "Current Opinion in Neurobiology" vol. 63, 31–41 (2020) (cited on page 86).

[176]T. Laviv, B. Scholl, P. Parra-Bueno, B. Foote, C. Zhang, L. Yan, Y. Hayano, J. Chu, and R. Yasuda: *In vivo imaging of the coupling between neuronal and CREB activity in the mouse brain*, "Neuron" (2019) (cited on page 86).

[177]S. A. Josselyn and S. Tonegawa: *Memory engrams: Recalling the past and imagining the future*, "Science" vol. 367, no. 6473 (2020) (cited on page 86).

[178]L. G. Reijmers, B. L. Perkins, N. Matsuo, and M. Mayford: *Localization of a stable neural correlate of associative memory*, "Science" vol. 317, no. 5842, 1230–1233 (2007) (cited on page 86).

[179]S. Ramirez, X. Liu, P.-A. Lin, J. Suh, M. Pignatelli, R. L. Redondo, T. J. Ryan, and S. Tonegawa: *Creating a false memory in the hippocampus*, "Science" vol. 341, no. 6144, 387–391 (2013) (cited on page 86).

[180]K. K. Tayler, K. Z. Tanaka, L. G. Reijmers, and B. J. Wiltgen: *Reactivation of neural ensembles during the retrieval of recent and remote memory*, "Current Biology" vol. 23, no. 2, 99–106 (2013) (cited on page 86).

[181]S. Ramirez, S. Tonegawa, and X. Liu: *Identification and optogenetic manipulation of memory engrams in the hippocampus*, "Frontiers in behavioral neuroscience" vol. 7, 226 (2014) (cited on page 86).

[182]W. Deng, M. Mayford, and F. H. Gage: *Selection of distinct populations of dentate granule cells in response to inputs as a mechanism for pattern separation in mice*, "Elife" vol. 2, e00312 (2013) (cited on page 86).

STATEMENT OF CONTRIBUTION

OHSCs and culture media were prepared by Iris Ohmert or Sabine Graf.

Supervision and technical assistance with the patch-clamp setup was provided by Christine E. Gee. Bas van Bommel and Antonio Virgilio Failla provided technical assistance with STED microscopy. Michaela Schweizer provided access to the confocal microscope. Thomas G. Oertner designed and constructed the in-incubator stimulation towers and off-axis stimulation pathway for the patch-clamp setup.

Christine E. Gee and Sabine Graf did the in-incubator stimulations to ensure the blinding.

CheRiff construct was kindly provided by Adam Cohen. ChrimsonR was a kind gift from Edward Boyden. Calmodulin was recieved from Simon Sandler (the laboratory of Prof. Dr. Henning Tidow). Iris Ohmert cloned and prepared plasmids. Ingke Braren (UKE Vector facility) prepared viruses.

Lennart Sobirey wrote the Matlab software to analyze the oSTDP data and provided substantial help with general automatization of data analysis.

Lennart Sobirey and Christine E. Gee proofread the thesis.

ACKNOWLEDGEMENTS

This work was not possible without many people, whom I would like to acknowledge here. Foremost, dear Thomas Oertner and Christine Gee, thank you for the opportunity to do my dissertation in your laboratory. Your technical knowledge, experience and opinions strongly pushed my scientific development through those years. I highly appreciate that you encouraged me and provided an opportunity to attend conferences, meetings, talks and the MBL summer school. Thank you for being very caring and attentive supervisors! I felt your support throughout my PhD and I highly appreciate that you were always there for me and always found time, when I needed your help.

I would also like to thank my secondary supervisor Prof. Dr. Robert Blick for being a valuable part of my mentoring and thesis committee.

A special thank goes to Iris Ohmert and Sabine Graf for an excellent technical support and for the weekly slice culture preparation. Additional thanks to Sabine Graf and Christine Gee for helping me with the in-incubator stimulations for both of my projects.

Liebe Heike Pehlke, vielen dank, dass du mir immer mit Bestellungen und Reisen geholfen hast! Danke für nette Unterhaltungen und gute Laune!

Thanks to all the lab members for your comprehensive support over the years. Oana, thank you very much for being my conference-buddy, we had many memorable trips together! Special thanks goes to Marie. Even though you just recently joined the laboratory, you became a very dear friend to me. Also thank you for sharing my frustration with Imaris and dragging me out for occasional coffee-breaks.

Dear now already my almost-husband Lennart, thank you for being there for me in the darkest moments and thank you for encouraging me to come to Europe. I would definitely not do it, if it was not because of you! Thank you for your love and support, I am looking forward to see what the coming years will bring us!

И конечно же огромное спасибо моим родителям Владимиру и Ольге Анисимовым за то, что поддержали меня в моем стремлении реализовать себя заграницей. Спасибо за то, что всегда были рядом, даже когда между нами были тысячи километров! Спасибо, что всегда помогали с учебой и мотивировали заниматься наукой!

Моя дорогая Светочка теперь уже Язвенко, а не Кузнецова, как тогда, когда мы познакомились в колледже. Спасибо, что оставалась самой близкой моей подругой все эти годы! С нетерпением жду нашей следующей встречи!

Вика Алёхина, мир действительно странное место, так как познакомились мы благодаря Японии, хотя многие годы жили практически в соседних домах. Спасибо, что ты была всегда готова меня выслушать и морально поддержать!

Алина Савилова, ты стала моим лучиком солнца в пасмурном Гамбурге. Я очень счастлива, что познакомилась с тобой и что из этого знакомства выросла такая прекрасная дружба! Спасибо за всю твою поддержку и спасибо, что помогла мне посмотреть на мою жизнь свежим взгядом и начать меняться к лучшему!

С получением этой докторской степени путь еще не пройден, все еще только начинается!

EIDESSTATTLICHE VERSICHERUNG

Hiermit versichere ich an Eides statt, die vorliegende Dissertationsschrift selbst verfasst und keine anderen als die angegebenen Hilfsmittel und Quellen benutzt zu haben.

Die eingereichte schriftliche Fassung entspricht der auf dem elektronischen Speichermedium.

Die Dissertation wurde in der vorgelegten oder einer ähnlichen Form nicht schon einmal in einem früheren Promotionsverfahren angenommen oder als ungenügend beurteilt.

Hamburg, den 27.07.2020

Margarita Anisimova